

**BRIDGE DECK CORNER CRACKING
ON SKEWED STRUCTURES**

Final Report to
Michigan Department of Transportation

Gongkang Fu, Jihang Feng, Jason Dimaria, and Yizhou Zhuang

Department of Civil and Environmental Engineering

Wayne State University

RC-1490

September 2007

Technical Report Documentation Page

1. Report No. Research Report RC-1490	2. Government Accession No.	3. MDOT Project Manager Roger Till	
4. Title and Subtitle Bridge Deck Corner Cracking on Skewed Structures		5. Report Date June 13, 2007	
7. Author(s) Gongkang Fu, Jihang Feng, Jason Dimaria, and Yizhou Zhuang		6. Performing Organization Code	
9. Performing Organization Name and Address Wayne State University, Center for Advanced Bridge Engineering Department of Civil and Environmental Engineering 5050 Anthony Wayne Dr., Detroit, MI 48202		8. Performing Org Report No. CE-2007-05	
12. Sponsoring Agency Name and Address Michigan Department of Transportation Construction and Technology Division P.O. Box 30049 Lansing, MI 48909		10. Work Unit No. (TRAIS)	
		11. Contract Number: 2002-0546	
		11(a). Authorization Number: 4	
15. Supplementary Notes		13. Type of Report & Period Covered Final report, July 2004 - August 2007	
		14. Sponsoring Agency Code	
16. Abstract This study had a focus on corner cracking in concrete decks of skew highway bridges. A survey of state transportation agencies in the U.S. was conducted on this subject. It found that deck corner cracking in skew bridges is commonly observed. Deck inspection for bridges in Michigan was also performed in this study. Cracking intensity in these decks was viewed as an effect of several possible causal factors, which was collected from 40 bridge decks, including 20 straight and 20 skewed structures. Analysis of the inspection results indicates no clearly agreeable causal relations. Two skew decks were instrumented using temperature and strain sensors for the concrete and the ambient environment. Concrete deck's temperature and strain response was collected to thermal-, shrinkage-, and truck-wheel-loads. Test results and thereby calibrated finite element analysis results show that the main cause of skew deck corner cracking is cement concrete's thermal and shrinkage load. Based on current Michigan practice of skew deck design and construction, additional reinforcement in the corner areas is therefore recommended to reduce concrete stresses. Further research is also recommended to develop solutions using optimal combinations of ingredients in concrete and to minimize the constraint between the deck and the supporting superstructure.			
17. Key Words Skew bridge, concrete deck, corner cracking, causes, cures		18. Distribution Statement No restrictions. This document is available to the public through the Michigan Department of Transportation.	
19. Security Classification (report) Unclassified	20. Security Classification (Page) Unclassified	21. No of Pages	22. Price

Table of Contents

I.	Introduction	---- 5
	I-1. Background	---- 5
	I-2. Research Objectives	---- 7
	I-3. Report Organization	---- 8
II.	State of the Art and Practice	---- 11
	II-1. Literature Review	---- 11
	II-2. Survey of State Transportation Agencies	---- 18
	II-3. Summary	---- 21
III.	Performance of Skew Decks in Michigan	---- 29
	III-1. Inspection Program	---- 29
	III-2. Analysis of Inspection Results	---- 41
IV.	Behavior of Typical Skew Decks Using Physical Measurement	---- 48
	IV-1. Experiment Program	---- 48
	IV-2. Instrumentation	---- 51
	IV-3. Measurement Results	---- 53
	IV-4. Discussions	---- 74
V.	Behavior of Skew Decks Using Finite Element Analysis	---- 75
	V-1. FEA Modeling and Validation	---- 75
	V-2. Analysis of Typical Skew Decks in Michigan	---133
	V-3. Discussions	---140
VI.	Discussions and Recommendations	----142
	VI-1. Recommended Cures for Skew Deck Corner Cracking	----142
	VI-2. Recommended Future Research Work	----144
	VI-3. Implementation Considerations	----144
	VI-4. Cost- Benefit Analysis	----145
	References	----146

Acknowledgements

The research work reported here was financially supported by the Michigan Department of Transportation in cooperation with the U.S. Federal Highway Administration. This support is gratefully appreciated. The direction of Mr. Roger Till and the Research Advisory Panel for the project has been very important to the successful completion of this study. Many student research assistants at Wayne State University have contributed to the this work, including Sarika Butala, Lixiang Yang, Dinesh Devaraj, Tapan Bhatt, Kiran Chiniva, Jian Ye, and Shubhada Gadkar. They assisted in various tasks reported therein.

CHAPTER I INTRODUCTION

I-1. Background

Reinforced concrete (RC) is a very common material for the highway bridge deck. It has a number of advantages: 1) Easy to construct with respect to deck dimensions.

2) Relatively lower requirement for maintenance and thus longer service life without maintenance, compared with other common construction materials, such as timber and steel. 3) Acceptable cost-effectiveness. On the other hand, along with increasing experience with concrete, there has been a growing concern with concrete for bridge decks. It is its longevity adversely affected by cracking. Figure I-1 shows an example of such cracking in a concrete bridge deck in Michigan, where cracks were marked using orange paint for a quantitative survey.

Historically, concrete structures have been primarily designed on the basis of strength only. The widespread decay of concrete structures in the infrastructure system, however, has indicated a need for design procedures that consider long-term durability.

Concrete is a composite material in which aggregate particles are bonded together using Portland cement and water. The water in the concrete serves two purposes. When concrete is still in the fluid state, it allows the composition to be workable. Water also participates in the chemical reaction (hydration) responsible for forming the “glue” that bonds the aggregates together. Typically, concrete is volumetrically stable if it remains in an environment of constant moisture and temperature. However, changes in the moisture and temperature of the surrounding

environment cause moisture movement within concrete, which results in a volumetric change. The amount of this volumetric change for a concrete mix is dependent on a variety of factors including the mix proportion, environmental condition, concrete age, structure size, etc. When this volumetric change is constrained by other necessary components (such as the supporting beams) in contact with concrete, the concrete can develop stresses significant enough to cause cracking.

In addition, thermal strains constrained by the supporting beams may also cause cracking due to a similar mechanism. The thermal strains may be caused by concrete hydration, and temperature variations due to climate change and/or daily cycling. Furthermore, there has also been concern with truck wheel loading that may cause or worsen cracking in a concrete deck.

In bridges with skew, such cracking has been seen more severe in the corner areas. Figure I-2 shows such cracks of a concrete deck in a bridge with a skew of about 29 degrees. These cracks typically start with a right angle to the deck edge that is along the direction of the supports (an abutment and/or a pier). This research project has a focus on this phenomenon, in order to increase the service life of the bridge deck and the entire structure the deck is supposed to protect.

I-2. Research Objectives

The research project's objective is to identify possible causes for corner cracking of skew concrete bridge decks, and to recommend viable options that may eliminate or reduce such cracking.

This research project was proposed to include the following tasks to reach the research objective.

Task 1: Review of state of the art and the practice including implementation efforts in addressing the subject issue. Task 2: Gathering field performance data from skewed and non-skewed RC decks to understand the severity of corner cracking in skew concrete decks in service in Michigan. Task 3: Statistical analysis of the performance data obtained in Task 2 to attempt to understand possible relations of deck cracking severity with a number of factors such as skew angle magnitude, slab thickness, span type, etc. Task 4: Testing typical skewed concrete decks to perform physical measurement for concrete strain response to thermal, shrinkage, and truck wheel loads. These data were thought to be important to understand the behavior of skew concrete decks and to provide a reference for calibrating the finite element analysis (FEA) model to be used in the next task. Task 5: FEA of selected straight and skewed concrete decks using the calibrated modeling method to analyze 12 cases of concrete decks with typical Michigan skew angles, beam spacings, and beam types. The analysis was to provide understanding of the effect of these parameters. Task 6: Determining possible causes of corner cracking in skewed RC decks using the data and information resulting from Tasks 4 and 5. This result will lead to the development of possible solutions to eliminate or reduce such cracking. Task 7: Prepare

quarterly reports and a final report. These reports were to record the progress to date in the project, present the research process, and document the final results.

I-3. Report Organization

This report includes five more chapters. These chapters are organized following the concept of project design presented above. Besides this chapter of introduction, Chapter II briefly presents state of the art and practice related to corner cracking of skew concrete decks. Chapter III summarizes the inspection program included in this research project for existing concrete decks in service. It is to quantitatively understand the severity of such cracking in concrete decks in Michigan. Chapter IV describes the experimental program for this research project, and presents and discusses the measurement results. Chapter V presents the study program of the finite element analysis and its results, which also exhibits possible causes of corner cracking in skew concrete decks. Chapter VI analyzes and synthesizes all the information gathered in this project, including the state agency survey results, the physical measurement results, and the finite element analysis results, and then develops recommendations to eliminate or reduce corner cracking. In addition, a process of implementation of the recommendations and a cost benefit analysis are presented to facilitate implementation of the research results.



Figure I-1 Concrete Deck Cracking Highlighted Using Orange Paint
(S11 of 12033, Pearl Beach Road over I-96)



Figure I-2 Corner Cracking of Skewed Concrete Deck
(S10-4 of 77111, I-94 WB over Gratiot in St. Clair County)

CHAPTER II STATE OF THE ART AND PRACTICE

II-1. Literature Review

A larger number of studies have been conducted on concrete bridge deck cracking and its effect on the deck durability. On the other hand, few reports, papers, or documented work have been found in this study directly addressing the issue of corner cracking in skewed bridges in the literature or with the surveyed state transportation agencies. Since deck cracking in general is relevant to the research objective here, this literature review also covers that aspect. It should also note that this review is not intended to be comprehensive but rather brief and covering the major issues and / or factors relevant to concrete deck cracking.

Purvis et al.,(1995) studied premature cracking of concrete bridge decks using a three-phase approach. The first phase included examination of existing bridge decks by visual inspection of 111 bridge decks in Pennsylvania. The inspected bridges were built within 5 years of the survey and an in-depth examination was conducted on 12 of the 111 bridge decks. The in-depth examination included the documentation of crack patterns, crack width, rebar location and depth, and finally concrete coring. The results of this phase indicated that almost all transverse cracks followed the line of the top transverse bars, regardless of the superstructure type. Coring of concrete showed that transverse crack depth extended to the level of the top transverse bars and beyond. It was also observed that transverse cracks often intersect coarse aggregate particles. This indicated that the cracks occurred in the hardened concrete as opposed to the plastic concrete. It was concluded that the cause of cracking was most likely drying shrinkage and

thermal shrinkage, rather than factors such as plastic shrinkage caused by surface evaporation prior to curing or settlement of plastic concrete between the top transverse bars.

The second phase of this study involved the observation of the construction of eight bridge decks to identify construction steps possibly contributing to shrinkage and cracking. The third phase involved laboratory experiments that focused on examining the effects of aggregate, cement, and fly ash on shrinkage. The result of this phase led to a conclusion that the main cause of transverse cracking is the shrinkage of hardened concrete. Further, the type of aggregate used in the concrete mix is a major factor associated with shrinkage cracking. Aggregate contributes to drying shrinkage of concrete in two different ways. First, certain aggregates need more water in the mix to produce the desired slump and workability, and the extra water increases shrinkage. Secondly, certain aggregates yield to the pressure from the shrinking paste and do not provide sufficient restraint against shrinkage. Therefore the study recommended using lower water content in the concrete mix in order to reduce drying shrinkage. Another important factor is the cement type. The study indicated that type II cement has lower heat of hydration and less drying shrinkage than type I cement. It was indicated that the less cement used, the less heat generated, the less water is required for hydration.

NCHRP Report 380 (Krauss and Rogalla 1996) is believed to have reported the most comprehensive study performed to date on transverse bridge deck cracking. The study included a survey of state departments of transportation in U.S. and several overseas transportation agencies, analytical studies, laboratory research, and field measurements of a bridge deck during and shortly after construction. However, the field measurement readings were not published.

Krauss and Rogalla (1996) also ranked the concrete material properties and material-related mechanisms that lead to early-age bridge deck cracking as shown in Table II-1. Other factors affecting cracking related to design and construction are also shown in the table. The study indicated that concrete material factors that are important in reducing early-age cracking include low shrinkage, low modulus of elasticity, high creep, low heat of hydration, and aggregates. Other material factors that are helpful in reducing the risk of cracking include reduction of cement content, use of shrinkage compensating cement and avoidance of silica fume admixtures and other materials that produce very high early compressive strength and modulus of elasticity. Concrete with these properties is prone to cracking because it creeps very little. It was also recommended that use of other cementitious materials with less drying shrinkage should be pursued. Air entrainment, water reducers, retarders, and accelerators were considered to have minimal effects on cracking.

A restrained ring test was also utilized in Krauss and Rogalla (1996) to measure the tendency of concrete to undergo drying shrinkage cracking, as well as to compare various concrete mixtures, curing, and environmental factors. The major advantage of using the restrained ring test is that it takes into consideration of all material factors that influence shrinkage cracking from the time of casting. Furthermore, it does not require complex calculations. The ring test was used to investigate the effects of many factors such as water to cement ratio, cement content, aggregate size and type, silica fume, set accelerators and retarder, air entrainment, cyclic temperature, evaporation rate, curing and shrinkage compensating cement. Rings cast with Type K expansive cement cracked much later than the control mix. Moreover, the mixes containing

silica fume cracked 5 to 6 days earlier than the companion mixes without silica fume. The test also showed that a mix with 28 percent of the Portland cement replaced with a Type F fly ash cracked only slightly later (4.3 days) than the control specimens.

Table II-1 Factors Relevant to Concrete Deck Cracking (Krauss and Rogalla 1996)

Factors	Effect			
	Major	Moderate	Minor	None
Design				
Restraint	√			
Continuous/simple span		√		
Deck thickness		√		
Girder Size		√		
Alignment of top and bottom reinforcement bars		√		
Form type		√		
Concrete cover			√	
Girder spacing			√	
Quantity of reinforcement			√	
Reinforcement bar sizes			√	
Dead-load deflections during casting			√	
Stud spacing			√	
Span length			√	
Bar type-epoxy coated			√	
Skew			√	
Traffic volume			√	
Frequency of traffic-induced vibrations				√
Materials				
Modulus of elasticity	√			
Creep	√			
Heat of hydration	√			
Aggregate type	√			
Cement content and type	√			
Coefficient of thermal expansion		√		
Paste volume---free shrinkage		√		
Water-cement ratio		√		
Shrinkage-compensating cement		√		
Silica fume admixtures		√		
Early compressive strength			√	
HRWRAs			√	
Accelerating admixtures			√	
Retarding admixtures			√	
Aggregate size			√	
Diffusivity			√	
Poisson's ratio			√	
Fly ash				√
Air content				√
Slump				√
Water content				√
Construction				
Weather	√			
Time of casting	√			
Curing period and method		√		
Finishing procedures		√		
Vibration of fresh concrete			√	
Pour length and sequence			√	
Reinforcement ties				√
Construction loads				√
Traffic-induced vibrations				√
Revolutions in concrete truck				√

To control thermal shrinkage, Babaei and Fouladgar (1987) recommended the use of a mix design with cement content as low as possible. When less cement content is used, less heat of hydration is generated. Pozzolans and slag can be used as partial substitutes for Portland cement. It was also recommended that Type II cement be used rather than Type I because Type II generates lower heat of hydration. Furthermore, as a means of controlling thermal shrinkage, use of retarders in the mix is recommended to delay the hydration process and reduce the rate of heat generated. The effect of aggregate type on drying shrinkage was also studied. A soft aggregate such as sandstone tends to result in increased drying shrinkage, while hard aggregates such as quartz, dolomite, and high limestone tend to result in decreased drying shrinkage. Also, use of less water in the mix resulted in decreased drying shrinkage.

Shah et al.(1998) observed that cracking has been shown to increase in higher strength concrete, especially with the addition of silica fume. It was recommended in this work that randomly distributed fiber reinforcement can be used to significantly reduce crack width. Different fiber compositions can alter the degree to which this occurs. It was also found that with a two percent addition of shrinkage reducing admixture (SRA) by weight of cement, drying shrinkage should be reduced by nearly 50 percent.

Similarly, French et al. (1998) investigated 72 bridges in the Minneapolis/St. Paul metropolitan area to address the issue of concrete cracking. In this study, the dominant material parameters associated with transverse cracking in bridge deck were identified as cement content, aggregate type and quantity, and air content. Data obtained from the material reports for 21 of the bridge deck mixes (including 12 prestressed- and 9 steel-beam bridges) show that cement content is a

major factor contributing to premature deck cracking. Namely, higher cement content causes more cracking. Increased aggregates and increased air content were also found respectively to have reduced cracking.

The earliest experimental investigation on skewed RC decks compared with their straight counterpart perhaps is Newmark et al (1946, 1947). The study used quarter-scaled RC deck models with 0, 30, and 60 degrees of skew. Using load testing, the maximum strain in the main (transverse) rebar was found to increase with the skew angle. For composite decks with respectively 30 and 60 degree skew, this strain was 1.23 and 1.29 times of the straight deck's counterpart, and 1.36 and 1.65 times for noncomposite decks with only natural bonding to the beams. This conclusion appears to be consistent with observations of corner cracking in skewed decks in Michigan and other states (Fu et al 1994, Castaneda 1995). It should be also noted that strains in concrete were not measured in this study.

It is relevant to note that the current AASHTO standard design code (2002) does not have specific provisions for skewed RC decks. Except an allowance for the transverse main reinforcement to follow the skew when the skew angle is smaller than 25 degrees, the AASHTO LRFD design code (2004) also has no considerations to skew in deck analysis and design. Both codes use a concept of isolating a "typical strip" of the deck for design. This approach, however, ignores the influence of the beam system supporting the deck, resulting in a simplistic model that possibly misses the governing stress/strain condition, depending on a number of factors including the magnitude of skew angle.

II-2. Survey of State Transportation Agencies

A survey of state transportation agencies was conducted in this study to understand whether they experience the problem of corner cracking in skewed concrete decks and to possibly learn their experience and solution to the problem. The survey included the following focus areas: 1) Observed severity of concrete deck corner cracking in skewed structures and its behavior (where in the deck, when cracked, what percentage of decks experiencing cracking, orientation of cracks, etc.) 2) Actions taken to address such cracking. 3) Special design requirements for skewed decks. 4) Special design requirements for reinforcement in skewed decks.

Out of the 52 state level agencies, 36 returned the questionnaire, representing a 69% return rate. The responses are summarized in Tables II-2 to II-5. Table II-2 focuses on the observed cracking in skew concrete decks. It is seen that out of the 36 agencies that responded, 17 have observed concrete deck corner cracking. In addition, two also reported transverse cracking, not necessarily in the corner area. Six other agencies did not know whether corner cracking was present in their bridge decks, and 13 said that there was no deck-corner cracking.

Out of the 17 agencies that indicated presence of corner cracking in their skew bridges, 5 said 0 to 25% of their decks have such cracking, 6 said 25 to 50%, 3 said 50 to 75%, and 3 said 75 to 100%. In other words, 12 out of 17 agencies said that more than 25% of their skew concrete decks have corner cracking. A majority of the states (10 out of 17) said that such cracking was observed within first 3 months of the deck life, 5 states said 3 to 12 months, and only 2 agencies said more than 12 months. A large number of the states (14 out of 17) indicated that the most

commonly seen cracking location is the acute angle area, with only one agency indicating the obtuse angle area. Two agencies responded with “do not know” as to in what areas in the deck cracking is more commonly seen. As far as the major direction of such corner cracking is concerned, the most often observed direction is perpendicular to the radial direction (7 agencies), followed by radial direction (5 agencies), transverse direction (3 agencies), longitudinal direction (one agency), and random directions (one agency).

It is appropriate to conclude that corner cracking in skewed concrete bridge decks is not a local issue. Such cracking is mostly observed in the early age of the deck (within 3 to 12 months), in the acute angle area, and in directions perpendicular to the radial direction.

Table II-3 includes the responses to the questions regarding actions or understanding after cracking is observed. Only a few agencies have taken action on corner cracking in skewed concrete bridge decks. Among them, Colorado developed new design, Delaware conducted research and added radial steel, New York conducted research, and Missouri used a new mix design that turned out to have also reduced cracking. For repair such cracking, deck sealing is seen in Table II-3 as the overwhelmingly common measure, if ever done. To the question on what type(s) of beam as seen to cause most cracking, most responding agencies either said “don’t know” or offered no comments. Others identified prestressed concrete beams (4 agencies) and steel beams (3 agencies), integral abutment (one agency), and precast flat slabs (one agency). All agencies except two indicated their interest in the result of this survey, showing a strong nationwide interest in the issue.

The questionnaire has also asked the state agencies for any special requirements for the design of concrete skew decks, which may be different from those for straight decks. The information obtained was used as leads for gathering more details, such as the web sites provided, excerpts of the specifications attached, follow-up phone conversations, etc. Tables II-4 and II-5 show summaries for the special requirements used by the responding agencies, which are discussed further next.

Four states have a specific requirement for the reinforcement orientation in skew decks. Table II-4 focuses on the cutoff skew angle at which the reinforcement will not follow the skew angle. It is seen that for the four states included, this cutoff angle ranges from 15 to 30 degrees. Note that the LRFD design code's counterpart is 25 degrees.

Table II-5 summarizes the findings from the survey and follow up investigations on the quantity of reinforcement in skew decks. It is seen that seven states have specific design requirements for additional reinforcement. Three of these states (Arizona, Arkansas, and Minnesota) did not indicate a cutoff threshold, so their respective requirements for additional steel are applied to all skew decks. The other four states have their requirements specified according to the cutoff thresholds. In general, skew requires more steel and to be specially arranged. As seen, some states require further more steel when the skew angle exceeds the threshold value.

II-3. Summary

The literature review and state survey can be summarized as follows.

- 1) Corner cracking in concrete skew bridge decks is not a local issue, and many other states observe the same problem.
- 2) Despite the commonly observed problem, very little research result has been reported or documented that directly addresses the issue of concrete deck corner cracking in skewed bridges. On the other hand, a large amount of research results are available regarding concrete deck cracking in general, which may be of interest to this research project.
- 3) A number of states have some special requirements for the design of concrete skew decks, including the reinforcement orientation and additional quantity. Nevertheless, the basis for these requirements has not been documented.

Table II-2 Survey Results 1 – Corner Cracking in Skewed Concrete Decks

State	Cracking detected in corner of RC decks?	Estimated percentage of decks with cracking	When is cracking observed	Where is cracking observed	What type of cracking is most profound
Alabama	no				
Alaska	no				
Arizona	no				
Arkansas	don't know				
California	don't know				
Colorado	yes	50-75%	3 months to 1 year	acute angle area	radial, from the corner
District of Columbia	no				
Delaware	yes	0-25%	0 to 3 months	acute angle area	radial, from the corner
Florida	don't know		0 to 3 months	don't know	transverse
Georgia	no				
Hawaii	don't know				
Idaho	yes	25%-50%	0 to 3 months	don't know	perpendicular to the radial direction
Illinois	no				
Indiana	yes	75%-100%	0 to 3 months	acute angle area	perpendicular to the radial direction
Kansas	yes	0-25%	3 months to 1 year	obtuse angle area	radial from the corner
Maine	no				
Michigan	yes	0 to 25%	3 months to 1 year	acute angle area	perpendicular to the radial direction also random difficult to describe

Table II-2 Survey Results 1 – Corner Cracking in Skewed Concrete Decks (cont'd)

State	Cracking detected in corner of RC decks?	Estimated percentage of decks with cracking	When is cracking observed	Where is cracking observed	What type of cracking is most profound
Minnesota	yes	25%-50%	0 to 3 months	acute angle area	perpendicular to the radial direction
Mississippi	no	0 to 25%	3 months to 1 year	acute angle area	transverse
Missouri	yes	75-100%	0 to 3 months	acute angle area	radial from the corner
Montana	don't know				
Nebraska	no				
Nevada	yes	0%-25%	more than 1 year	acute angle area	random, difficult to describe
New Jersey	no				
New Mexico	no				
New York	yes	50%-75%	0 to 3 months	acute angle area	perpendicular to the radial direction
North Carolina	no				
North Dakota	don't know				
Oklahoma	yes	50%-75%	3 months to 1 year	no comment	longitudinally and transvers
South Carolina	yes	75%-100%	0 to 3 months	acute angle area	transverse

Table II-2 Survey Results 1 – Corner Cracking in Skewed Concrete Decks (cont'd)

State	Cracking detected in corner of RC decks?	Estimated percentage of decks with cracking	When is cracking observed	Where is cracking observed	What type of cracking is most profound
Tennessee	yes	25%-50%	0 to 3 months	acute angle area	random, difficult to describe
Texas	no				
Utah	yes	25-50%	3 months to 1 year	acute angle area	transverse
Virginia	yes	0 to 25%	more than 1 year	acute angle area	perpendicular to the radial direction
Washington	yes	25-50%	0 to 3 months	acute angle area	radial from the corner
Wyoming	yes	25%-50%	0 to 3 months	acute angle area	perpendicular to the radial direction

Table II-3 Survey Results 2 – Actions for Observed Cracking

State	Action taken	RC deck cracking repair	Girder types causing most severe cracking	Interested in survey results?
Alabama				yes
Alaska				yes
Arizona				yes
Arkansas				yes
California				yes
Colorado	developed new design and revised concrete bridge policy	sealing	don't know	yes
District of Columbia				yes
Delaware	conducted research and added radial steel rebars	sealing	steel	yes
Florida	no	sealing	precast flat slabs	yes
Georgia				yes
Hawaii				yes
Idaho	no		prestressed concrete	yes
Illinois				yes
Indiana	no	epoxy injection	steel	yes
Kansas	no	sealing	steel	yes
Maine				yes
Michigan	conducted research, also ongoing research	sealing/epoxy injection or epoxy floodcoat	don't know	yes

Table II-3 Survey Results 2 – Actions for Observed Cracking (cont'd)

State	Action taken	RC deck cracking repair	Girder types causing most severe cracking	Interested in survey results?
Minnesota	no	sealing/epoxy penetrating sealers	don't know	yes
Mississippi	no		prestressed concrete	yes
Missouri	no, new mix desin was used but reduction of cracks were not intended, though they were reduced	sealing	prestressed concrete	yes
Montana				yes
Nebraska		sealing		yes
Nevada	yes	square off corner with brdge rail or sidewalk, sealing epoxy injection as applicable.	don't know	yes
New Jersey				yes
New Mexico				no
New York	yes, conducted research	research and sealing	integral abutments	yes
North Carolina				yes
North Dakota				no
Oklahoma	no	sealing	prestressed concrete	yes
South Carolina	no	sealing	don't know	yes

Table II-3 Survey Results 2 – Actions for Observed Cracking (cont'd)

State	Action taken	RC deck cracking repair	Girder types causing most severe cracking	Interested in survey results?
Tennessee	no	sealing, when necessary, methylmethacrylate or epoxy injection	all types induce this problem, most frequent is steel girder type	yes
Texas				yes
Utah	no	sealing, injection if larger cracks	don't know	yes
Virginia	no		don't know	yes
Washington	no	sealing, goal is to reduce further reinforcement damage not to provide structural repair. effectiveness of repair is inconclusive	don't know, cracking seems to irrelevant to girder type	yes
Wyoming	no		don't know	yes

Table II-4 Threshold Skew Angles beyond Which Reinforcement Not To Follow Skew Direction

State	Threshold Skew Angle Dictating Reinforcement Direction* (degree)	Remarks
CO	25 (to be approved)	transition from along-skew to perpendicular-to-girder is allowed for small skew
FL	15	
NY	30	
TX	15	

* When skew angle is smaller than threshold, reinforcement will be parallel to skew, otherwise perpendicular to girder.

Table II-5 Additional Steel Reinforcement Requirements for Skew Decks

	If skew angle < threshold angle	If skew angle > threshold angle
AR	yes	yes
AZ	yes	yes
FL*		3 No.5@6" along skew plus doubled longitudinal steel
MN	fanned steel in acute angle area	fanned steel in acute angle area
NC	splayed	splayed
NY*		#13 @ 100mm along skew over one-girder spacing
TX*	at 6" over 42" of deck length plus 4 bars from fascia edge to fascia beam	8 bars over 44"/cos(skew angle) of deck length plus 4 bars from fascia edge to fascia beam

* Threshold angle given in Table II-4

CHAPTER III PERFORMANCE OF SKEW DECKS IN MICHIGAN

III-1. Inspection Program

In order to understand the performance of concrete skew bridge decks in Michigan, inspection of decks was performed in this study for bridges in Michigan. The intention was to understand how severe the situation is for these decks. It was also hoped that the inspection data might provide some information on the possible causes of corner cracking in these decks.

A total of 24 decks were included in this inspection program, which were located around the state. The intention was to compare 20 skewed structures with 20 straight ones, including 14 skewed and 10 straight decks inspected in this study and 6 skewed and 10 straight decks from a recent previous study (Aktan et al 2003). This section presents the scope and details of the inspection program. The next section will discuss the inspection data and the result of their statistical analysis.

Tables III-1 and III-2 show the sample of decks for this inspection program. Also included are the 10 straight decks shaded in Table III-1 taken from the previous project (Aktan et al 2003) to maximize the use of available data. Besides the ID, a number of other characteristic factors are also listed in the tables, including length of the span inspected (not the total bridge length), aspect ratio as the ratio of bridge width to the inspected span length, span type (simple or continuous), girder type, deck slab thickness, deck age at the time of inspection, and skew angle. Girder types include steel, prestressed concrete I (PCI), concrete T (reinforced concrete T cross

section), and adjacent box (prestressed concrete boxes adjacent to on another) beams. Table III-2 contains the same information for skew decks included in this study, for 6 shaded decks taken from the earlier study plus the 14 inspected in this project.

Table III-1. Deck Crack Density of Inspected Straight Bridges and Their Parameters

Bridge ID	Crack Density (in/sqft)	Span Length (ft)	Aspect Ratio (Width/ Span Length)	Span Type	Girder Type	Slab Thickness (in)	Age (years)	Skew Angle (degree)
B01 of 06071	0.0106100	25.00	2.80	Continuous	Adjacent Box	6	4	0
B01 of 44012	0.0116893	64.99	0.70	Simple	Steel	9	3	0
B02 of 06071	0.0125310	32.00	2.26	Continuous	Steel	8	4	0
B03 of 64012	0.0008217	50.98	0.93	Simple	Adjacent Box	6	1	0
B03 of 73031	0.0102346	50.00	1.10	Simple	PCI	8	2	0
S03 of 82192	0.0067657	38.00	1.47	Simple	Steel	9	1	0
S06 of 82192	0.0045959	29.50	1.99	Simple	Steel	9	1	0
S09 of 82252	0.1430590	24.75	2.84	Continuous	Steel	9	5	0
S15 of 25032	0.0880100	32.81	2.83	Simple	Adjacent Box	6	3	0
S19 of 82023	0.1103213	28.08	2.91	Simple	Steel	8	5	0
B01 of 29021	0.0372469	91.00	0.50	Simple	PCI	9	4	0
B02 of 78061	0.0125686	88.91	0.58	Simple	Adjacent Box	6	5	0
B01 of 78061	0.0115066	60.00	0.98	Simple	Adjacent Box	6	4	0
S11 of 12033	0.0113491	108.00	0.30	Continuous	Steel	7	5	0
B01 of 38021	0.0455776	45.91	1.03	Simple	Adjacent Box	6	4	0
B02 of 46062	0.0495825	28.00	1.22	Simple	Steel	6	4	0
S03 of 82192	0.0023850	33.00	1.70	Continuous	Steel	9	3	0
S03 of 63043	0.0209660	48.00	1.32	Simple	Adjacent Box	6	5	0
S30 of 82112	0.0690398	55.30	1.25	Simple	Steel	9	4	0
S02 of 82195	0.0914714	33.00	2.71	Continuous	Steel	9	5	0

Table III-2. Deck Crack Density of Inspected Skewed Bridges and Their Parameters

Bridge ID	Crack Density (in/sqft)	Span Length (ft)	Aspect Ratio (Width/ Span Length)	Span Type	Girder Type	Slab Thickness (in)	Age (years)	Skew Angle (degree)
S03 of 63022	0.0082966	112.50	0.40	Simple	Adjacent Box	6	3	24
S04 of 82062	0.0099710	62.50	1.00	Continuous	Steel	8	4	28
S11 of 82025	0.0271360	39.00	1.79	Simple	Steel	8	5	50
S17 of 82112	0.0091386	73.95	1.65	Continuous	Steel	9	2	22
S27 of 41064	0.0004132	131.56	0.46	Simple	PCI	9	4	19
S28 of 41064	0.0030582	131.56	0.46	Simple	PCI	9	4	19
S44 of 25132	0.0247323	42.00	1.04	Simple	Steel	9	5	49
B01 of 25051	0.0496383	40.00	2.37	Simple	PCI	9	2	24
S02 of 18033	0.0355179	93.63	0.72	Simple	Steel	9	3	40
S02 of 09101	0.0173882	105.00	0.90	Continuous	Concrete T	9	5	30
B03 of 11112	0.0092593	78.25	0.91	Simple	PCI	9	4	45
S04 of 11016	0.0519442	104.00	0.81	Simple	Adjacent Box	6	4	24
S02 of 11112	0.0179297	45.80	1.03	Simple	PCI	9	5	26
B01 of 58011	0.0496383	65.62	0.72	Simple	Adjacent Box	6	1	20
S07 of 47065	0.0370477	54.50	0.65	Simple	Steel	9	4	48
S04 of 50015	0.0451475	68.00	0.71	Simple	PCI	9	2	44
S03 of 63022	0.0270707	122.60	0.37	Simple	Adjacent Box	6	5	23
B01 of 77041	0.0462953	116.70	0.40	Simple	Adjacent Box	6	5	22
S04 of 63022	0.0001943	122.10	0.38	Simple	Adjacent Box	6	1	23
S03 of 82195	0.0000000	33.00	0.74	Simple	Steel	9	1	63

To minimize the influence to traffic during deck inspection, only the driving lane of the first span was inspected for each of these bridges. The width of the inspected lane is typically 12 ft. The columns of “Span Length” in Tables III-1 and III-2 give the length of the span inspected. The focus here was on cracking of the concrete deck. Cracks were marked by spray paint next to them to make them more visible for measurement and mapping. Crack lengths were measured using a tape measure, and width using a crack width ruler. Figures III-1 to III-13 show the cracks mapped for the skew decks inspected in this project, except S03 of 82195 that showed no cracking. Note that the horizontal outlines in these crack maps are lane lines, indicating a 12 ft wide lane. Also the lengths of these inspected lane sections are the same as the span lengths recorded in Table III-2.

As seen in the crack maps, cracks extend in the longitudinal direction (along the traffic or beam direction), transverse direction (perpendicular to the traffic or beam direction), diagonal direction, and some other random directions. Note that diagonal cracking is seen mostly in the deck end areas. The total length of the observed cracks for each deck is divided by the inspected deck area to arrive at a crack density in in./sqft to quantify the severity of cracking. This density is recorded in Tables III-1 and III-2 for each deck inspected.



Figure III-1 Cracking Map for S02 of 09101



Figure III-2 Cracking Map for S44 of 25132

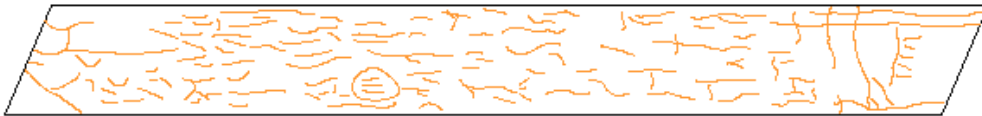


Figure III-3 Cracking Map for S04 of 11016



Figure III-4 Cracking Map for B01 of 25051

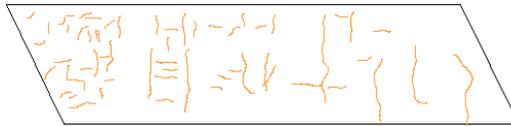


Figure III-5 Cracking Map for S02 of 11112



Figure III-6 Cracking Map for B03 of 11112



Figure III-7 Cracking Map for S02 of 18033



Figure III-8 Cracking Map for B01 of 58011

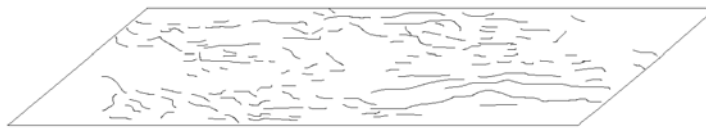


Figure III-9 Cracking Map for S07 of 47065



Figure III-10 Cracking Map for S04 of 50015



Figure III-11 Cracking Map for S03 of 63022

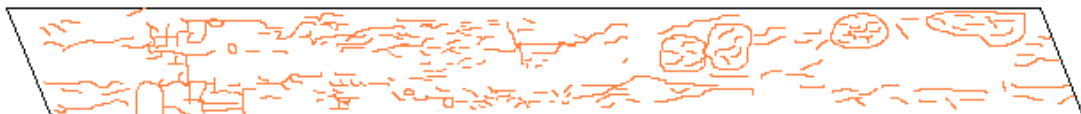


Figure III-12 Cracking Map for B01 of 77041



Figure III-13 Cracking Map for S04 of 63022

Figures III-14 to III-23 show crack maps for the ten straight bridge decks inspected in this research project. It is seen that these cracks all generally follow the longitudinal and transverse directions. Almost no crack extended in a diagonal direction. In comparison, noticeably more diagonal cracks are observed in the skew decks as shown in Figures III-1 to III-13, as well as in Figure I-2 seen earlier. These are the very focus of this study.

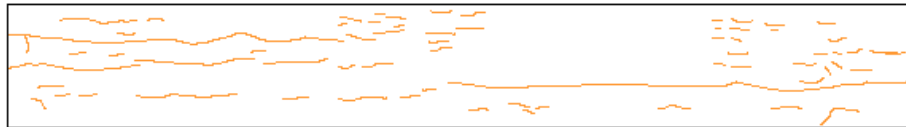


Figure III-14 Cracking Map for B02 of 78061

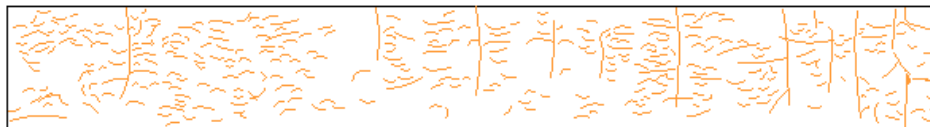


Figure III-15 Cracking Map for B01 of 29021



Figure III-16 Cracking Map for S11 of 12033



Figure III-17 Cracking Map for B01 of 78061

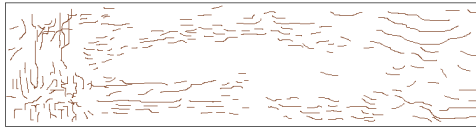


Figure III-18 Cracking Map for B01 of 38021

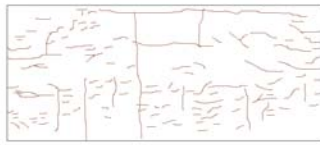


Figure III-19 Cracking Map for B02 of 46062

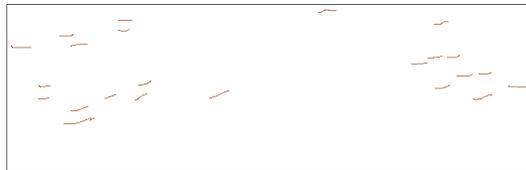


Figure III-20 Cracking Map for S03 of 82192



Figure III-21 Cracking Map for S03 of 63043



Figure III-22 Cracking Map for S30 of 82112



Figure III-23 Cracking Map for S02 of 82195

III-2. Analysis of Inspection Results

To examine relationships between the crack density and other possible causal factors, Figures III-24 to III-28 plot crack density versus a possible causal factor in each for the 20 skew decks. These factors are deck age, span length, slab thickness, skew angle, and aspect ratio. Inspection of these plots indicates, however, no noticeable statistical correlation between the crack density and any of these parameters.

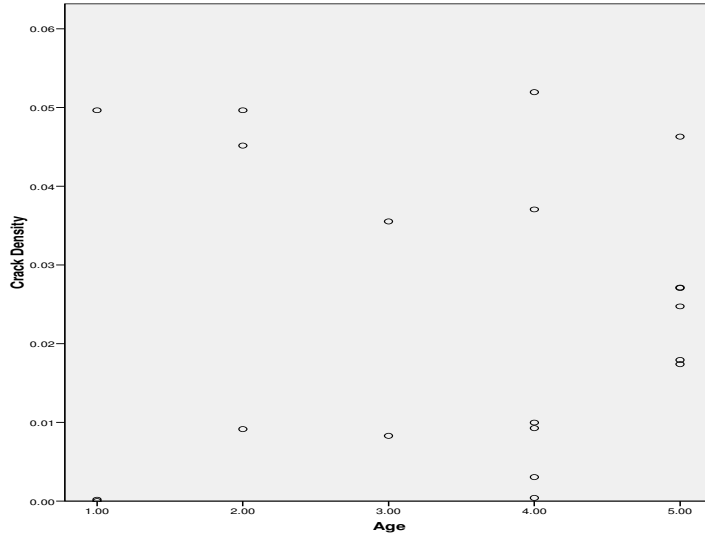


Figure III-24 Relation between Crack Density and Deck Age (yrs) for Skew Bridges

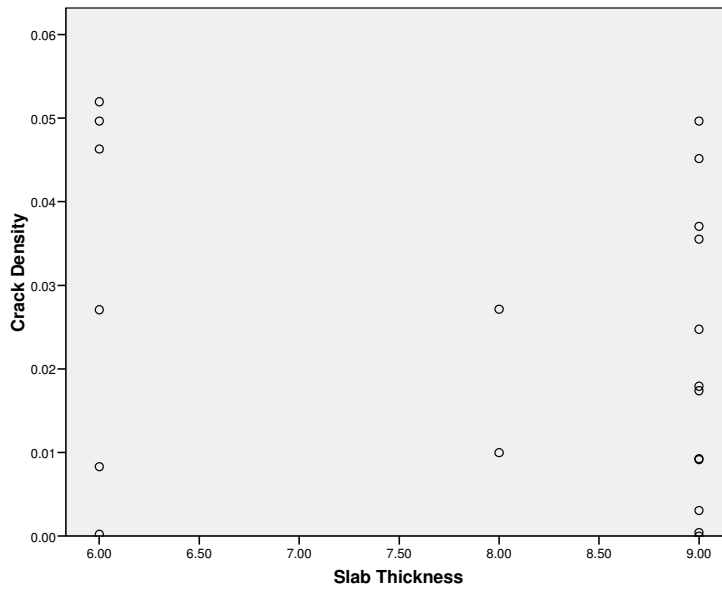


Figure III-25 Relation between Crack Density and Deck Slab Thickness (in.) for Skew Bridges

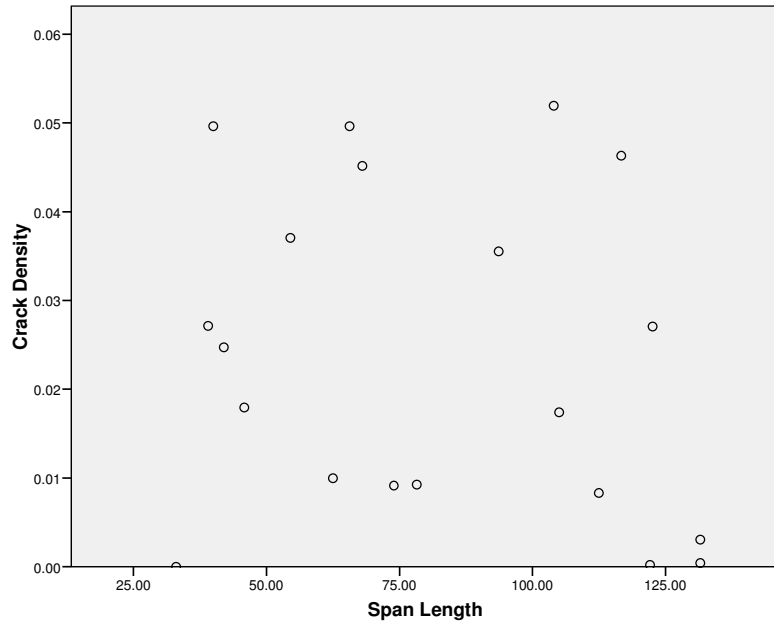


Figure III-26 Relation between Crack Density and Span Length for Skew Bridges

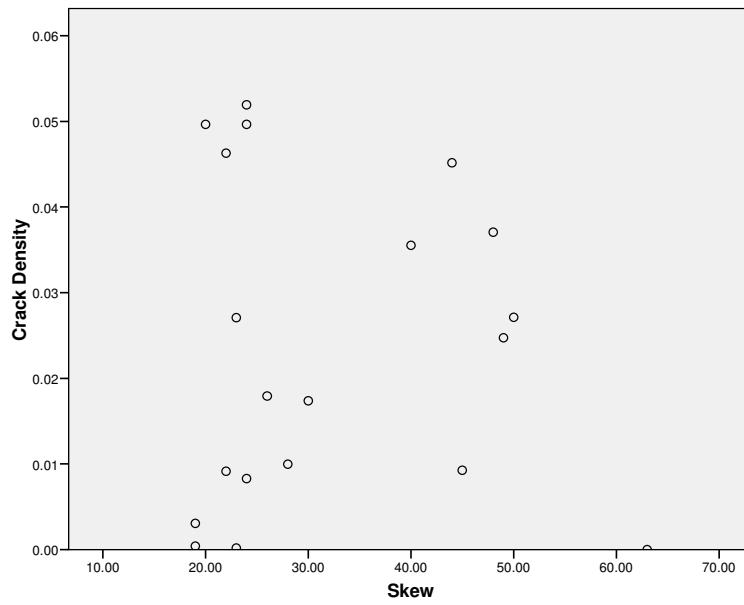


Figure III-27 Relation between Crack Density and Skew Angle (degree) for Skew Bridges

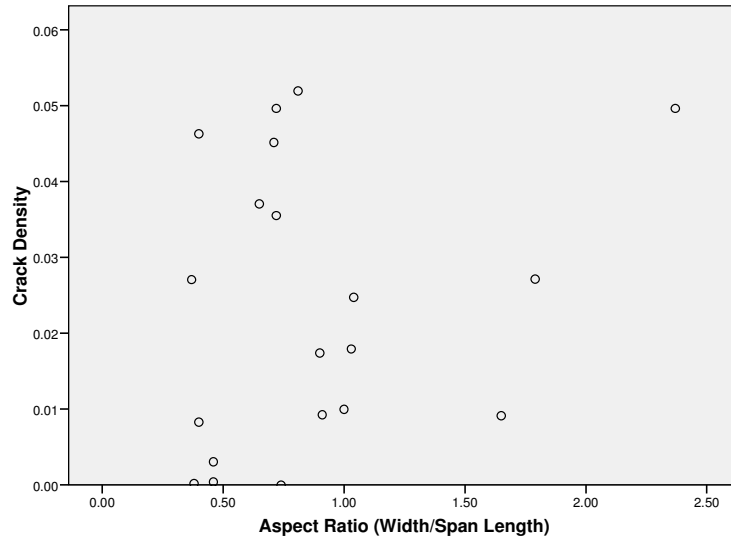


Figure III-28 Relation between Crack Density and Aspect Ratio for Skew Bridges

Figures III-29 to III-32 continues this examination for the 20 straight decks covered in this study. It appears that the same conclusion can be drawn, that no apparent correlation is observed between the crack density and any of the possible causal factors.

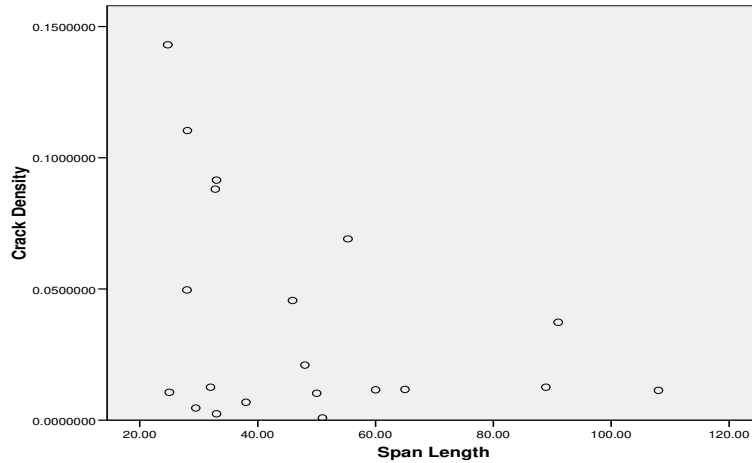


Figure III-31 Relation between Crack Density and Span Length for Straight Bridges

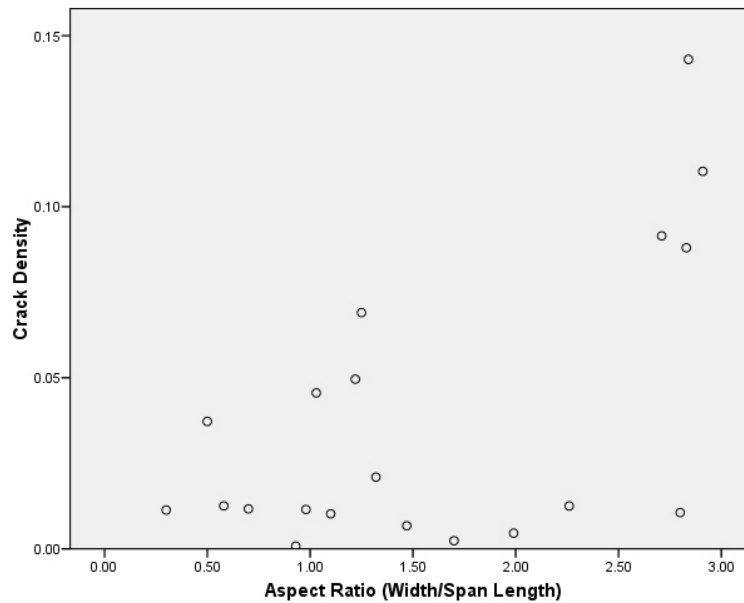


Figure III-32 Relation between Crack Density and Aspect Ratio for Straight Bridges

It appears to be appropriate to conclude that the included parameters, including span length, deck age, slab thickness, and skew angle magnitude, are not statistically correlated with cracking severity. Nevertheless, if one ignores a few data points in the plots for the straight decks for low crack densities at older ages, shorter span lengths, and lower aspect ratios, a trend of crack

density increase is seen with age increase, span length decrease, and aspect ratio increase. Of course these trends are not obvious. Comparison of the crack maps for the skewed and straight decks also shows that diagonal cracking (not along or perpendicular to the beams) is more often observed in the corner areas. Such cracking appears to be associated with skew structures.

CHAPTER IV

BEHAVIOR OF TYPICAL SKEW DECKS USING PHYSICAL MEASUREMENT

Cracking in Portland cement concrete decks can be caused by a number of factors as discussed in Chapter II. These factors may also interact with each other. In order to understand the behavior of concrete deck in both stages of strength development and service, an experimental program was designed in this project for physical measurement of interested quantities. This experiment program had two main purposes: 1) To quantitatively understand the strain/stress behavior of concrete in the field condition for critical stages of its life starting from hydration. 2) To provide measurement data for the calibration of finite element modeling, so that the numerical analysis method can be reliably used to understand the behaviors of a larger number of skew concrete decks. Relatively, the second purpose was more emphasized here, because field instrumentation and testing of many bridges can be prohibitively costly, and calibrated numerical modeling and analysis using the finite element method is the only viable approach to understanding the behaviors of different bridge decks.

IV-1. Experiment Program

The experiment program included two skew concrete decks constructed in the summer of 2005. One of them had a steel I-beam superstructure supporting a 9” concrete deck on Grove Street over I-94 (S02-81063); the other a prestressed I-beam superstructure with a 9” deck carrying the ramp from US-127 to M-50 (S02-38131). These two bridges are referred to as the Grove Street

and M50 bridges hereafter in this report. Figures IV-1 and IV-2 show their deck planes, respectively.

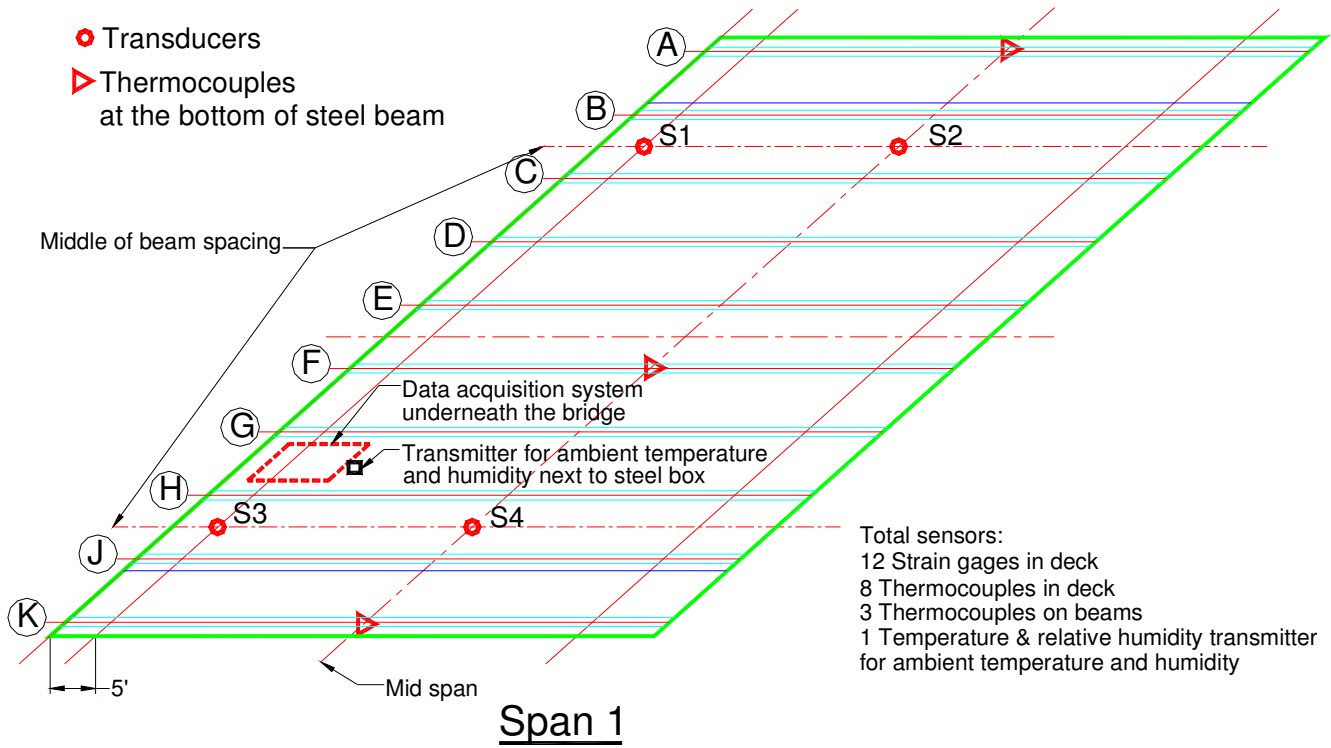


Figure IV-1 Grove Street Bridge (S02-81063) Deck Span 1 and Instrumentation

girders themselves are straight. The bridge includes four continuous spans, with various skew angles. Only one span of length 45ft at the end of the ramp was instrumented, which has a skew angle of 46°. More details of the instrumentation are presented in the next section.

Results from this experiment program were also used in the calibration of finite element modeling for skew bridges typical in Michigan, along with their straight counterparts. Two superstructure types are considered (steel I-beams and prestressed concrete I-beams) for 3 skew angles (0, 30, and 45 degrees) and two beam spacings (6 and 10 ft). This makes a total of 12 cases of bridges designed according to the AASHTO standard specifications. More details and the results of these cases are included in Chapter V.

IV-2. Instrumentation

Both the Grove Street and the M-50 bridges were instrumented with 12 separate strain gages in the concrete at four locations identified as S1, S2, S3, and S4 shown in Figures IV-1 and IV-2 respectively. Each of the four locations in the deck had three one-arm strain gages, one at the depth of the top reinforcement in the bridge's longitudinal direction, and the other two at the depth of the lower reinforcement in the longitudinal and transverse directions. Figure IV-3 includes a vertical cross section of the deck to show the detail of this arrangement. The strain gages and locations were selected to provide strain measurements for short and long term behaviors of the deck, as well as possible maximum strain response to truck wheel load.

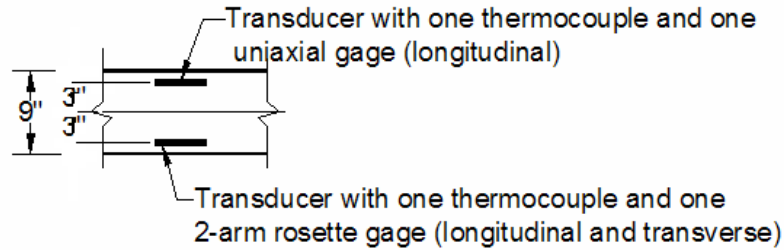


Figure IV-3 Strain Gage and Thermal Couple Depth Locations in Deck

In addition, eight thermocouples were installed in each of the two decks and next to the top strain gage and the bottom strain gages, as shown in Figures IV-1 and IV-2, to obtain temperature measurements, because the strains can be an effect of temperature change and in turn they may cause concrete cracking while the concrete strength is still low and developing. Three more thermal couples were attached to the bottom flange of the two fascia beams and one middle beam of both bridges. In addition, another temperature gage was placed below the deck at the abutment, as shown in Figures IV-1 and IV-2 as a dashed line square. These sensors were intended to provide ambient temperature readings for the temperature field. The heat transfer and dissipation in the deck during hydration depends on the ambient temperature, and thus the finite element modeling of the deck hydration will use the measured ambient temperature as its boundary condition. Furthermore, a humidity sensor was placed under the deck, next to the temperature transmitter, as shown in Figures IV-1 and IV-2, to gather humidity readings for the finite element modeling.

IV-3. Measurement Results

IV-3.1 Behavior in Hydration Process

Temperature, strain, and humidity data were collected for the first three days of concrete deck curing for the Grove Street structure and the M-50 structure. The Grove Street bridge deck was constructed in two phases, one traffic direction in each phase. Phase 1 included the East Bound half of the bridge, including sensor locations S3 and S4 shown in Figure IV-1. For Phase 2 of the bridge, we were able to continue data recording for about 21 days starting from concrete placement. The data were acquired using an Omega Log-book data acquisition system, as shown in Figure IV-4, powered by batteries.

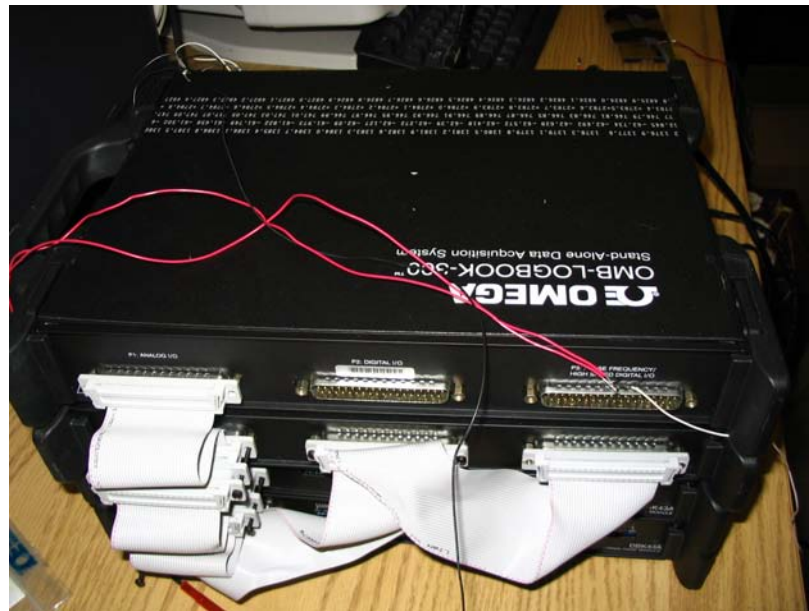


Figure IV-4 Omega Data Logbook System

Grove Street Bridge

Figure IV-5 shows the temperature readings recorded using the thermocouples in the deck and Figure IV-6 for the transducers for the environment condition. Those temperatures marked as S3 and S4 are thermocouples embedded in the concrete deck at the respective locations indicated in Figure IV-1. At each location, two temperature curves are shown, one for the thermal couple at the top- and the other at the bottom-reinforcement level. The other two temperature records in Figure IV-6 were obtained from a thermocouple attached to an exterior beam on the East Bound side and the temperature transmitter underneath the deck near the abutment, also shown in Figure IV-1. Figure IV-7 exhibits the relative humidity readings underneath the bridge deck for the ambient humidity condition.

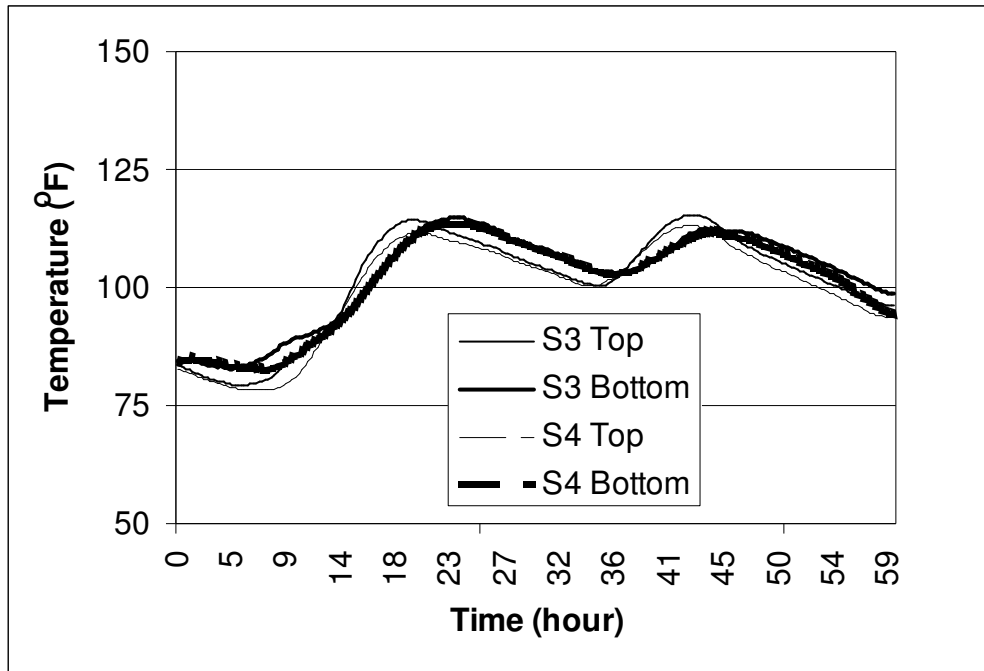


Figure IV-5 Temperature in Deck for Grove Street Bridge (Phase 1 Construction)

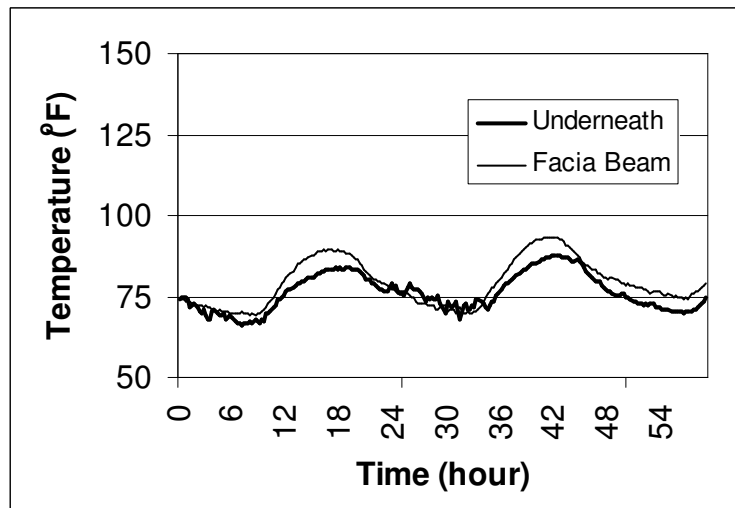


Figure IV-6 Environment Temperature for Grove Street Bridge (Phase 1 Construction)

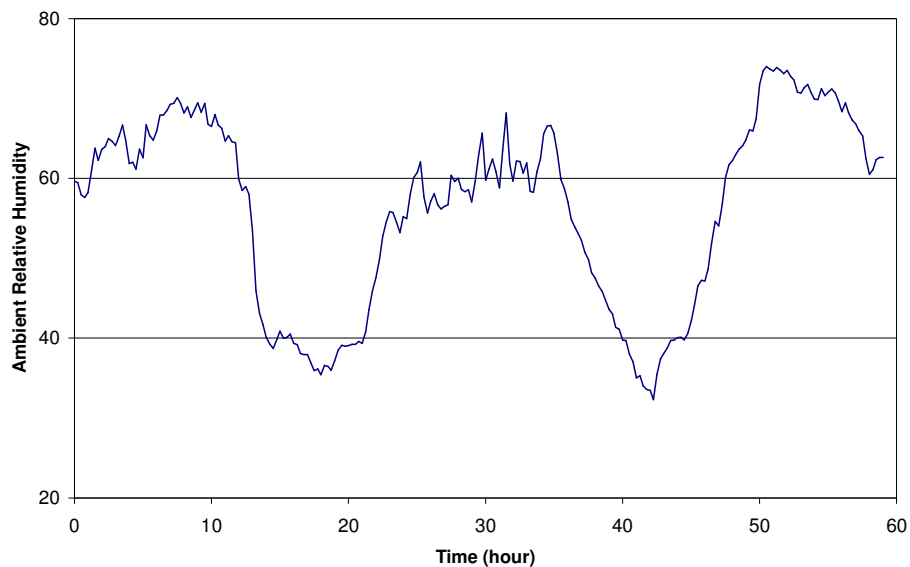


Figure IV-7 Environment Humidity for Grove Street Bridge (Phase 1 Construction)

These results show that the two sensors for environmental temperature recorded similar temperatures, exhibiting essentially a daily variation. Those sensors in the deck also followed this cycle, with a little time lag behind the cycle of the two sensors for the ambient environment. Note also that the deck temperatures exhibited a general trend of increase besides the daily cycle.

Figure IV-8 shows the concrete strains recorded through the strain gages at location S3 in the deck, for the same time period in Figures IV-5 to IV-7. They appear to follow the daily cycle as well, but not as clearly seen as for the temperatures. The strain gages near the deck bottom surface show a clearer daily cycle than the one near the top surface. The maximum strain for this time period is about ± 300 microstrains.

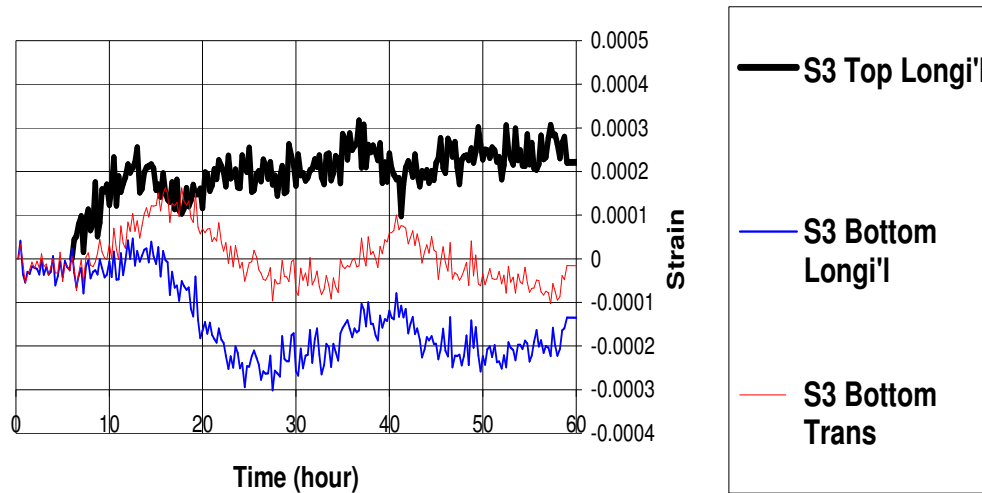


Figure IV-8 Strains at S3 Location in Grove Street Bridge Deck (Phase 1 Construction)

Figure IV-9 shows the same as Figure IV-8 but for the strain gages at location S4. Again the strain gages near the bottom surface of the deck show a more clearly seen daily cycle, compared with that near the top. The maximum strain has reached +200 and -100 microstrains. Also note that the strains at S3 and S4 are different, due to effects of the skew angle and the constraints. Since S3 is closer to the end of the deck slab, the skew may have more profound influence.

The temperature and strain readings for Phase 2 of the Grove Street Bridge deck will be presented in Section IV-3.3 Long Term Thermal and Shrinkage Behavior because much longer time was covered to observe long term behavior.

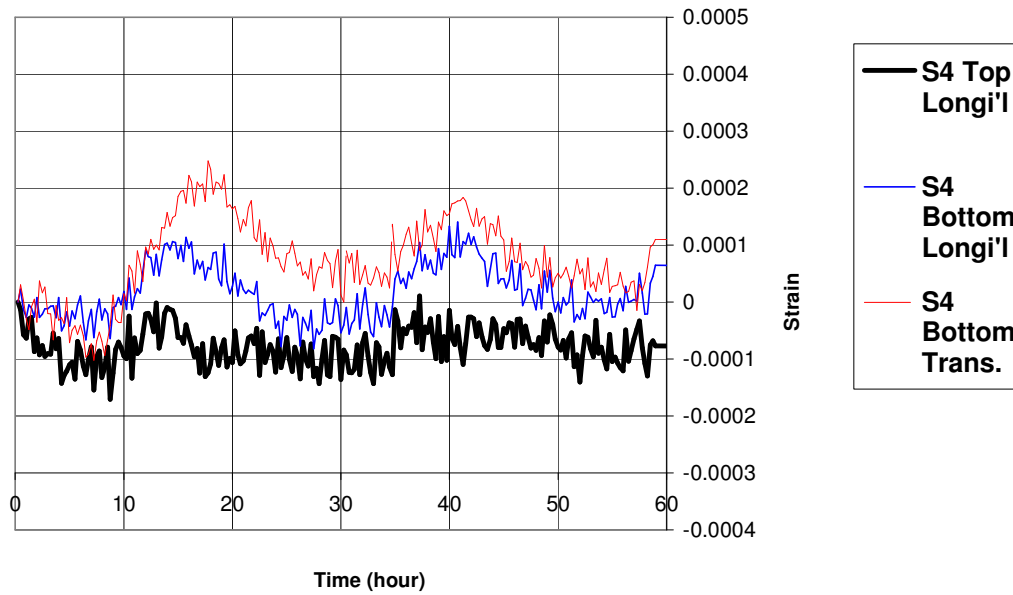


Figure IV-9 Strains at S4 Location in Grove Street Bridge Deck (Phase 1 Construction)

M-50 Bridge

Figures IV-10 to IV-13 show the temperature and humidity readings for the M50 bridge deck for the first 3 to 4 days. Except the humidity in Figure IV-13, they are grouped in three figures for S1 and S2, S3 and S4, and the environmental locations, respectively. The internal thermal couples at S1 to S4 locations appear to show little cyclic behavior due to the environment, and the external temperature readings exhibit some cyclic behavior largely due to weather. It appears that this deck's hydration process is dominant for the temperature observed, so that the daily cycling in temperature is not clearly seen.

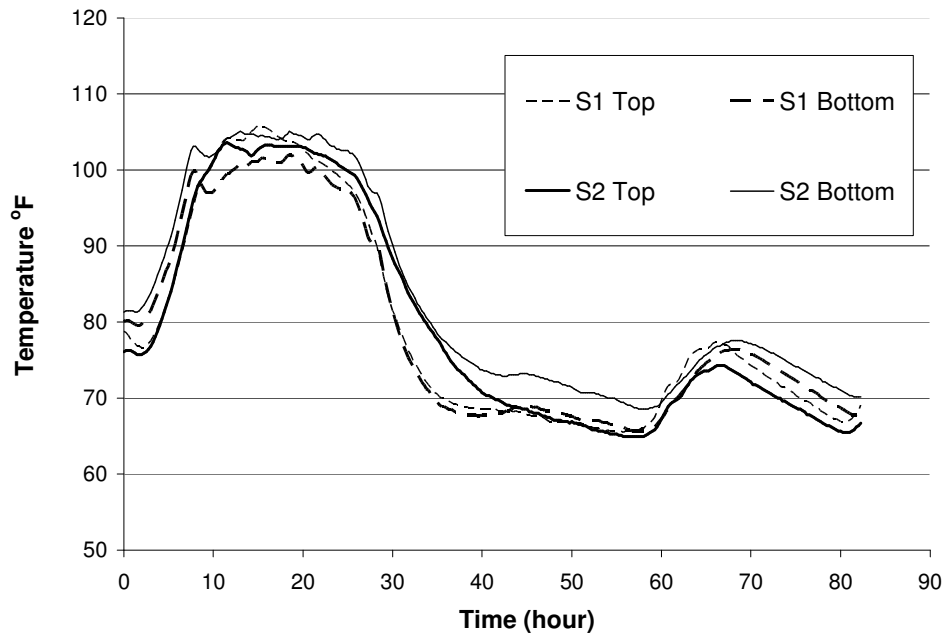


Figure IV-10 Temperature in Deck for M-50 Bridge (Locations S1 and S2)

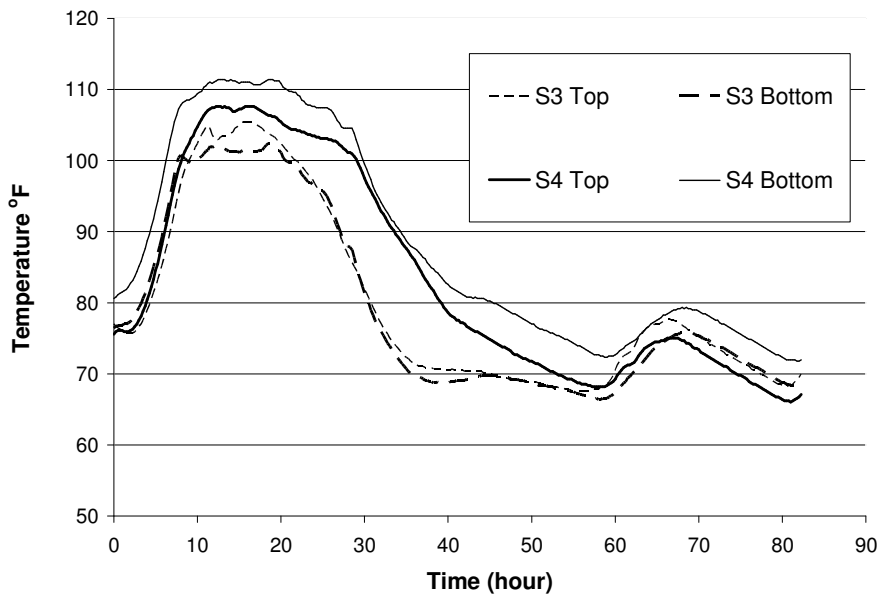


Figure IV-11 Temperature in Deck for M-50 Bridge (Locations S3 and S4)

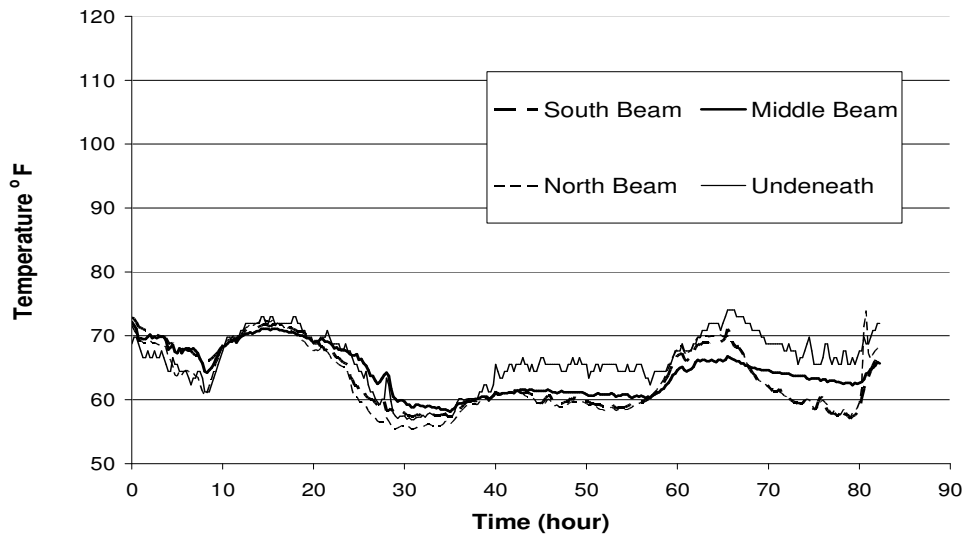


Figure IV-12 Environment Temperature for M-50 Bridge

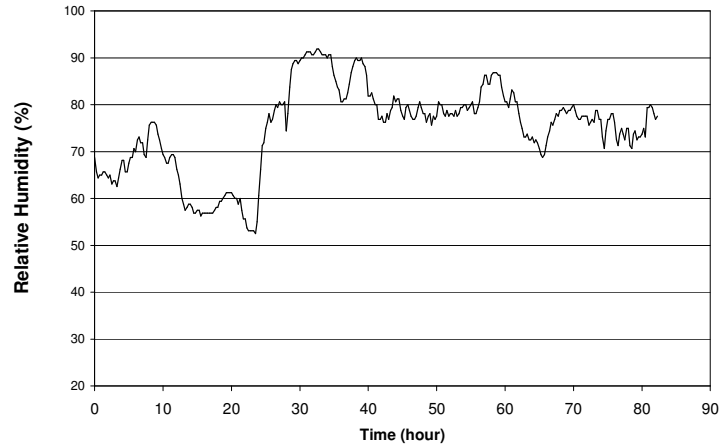


Figure IV-13 Environment Humidity for M-50 Bridge

Figures IV-14 to 17 shows the strain readings at the M-50 bridge deck using the strain transducers at locations S1 through S4, respectively. The maximum strains in the M-50 bridge deck are similar to those seen for the Grove Street Bridge, consistent with the temperature readings shown in Figures IV-10 to 12, the strains mainly due to hydration largely reduced at approximately 30 to 35 hours of the deck age.

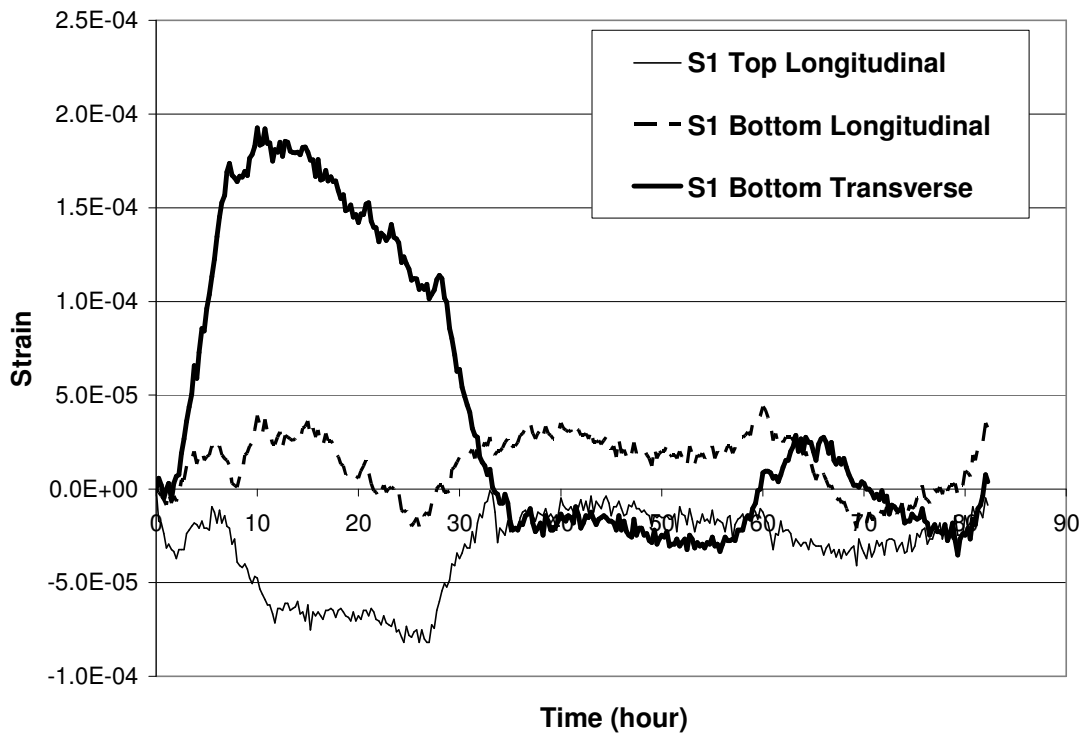


Figure IV-14 Strains at S1 Location in M-50 Bridge Deck

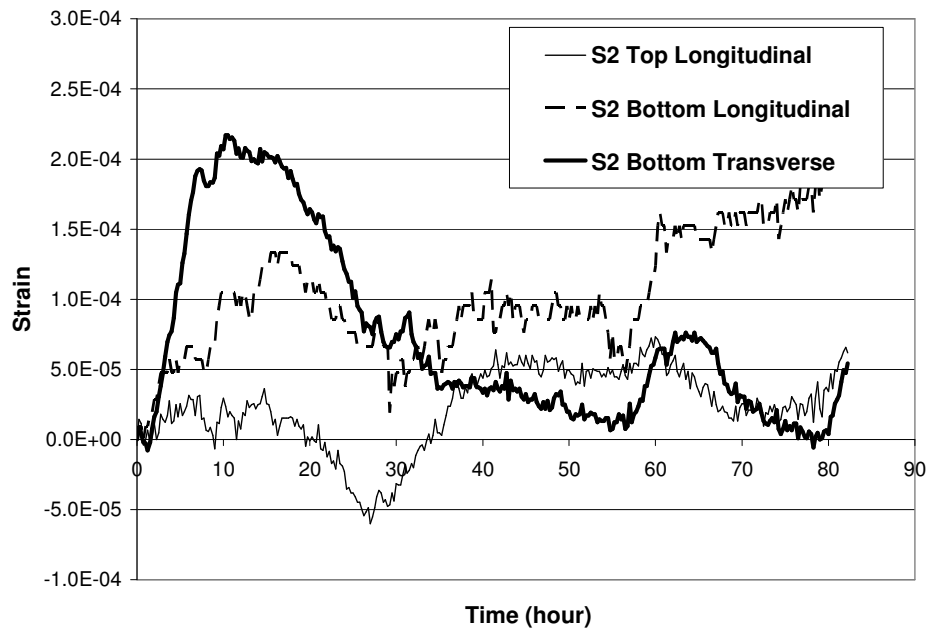


Figure IV-15 Strains at S1 Location in M-50 Bridge Deck

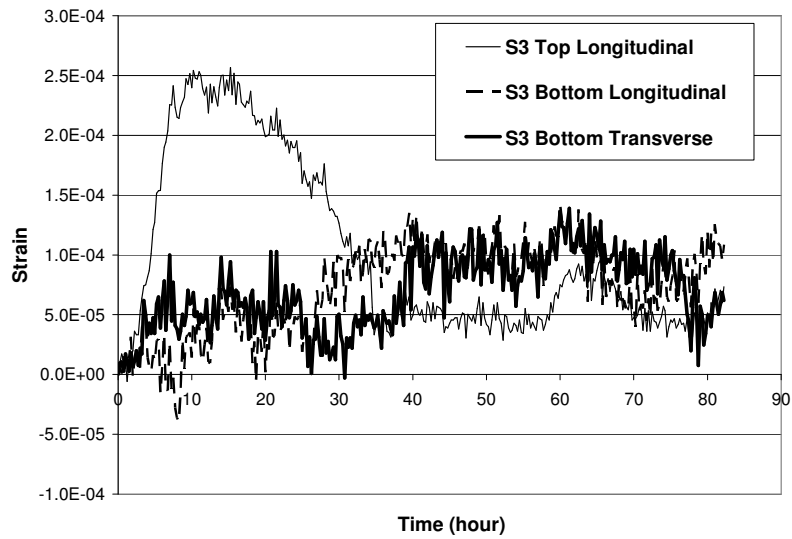


Figure IV-16 Strains at S3 Location in M-50 Bridge Deck

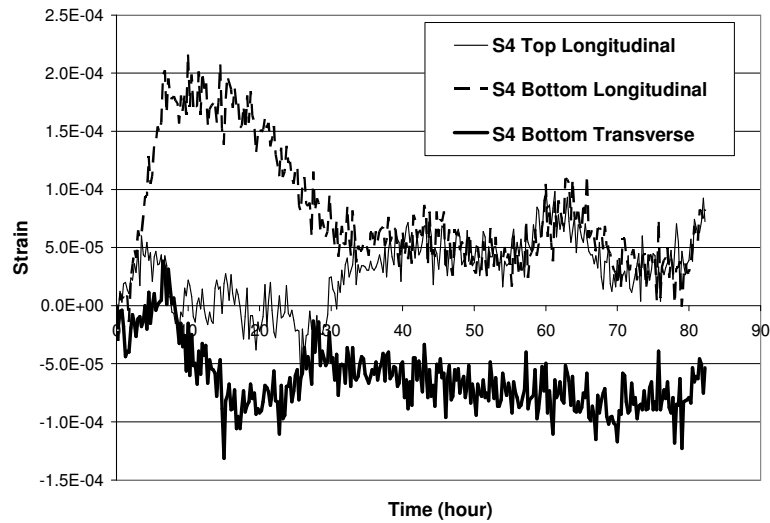


Figure IV-17 Strains at S4 Location in M-50 Bridge Deck

IV-3.2 Behavior under Truck Load

In addition to monitoring temperature, strain, and humidity during the hydration and curing process, truck load testing was carried out to determine the concrete deck's strain response to truck wheel loading. Test readings were taken with the truck load on and off the structure to obtain the load response for each strain gage. The truck was driven over the bridge with one side (i.e., one wheel line) of the truck going along the central line between two beams to maximize the bending strain in the deck, where the strain gages were embedded.

The truck load-induced strains were recorded using an Invocon wireless data acquisition system, as shown in Figure IV-18. The reason for the use of this system for load-induced strains is that the Invocon system offers a much higher resolution although its memory capacity is much smaller and not suitable for long-term data acquisition.



Figure IV-18 Radio-based Invocon Strain Data Acquisition System

Grove Street Bridge



Figure IV-19 A 6-Axle Truck Loading Grove Street Bridge Deck (Phase 1)

Figure IV-19 shows the truck with 6-axles used to load the Grove Street bridge deck. Before loading, the axle weights and spacings were measured and recorded to be used in the simulation

analysis using the finite element method. The axle weights were 14,380, 15,700, 15,250, 11,840, 14,530, and 15,850 lbs, and the corresponding axle spacings were 12, 4.67, 9.92, 3.75, and 4.75 ft. Figures IV-20 and IV-21 show typical strain responses of the concrete deck under the truck load from the strain gages at locations S3 and S4. The truck was driven backward or forward in each loading run, starting from a location off the span. The truck load path was restricted within the length of the continuous beams (64').

Each of these strain curves in Figures IV-20 and 21 shows accordingly six peaks corresponding to the wheels going over the gage in the backward movement for this case. All the gages did not experience much strain, not more than 15 microstrains. Note again that these results were obtained using a data acquisition system with wireless (radio wave) transmission capability. The system records very low noise and is able to pick up small signals as shown.

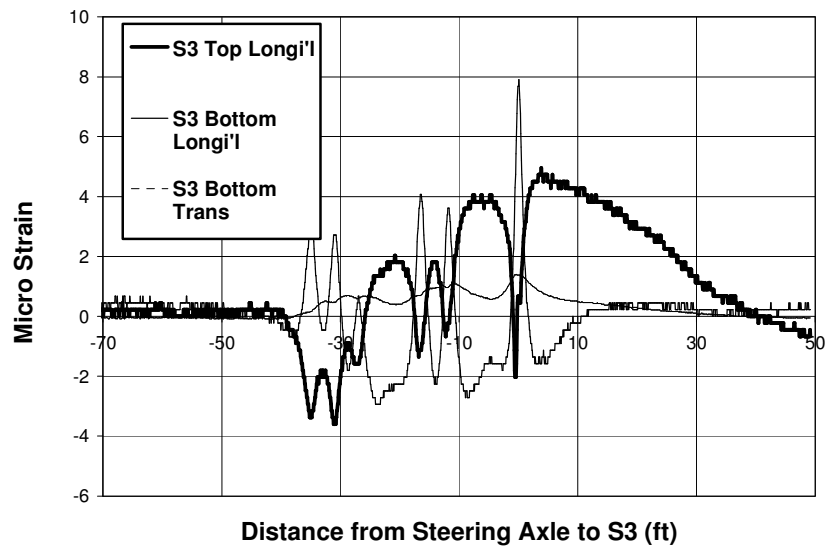


Figure IV-20 Strains at S3 Location in Grove Street Bridge due to Truck Load

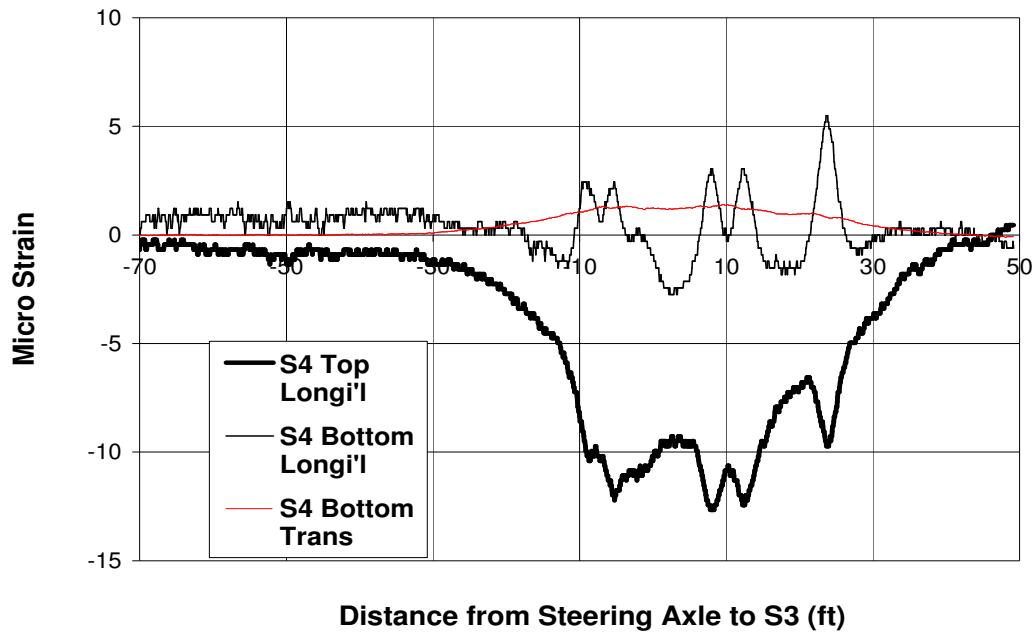


Figure IV-21 Strains at S4 Location in Grove Street Bridge due to Truck Load

For the other half of the deck constructed in Phase 2 about a month later, a different 6-axle truck was used to apply load. The axle weights were 18,000, 16,000, 16,000, 13,000, 13,000, and 13,000 lbs, and the axle spacings were correspondingly 12.17, 4.25, 10.17, 3.75, and 3.75 ft. Figures IV-22 and IV-23 show strain readings at the S1 and S2 locations for a typical truck run. The curves in each figure may be viewed as the influence lines for the strains at each respective location. As observed in Phase 1 load test for the S3 and S4 locations, the maximum strains are below 30 microstrains for both tension (+) and compression (-).

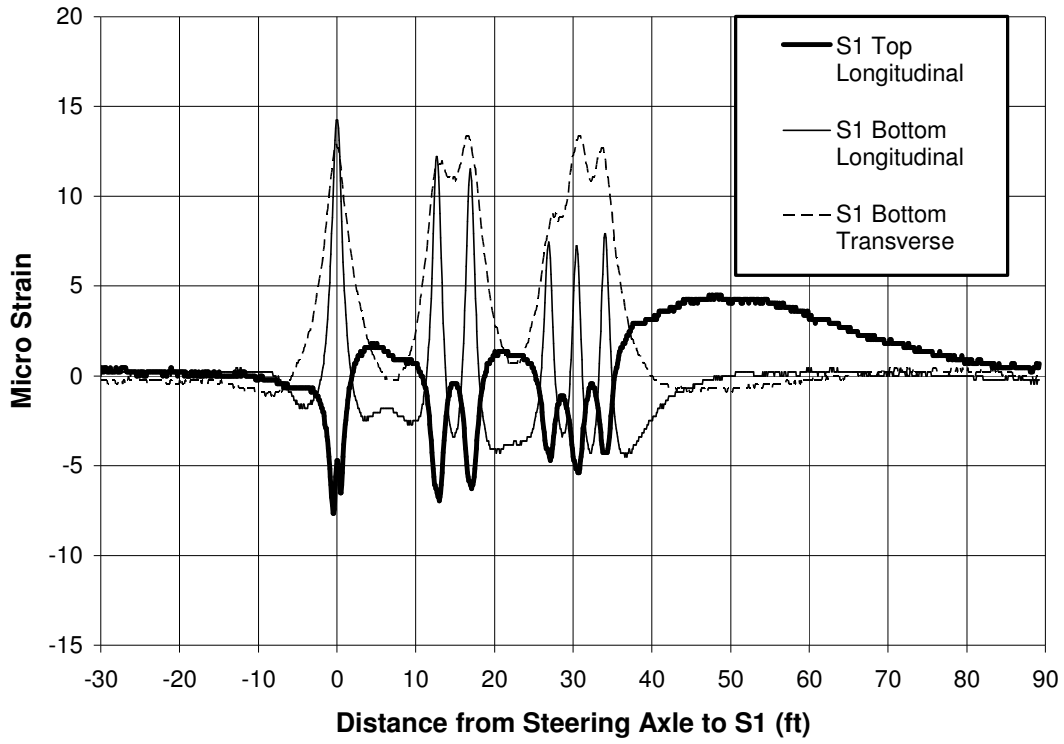


Figure IV-22 Strains at S1 Location in Grove Street Bridge due to Truck Load

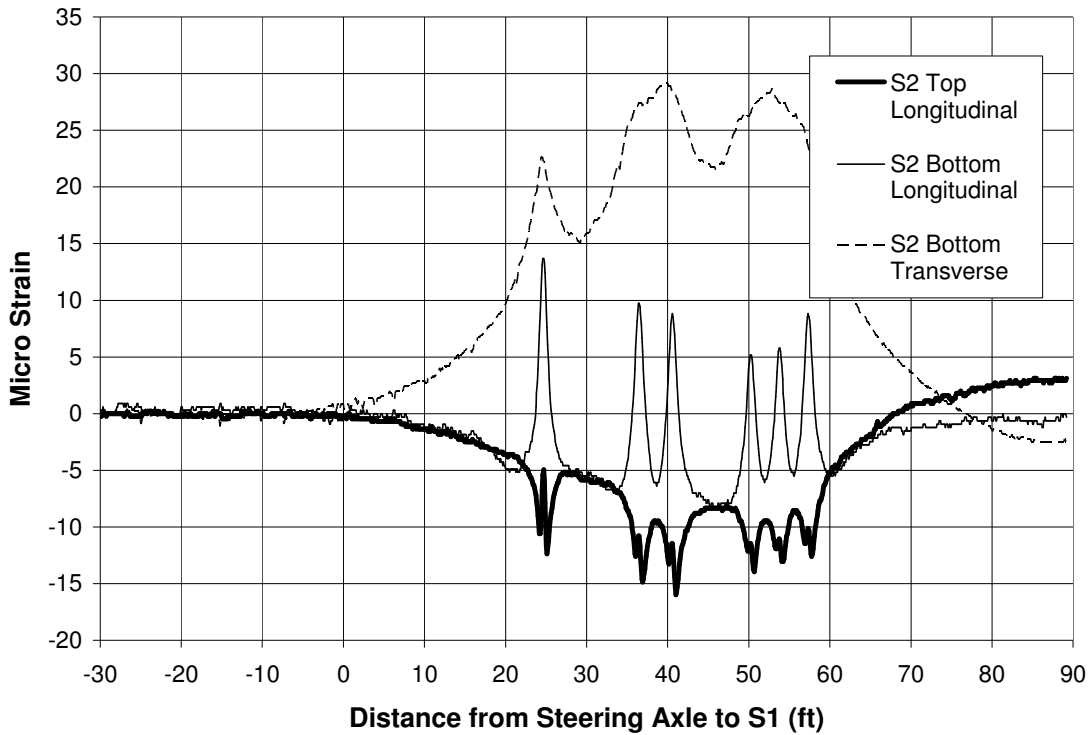


Figure IV-23 Strains at S2 Location in Grove Street Bridge due to Truck Load

M-50 Bridge

For the M-50 Bridge, a 5-axle truck was used for loading the deck, as shown in Figure IV-24. The resulting strains from the embedded strain transducers were recorded using the same approach as for the Grove Street Bridge. Figures IV-25 to IV-28 show the strain readings for a typical truck run on the deck, as influence lines. The observed strains due to truck load are relatively small, as seen for the Grove Street Bridge. They are within -10 (compression) and +20 (tension) microstrains.



Figure IV-24 A 5-axle Truck Loading M-50 Bridge Deck

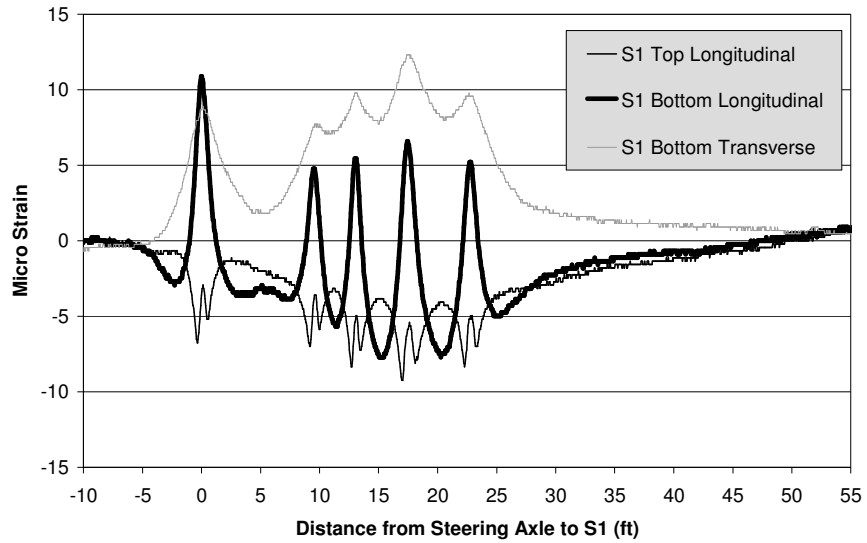


Figure IV-25 Strains at S1 Location in M-50 Bridge Deck due to Truck Load

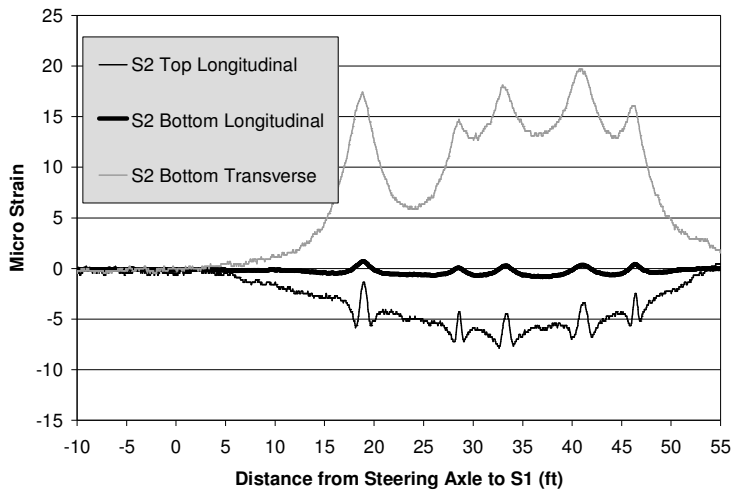


Figure IV-26 Strains at S2 Location in M-50 Bridge Deck due to Truck Load

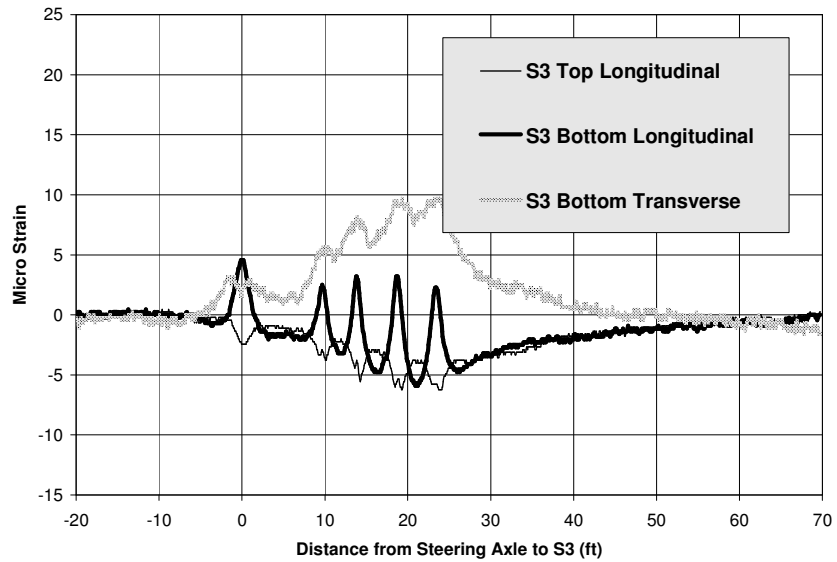


Figure IV-27 Strains at S3 Location in M-50 Bridge Deck due to Truck Load

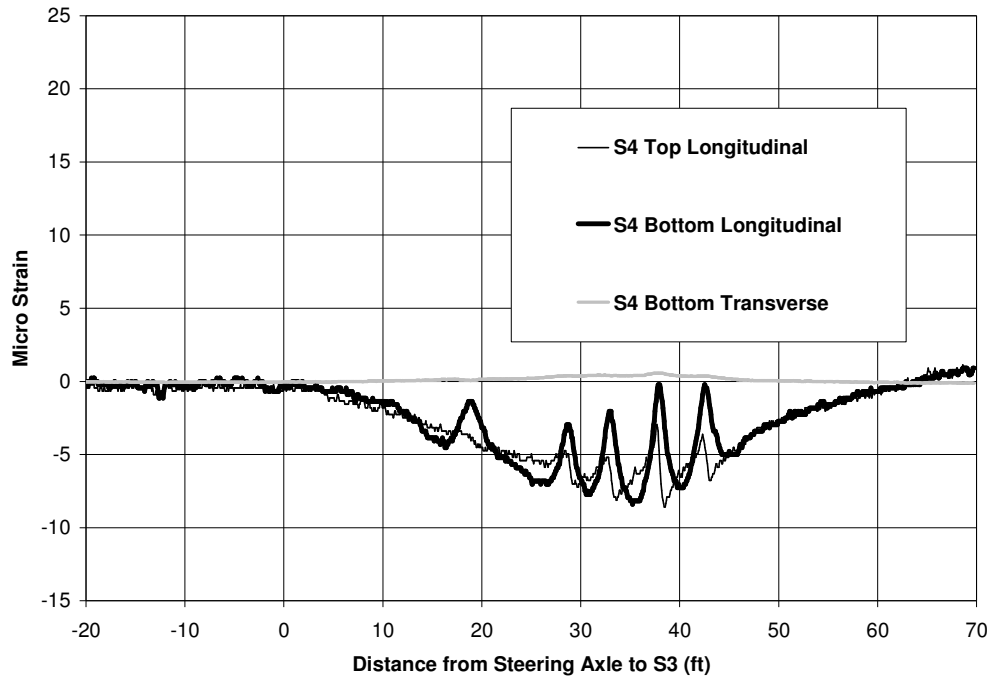


Figure IV-28 Strains at S4 Location in M-50 Bridge Deck due to Truck Load

IV-3.3 Long Term Thermal and Shrinkage Behavior

Figure IV-29 shows the recorded temperature from the thermal couples in the Grove Street bridge deck. Figure IV-30 displays the ambient temperature readings at three locations, two at the bottom flanges of the fascia beams and an internal beam in addition to one underneath the bridge superstructure near the abutment. It is seen that the thermal couples at S1 and S2 locations show higher temperatures in the first two days, apparently due to hydration of that half of the deck placed in Phase 2. Other temperature readings all show cycling behavior, with a general trend downward, because the climate was becoming colder in general.

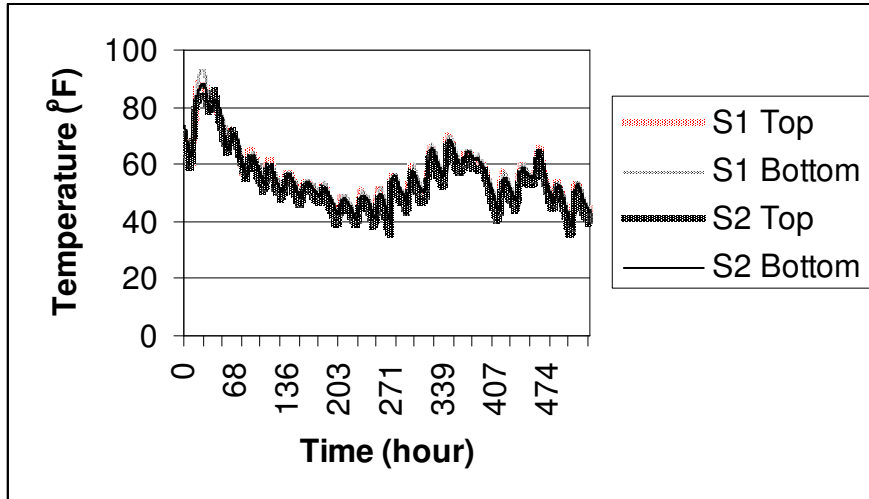


Figure IV -29 Temperature Readings in Grove Street Bridge Deck (Phase 2)

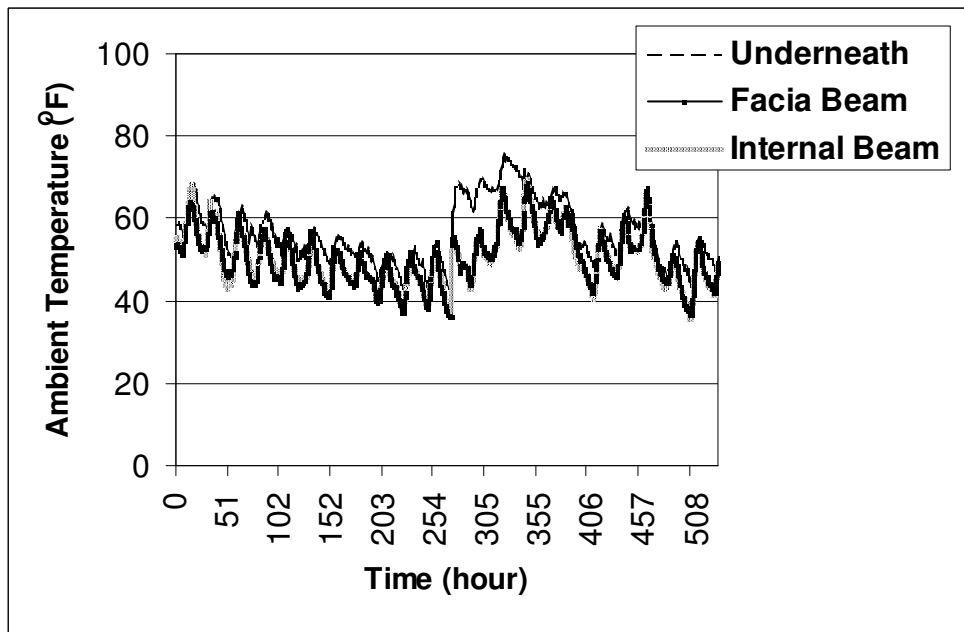


Figure IV-30 Ambient Temperature at Grove Street Bridge (Phase 2)

Figures IV-31 and IV-32 show the strain readings at locations S1 and S2. The tensile strains are in the range of about 100 microstrains. Note that the concrete in the S3 and S4 locations completed curing about a month earlier than the S1 and S2 locations.

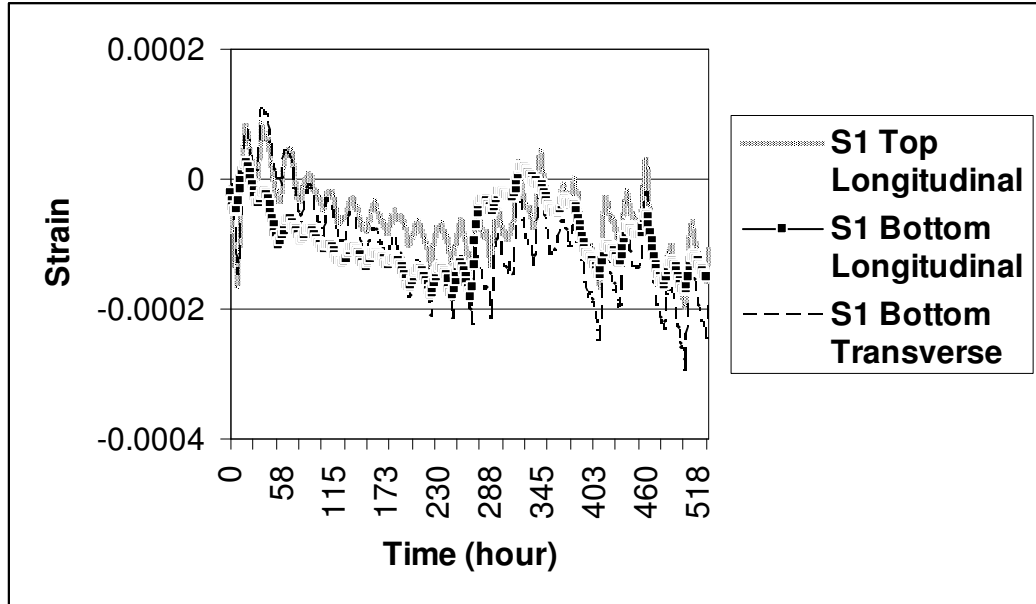


Figure IV-31 Strain Readings at S1 in Grove Street Bridge Deck (Phase 2)

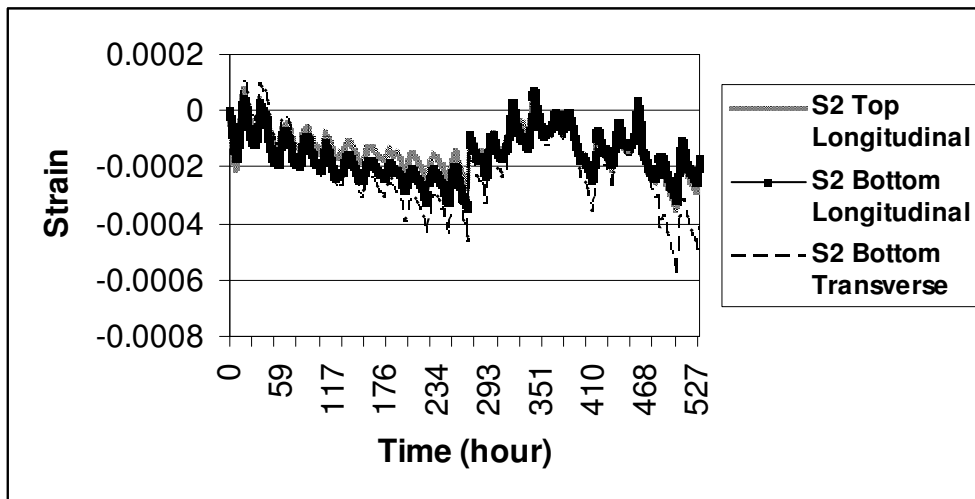


Figure IV-32 Strain Readings at S2 in Grove Street Bridge Deck (Phase 2)

IV-4. Discussions

It is seen that the strains induced by the truck wheel load are much lower compared with the strains recorded in the fast strength-development stage and immediately after. It should also be noted that a certain amount of strains are due to free thermal or shrinkage strain that do not cause stress. In other words, the constraint that limits the thermal strain and shrinkage strain causes stress, which may crack the concrete depending on the strength of concrete at the time.

CHAPTER V

BEHAVIOR OF SKEW DECKS USING FINITE ELEMENT ANALYSIS

Physical measurement of skew bridge decks can be only performed on a limited number of structures and at a limited number of perceived critical locations. However, these measurements are important and can be used here to calibrate numerical modeling of the measured structures to provide validation. Finite element analysis (FEA) is considered the most generally applicable and powerful tool for such modeling. This chapter presents the process and the results of calibration using the measured data from the Grove Street and M-50 bridges. Section V-1 below covers the model validation, and Section V-2 summarizes the modeling and the results for 12 decks typical in Michigan, including 8 cases of skew decks compared with 4 cases of straight decks. Section V-3 summarizes and discusses the results for this chapter, in order to lead to the identification of the causes and recommendation of possible solutions to eliminate or reduce corner cracking in skew concrete decks.

V-1. FEA Modeling and Validation

DIANA, a 3-D FEA software program, was used in this study to perform the analysis. This section presents the process and results for the modeling and its validation using the measured data.

V-1.1 Selection of Modeling Elements

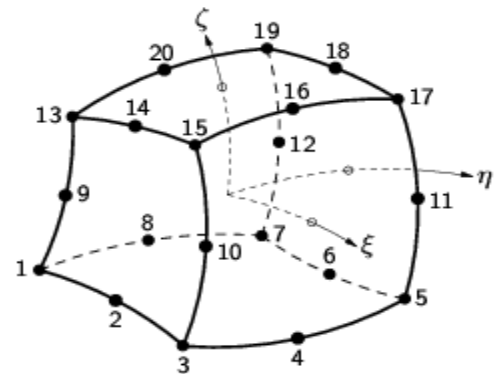
In this analysis covering thermal, shrinkage, creep, and truck wheel load effects, the 3-D solid element CHX60 of the DIANA program is used for modeling the concrete deck and the concrete beams, curved shell element CQ40S for the steel beams, and 3-D general potential flow element BQ4HT for the boundaries of the concrete deck involved in heat transferring. These elements are discussed next in more detail.

Element CHX60

CHX60 in DIANA is a 20-nodes iso-parametric solid brick element. It is based on quadratic interpolation and Gauss integration. The basic variables in the nodes of the solid element are the translations u_x , u_y , and u_z in the three orthogonal local directions. The polynomial for the translations u_i ($i=x, y, z$) is expressed as:

$$\begin{aligned}
 u_i(\xi, \eta, \zeta) = & a_0 + a_1\xi + a_2\eta + a_3\zeta + a_4\xi\eta + a_5\eta\zeta + a_6\xi\zeta + a_7\xi^2 + a_8\eta^2 \\
 & + a_9\zeta^2 + a_{10}\xi\eta\zeta + a_{11}\xi^2\eta + a_{12}\xi^2\zeta + a_{13}\xi\eta^2 + a_{14}\xi\zeta^2 + a_{15}\eta^2\zeta + a_{16}\eta\zeta^2 \\
 & + a_{17}\xi^2\eta\zeta + a_{18}\xi\eta^2\zeta + a_{19}\xi\eta\zeta^2
 \end{aligned} \tag{V-1}$$

Figure V-1 Definitions of Nodes and Coordinate System for Element CHX 60



where ξ , η , and ζ are the coordinates of a point in the element as shown in Figure V-1.

Typically, a rectangular brick element in DIANA using polynomial approximates the strain and stress distribution over the element volume. The normal strain and stress in the x direction vary linearly in the x direction and quadratically in the y and z directions. The normal strain and stress in the y direction vary linearly in the y direction and quadratically in the x and z directions. The normal strain and stress in the z direction vary linearly in the z direction and quadratically in the x and y directions. The stress condition of CHX60 is three-dimensional, and the loading may be arbitrary. The CHX60's dimensions in the three axial directions X , Y , and Z should be in the same order of magnitude. For the bridge decks here, steel reinforcement in the deck was added into the solid element according to the reinforcement cross section area.

Element CQ40S

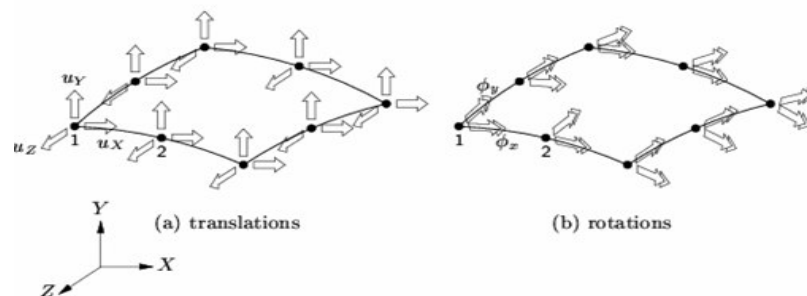


Figure V-2 Displacements and Coordinate System for Curved Shell Element CQ40S

CQ40S is an eight-node quadrilateral iso-parametric curved shell element. It is also based on quadratic interpolation and Gauss integration over the $\xi\eta$ element area. The polynomials for the translations u_i and rotations ϕ_i ($i=x,y,z$) can be expressed as:

$$\begin{aligned} u_i(\xi, \eta) &= a_0 + a_1\xi + a_2\eta + a_3\xi\eta + a_4\xi^2 + a_5\eta^2 + a_6\xi^2\eta + a_7\xi\eta^2 \\ \phi_i(\xi, \eta) &= b_0 + b_1\xi + b_2\eta + b_3\xi\eta + b_4\xi^2 + b_5\eta^2 + b_6\xi^2\eta + b_7\xi\eta^2 \end{aligned} \quad (V-2)$$

Element BQ4HT

BQ4HT is a four-node isoparametric quadrilateral element to describe boundaries in three-dimensional potential flow analysis. It is based on linear interpolation and Gauss integration.

V-1.2 Material Property and Behavior Modeling

Each of the bridge models is made of the above 3 types of elements. Each type has its own material properties. The solid element CHX60 is used for modeling the concrete deck and concrete beams. The curved shell element CQ40S is used for modeling steel beams. The potential flow element BQ4HT is used for modeling the interface between the concrete and surrounding environment for heat transfer.

The concrete material properties in this model are divided into two groups: structure analysis properties and thermal analysis properties. For concrete still in the development stage, the ACI 209 model (1982) is referred to in modeling the shrinkage and creep behavior.

Concrete material properties for structural analysis

Concrete mechanical properties vary with time and its variation is modeled here using the ACI formulas as follows (DIANA 2003, ACI 1982).

- Compressive strength $f_c(t)$ in psi at any time t (in day) :

$$f_c(t) = \frac{t}{\alpha + \beta t} f_{c28} \quad (\text{V-3})$$

where f_{c28} is the concrete compressive strength at 28 day in psi, α and β are model parameters depending on cement and curing type. For example, $\alpha = 4.0$ and $\beta = 0.85$ are used in this study for Cement Type 1 using moist curing.

- Modulus of elasticity (Young's Modulus):

$$E_c(t) = \sqrt{\frac{t}{\alpha + \beta t}} E_{c28} \quad (\text{V-4})$$

where E_{c28} is the concrete's Young's modulus at 28 day in psi, $E_c(t)$ is the concrete's Young's modulus at time t (in day), and α , β , and t have been defined above.

- Creep function $J(t, t_0)$ according to the ACI 209 model (1982):

$$J(t, t_0) = \frac{1}{E_c(t)} (1 + \phi(t, t_0)) \quad (\text{V-5})$$

where the creep coefficient $\phi(t, t_0)$ is defined as:

$$\phi(t, t_0) = \frac{(t - t_0)^{0.6}}{10 + (t - t_0)^{0.6}} \phi_u \quad (\text{V-6})$$

where,

$$\phi_u = 2.35 \phi_{LA} \phi_{RH} \phi_{VS} \phi_{SL} \phi_{FA} \phi_{AC} \quad (\text{V-7})$$

According to the ACI model, ϕ_{LA} , ϕ_{RH} , ϕ_{VS} , ϕ_{SL} , ϕ_{FA} , and ϕ_{AC} in Eq.(V-7) are correction factors for loading age, relative humidity, volume-surface ratio, slump, fine aggregate percentage, and air content, respectively. Their values for the two instrumented bridge decks are given in Table V-1.

Table V-1 Values of Correction Factors in Eq.(V-7)

	ϕ_{LA}	ϕ_{RH}	ϕ_{VS}	ϕ_{SL}	ϕ_{FA}	ϕ_{AC}
Grove Street Bridge	0.994	0.893	0.673	1.202	0.978	1.000
M-50 Bridge	0.994	0.768	0.673	1.202	0.978	1.072

- Total shrinkage strain at age t (in day)

$$\epsilon_s(t - t_s) = \begin{cases} \frac{(t - t_s)}{35 + (t - t_s)} \epsilon_{su} & \text{for moist curing } (t_s \geq 7 \text{ days}) \\ \frac{(t - t_s)}{55 + (t - t_s)} \epsilon_{su} & \text{for steam curing } (t_s \geq 1 \text{ days}) \end{cases} \quad (\text{V-8})$$

where t_s is the duration of initial wet curing and ϵ_{su} is given by

$$\varepsilon_{su} = -(780\gamma_{MC}\gamma_{RH}\gamma_{VS}\gamma_{SL}\gamma_{FA}\gamma_{CC}\gamma_{AC})\times 10^{-6} \quad (V-9)$$

where γ_{MC} , γ_{RH} , γ_{VS} , γ_{SL} , γ_{FA} , γ_{CC} , and γ_{AC} are correction factors for moist curing duration, ambient relative humidity, volume-surface ratio, slump, fine aggregate percentage, and cement content, and air content, respectively. The ambient relative humidity, concrete slump, and concrete air content of the deck were based on measurement. The volume-surface ratio, fine aggregate percentage, and cement content were based on the mix design. The values for the correction factors in Eq. (V-9) are shown in Table V-2.

Table V-2 Values of Correction Factors in Eq. (V-9)

	γ_{MC}	γ_{RH}	γ_{VS}	γ_{SL}	γ_{FA}	γ_{CC}	γ_{AC}
Grove Street Bridge	1.000	0.838	0.408	1.123	0.874	0.967	0.996
M-50 Bridge	1.000	0.651	0.408	1.123	0.874	0.990	1.004

Material properties for thermal analysis

- Thermal conductivity

For 3-D heat flow analysis to model the process of concrete hydration, the concrete conductivity k is used to measure the ability of the material to conduct heat when the heat transfer is dependent only on the temperature gradient. The conductivity of ordinary concrete depends on its composition and, and it ranges generally between about 0.46 and 1.16 $Btu/h\ ft\ ^\circ F$ (Weiss 1999)

- Thermal capacity

Thermal capacity is defined as the amount of heat necessary to change the temperature of unit mass (e.g., 1 lb) by unit temperature change (e.g., 1°F). The heat capacity c of concrete is little affected by the mineralogical character of the aggregate, but is considerably increased by increase in moisture content of the concrete. The capacity also increases with temperature and with a decrease in the concrete density. The common range of thermal capacity for concrete is between 0.20 and 0.28 $Btu/lb^{\circ}F$.

- Coefficient of thermal expansion

Like most engineering materials, concrete has a positive coefficient of thermal expansion, but its value depends both on the composition of the mix and on its hydration state at the time of the temperature change. The influence of the mix proportions arises from the fact that the two main constituents of concrete, hydrated cement paste and aggregate, have dissimilar thermal coefficients, and the coefficient for the concrete matrix is a resultant of the two material properties. The linear coefficient of thermal expansion of hydrated cement paste varies between about 6×10^{-6} and 11×10^{-6} per $^{\circ}F$ (Nevelle 1995). It is higher than the coefficient for aggregate. An average linear thermal expansion coefficient of concrete may be taken as $5.5 \times 10^{-6} / ^{\circ}F$, but the range may be from about $3.2 \times 10^{-6} / ^{\circ}F$ to $7.8 \times 10^{-6} / ^{\circ}F$, depending upon the type and quantities of the aggregates, the mixture proportions and other factors (Cook 1966).

- Adiabatic hydration curve

The adiabatic temperature rise measured under the thermally isolated situation is directly proportional to the heat released on a cumulated basis, because the heat capacity can be assumed constant due to the large volume occupied by aggregates having thermal stability.

To model heat production using DIANA, an adiabatic temperature rise curve needs to be specified as a function of time. Suzuki et al. (1997) systematically carried out a series of adiabatic temperature rise tests with several types of Portland cement, including early hardening cement, ordinary cement, moderate-heat cement and binary blended cement including blast furnace slag or fly ash and ordinary Portland cement. Three casting temperatures ($50^{\circ}F$, $68^{\circ}F$, $86^{\circ}F$) and three unit cement weights (41.0 lb/ft^2 , 61.5 lb/ft^2 and 81.9 lb/ft^2) were used in these tests. This set of results is the main source in this study to select appropriate models for analysis.

For the Grove Street and M50 bridges, the cement used is blended cement including blast furnace slag and fly ash and ordinary Portland cement. The curing temperature was between $50^{\circ}F$ and $86^{\circ}F$, according to the field measurement presented earlier. So the adiabatic temperature curve for binary blended cement is used in the FEA models. Two cases of the adiabatic curve were used to envelope the real situation, designated as the maximum and minimum adiabatic temperature rise, respectively, as follows in Table V-3.

Table V-3 Parameters Used in Adiabatic Temperature Rise Curves

Parameter	Maximum adiabatic temperature rise	Minimum adiabatic temperature rise
Initial casting temperature	86 °F	50 °F
Slag or fly ash content	81.9 lb/ft ²	41.0 lb/ft ²

Properties of steel

The properties of steel also include two groups used in this study, the mechanical properties and the thermal properties. They are largely constant for different steels. In the DIANA FEA process used here, the properties are adopted as shown in Table V-4.

Table V-4 Steel Properties Used in DIANA Analysis

Steel Property	Selected Value
Conductivity	8.67 Btu/h ft °F
Capacity	56.9 Btu/ft ³ °F
Density	490 lb/ft ³
Young's Modules	29,000 ksi
Poison Ratio	0.2
Coefficient of Thermal Expansion	6.67 × 10 ⁻⁶ /°F

Properties of interface

As discussed earlier, the interface element BQ4HT allows the heat flux in the concrete to interact with that of the surrounding environment. It uses one parameter, the conduction coefficient K , to model this process. During curing, concrete is covered using wet burlap on the top surface, plywood forms on the sides, and steel stay-in-place forms for the bottom surface. Accordingly, the thermal conduction coefficients for these different materials are selected as shown in Table V-5.

Table V-5 Thermal Conduction Coefficients for Boundary Conditions

Interface Material	Conduction Coefficient
Steel Forms	$3.30 \text{ Btu/h ft}^2 \text{ }^\circ\text{F}$
Plywood Forms	$1.03 \text{ Btu/h ft}^2 \text{ }^\circ\text{F}$
Wet Burlap	$1.76 \text{ Btu/h ft}^2 \text{ }^\circ\text{F}$

V-1.3 Selection of Parameters for Analysis

The DIANA FEA is intended to cover the effects of thermal, shrinkage, and truck loading.

There are a number of material parameters that need to be selected for the analysis as follows.

Thermal conductivity of concrete

- VII. Thermal capacity of concrete
- VIII. Coefficient of thermal expansion of concrete
- IX. Young's modulus of concrete (28 day)
- X. Poisson's ratio of concrete
- XI. Density of concrete
- XII. Slump of concrete
- XIII. Amount of fine aggregate
- XIV. Air content in concrete
- XV. Surface area in contact with ambient air
- XVIII. Curing length
- XIX. Curing type
- XX. Ambient relative humidity
- XXI. Cement content
- XXII. Cement type
- XXIII. Thermal conductivity of wet burlap used to cover concrete for curing
- XXIV. Thermal conductivity of plywood form in contact with concrete
- XXV. Thermal conductivity of steel in contact with concrete
- XXVI. Adiabatic temperature rise curve

These parameters are included in the analysis to understand the behavior of concrete deck during strength development and the service stages. If two values (or behaviors for the case of adiabatic curves), such as a maximum and a minimum, of each of these 19 parameters are used

for analysis, there would be $2^{19} = 524,288$ cases to consider in the analysis program. In order to keep the number of analysis cases practical, the following parameters were selected as constants based on the daily concrete reports and the concrete strength reports for the two instrumented bridge decks.

Table V-6 Properties Selected According to Concrete Test Reports

Parameter	Value
Density of concrete	145 <i>lb/ft</i> ³
Slump of concrete	5.7 in.
Fine aggregate	40.6%
Air content	5.8% for Grove Street and 6.8% for M-50

In addition, the curing length is set at 7 days as the time period in which wet burlap is used to cover the deck, and the curing type referring to curing method is set here as moist curing in the field using wet burlap coverage.

The surface area of concrete, ambient relative humidity, cement content, and cement type are dependent on the bridge analyzed. They were fortunately either measured by the research team or available via construction reports. However, there are still 6 required parameters yet to be selected as summarized in Table V-7.

Table V-7 Required Parameters with Respective Estimated Range

Concrete Parameter	Range
Thermal Conductivity	0.46 and 1.16 <i>Btu/h ft °F</i>
Thermal Capacity	0.20 ~ 0.28 <i>Btu/lb per °F</i>
Coefficient of Thermal Expansion	3.22 to $7.78 \times 10^{-6} / ^\circ F$
Young's Modulus (28 day)	3,400 ~4,070 ksi
Poisson's Ratio	0.15~0.3
Adiabatic Temperature Rise Curve	Minimum Curve ~Maximum Curve

The minimum and maximum curves in Table V-7 refer to the adiabatic temperature rise curves, respectively, to produce minimum and maximum amounts of heat in a given time period for curing. For these six parameters, there could be still a large number of possible combinations for their values. If only a minimum and a maximum case are used for each parameter, there could be 64 cases to consider. In order to envelope these combinations, a perceived maximum stress case and a minimum stress case were developed as shown in Table V-8, and used in the FEA program in this study.

Table V-8 Minimum and Maximum Cases for FEA

Minimum Stress Case	Maximum Stress Case
Maximum Thermal Conductivity	Minimum Thermal Conductivity
Minimum Thermal Capacity	Maximum Thermal Capacity
Minimum Difference in Coefficients of Thermal Expansion between Concrete Deck and Constraining Beams	Maximum Difference in Coefficients of Thermal Expansion between Concrete Deck and Constraining Beams
Minimum Young's Modulus(28 day)	Maximum Young's Modulus(28 day)
Minimum Poisson's Ratio	Maximum Poisson's Ratio
Minimum Adiabatic Temperature Curve	Maximum Adiabatic Temperature Rise Curve

V-1.4 Failure Criteria

The failure criterion refers in general to the threshold used to judge if a material has failed under the mechanically loaded condition. For simple loading conditions such as uniaxial loading the failure criterion is simple, such as the tensile or compressive strength. When the stress condition is more complex, as in the concrete deck interested here, the failure criterion becomes significantly more complicated. Therefore, a failure criterion in this report is a mathematical model to predict or identify the failure of a material subjected to combined stresses, based on the strength of that material measured in a uniaxial stress state.

A number of failure criteria have been proposed for different materials in the literature. A brief review is provided next to cover several commonly used ones. On the other hand, which failure criterion is most appropriate for the concretes used in the tested decks as well as the typical decks analyzed in this study is yet unknown, until a comprehensive test program is carried out for samples from these decks. Such a test program is expensive and is beyond the scope of this study.

The so called Trasca criterion is a failure criterion based on maximum shear stresses. Thus, it is also referred to as the maximum shear stress criterion and often used to predict the failure of ductile materials. A given point in the loaded material is considered safe as long as the maximum shear stress at that point is under the yield shear stress σ_y obtained from a uniaxial tensile test. The mathematical formula for no failure is written as:

$$\text{Max} (|\sigma_1 - \sigma_2|, |\sigma_2 - \sigma_3|, |\sigma_1 - \sigma_3|) \leq \sigma_y$$

$$\text{Max} (|\sigma_1|, |\sigma_2|, |\sigma_3|) \leq \sigma_y$$

where σ_1 , σ_2 , and σ_3 are the three principal stresses due to the loading. For a 2-D situation, the no failure region is given as the inside of the dotted line in Figure V-3.

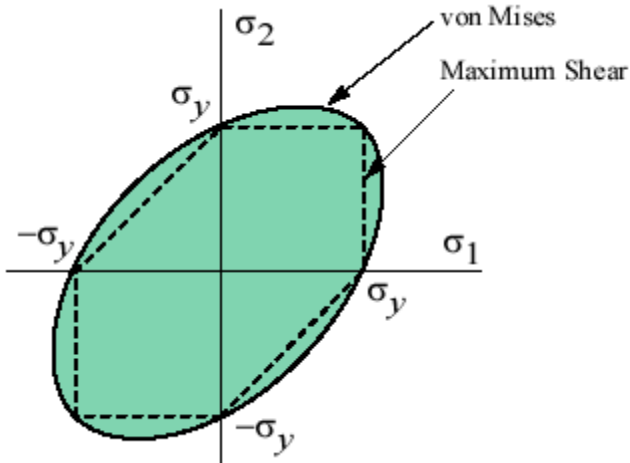


Figure V-3 Maximum Shear and von Mises Criteria for 2-D Stress Condition

Also shown in Figure V-3 is the so called von Mises criterion often used to estimate the yield of ductile material. Its mathematical expression for no failure is

$$\frac{1}{2}[(\sigma_1 - \sigma_2)^2 + (\sigma_2 - \sigma_3)^2 + (\sigma_3 - \sigma_1)^2] \leq \sigma_p^2$$

It is seen in Figure V-3 that the maximum shear criterion is more restrictive but the difference between the two criteria is not significant.

The maximum normal stress criterion is another failure criterion, also known as Coulomb, or Rankine criterion, widely used for failure prediction especially for brittle materials. It states that failure occurs when a maximum normal (principal) stress reaches either the uniaxial tension strength σ_t , or the *uniaxial* compression strength σ_c . For the case of 2-D situation, the no failure region is shown as the inside of the dotted line in Figure V-4, where another failure criterion, known as the Mohr's criterion, is also graphed for comparison.

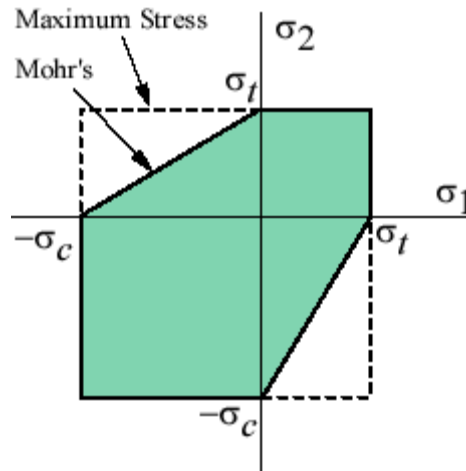


Figure V-4 Maximum Normal Stress and Mohr's Criteria for 2-D Stress Condition

As mentioned earlier, which failure criterion is most appropriate is unknown specifically for the concretes used in the tested decks as well as the typical decks analyzed in this study, until a comprehensive test program is carried out for samples from these decks. On the other hand, it is known that the controlling parameters for appropriate failure criteria for concrete are the principal stress and principal strains. Furthermore, the difference among available failure criteria is not significant as seen above. Accordingly, the first principal stress (namely the maximum tensile stress) in the concrete deck is used in this study to estimate the potential of cracking. This is actually equivalent to the maximum normal stress criterion.

It is also worth mentioning that one should keep in mind that since the failure criterion is not a deterministic threshold (with respect to available knowledge to the profession), whether a concrete deck cracks or not needs to be understood on a probabilistic base as well. This approach is used in Section V-2 when examining the analysis results and judging if the concrete has cracked.

V-1.5 Analysis Process

The FEA process of the bridge deck models is divided into two steps: the transient heat flow analysis to find the temperature distribution as a result of hydration, and the flow-stress analysis to determine the strain and stress fields for the concrete deck. The first step produces the temperature, maturity, shrinkage, and viscous-elasticity of the modeled concrete to be used as the condition for the following flow-stress analysis. Finally, strain, stress, and displacement are output as the result. As discussed above, in the second step of FEA the resulting principal stress is used to identify cracking in the concrete deck, which can lead us to the possible causes of cracking.

The transient heat flow analysis requires the initial condition and boundary condition to start. The initial condition includes the initial temperature of the concrete when poured. The boundary condition for the heat flow analysis is the ambient temperature as a function of time. Fortunately, both were measured using the thermal couples and the temperature transmitter embedded in the concrete or exposed to the ambient environment. Depending on the purpose of analysis, different time step lengths may be used, and the DIANA program is restricted to a total of 100 time steps of analysis. For example, to analyze the first hydration-intensive stage of concrete development, a time step of 0.75 hours was used for 80 steps or the first two and a half days ($0.75 \text{ hours} \times 80 = 60 \text{ hours} = 2.5 \text{ days}$).

As a result, the temperature output will be available on the element nodes and on the integration points as functions of time. These results can then be used in the next step of flow-stress

analysis as input. The flow-stress analysis involves nonlinear structure analysis, taking into account temperature effects on strains and stresses and viscous-elastic concrete material behavior. Therefore, this step takes more computation time, and reliably predicting reality is certainly more challenging.

V-1.6 Validation of Modeling Using Measured Responses

The validation was performed on the two instrumented bridge decks, the Grove Street bridge and the M50 bridge, respectively. In presenting the validation results below, the concrete development stage is discussed first, followed by the truck load test stage.

V-1.6.1 M50 Bridge Deck in Development (S02-38131)

Figures V-5 to V-12 show the comparison of the temperature results by FEA using DIANA and measurement using the instrumentation presented in Chapter IV for the M-50 bridge. It covers the first three and a half days, in which a significant percentage of the hydration process was believed to have completed. This comparison uses all the available measured data for this bridge. As discussed earlier, a number of material properties were not available so that a minimum and a maximum value was used to try to envelope the responses. These figures include the results using the two respective sets of perceived bounding values.

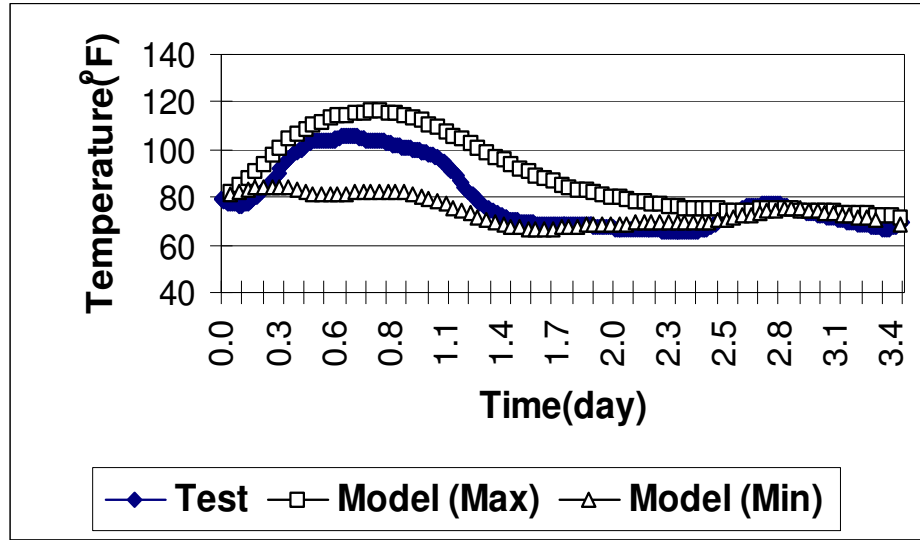


Figure V-5 Comparison for M-50 Bridge Temperature at S1 Top

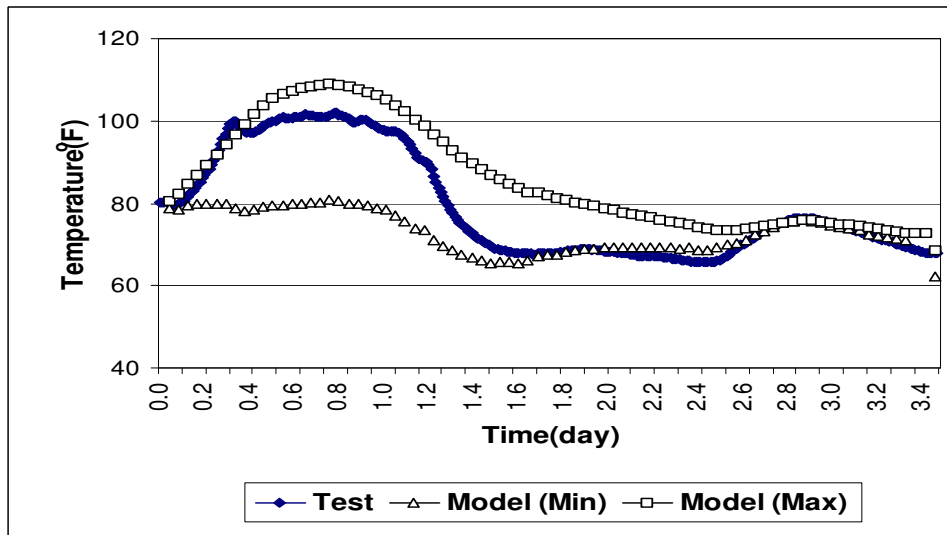


Figure V-6 Comparison for M-50 Bridge Temperature at S1 Bottom

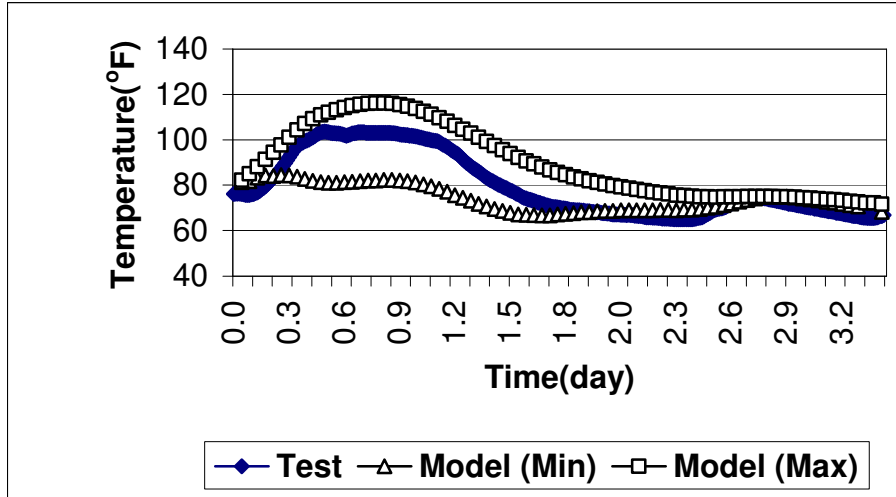


Figure V-7 Comparison for M-50 Bridge Temperature at S2 Top

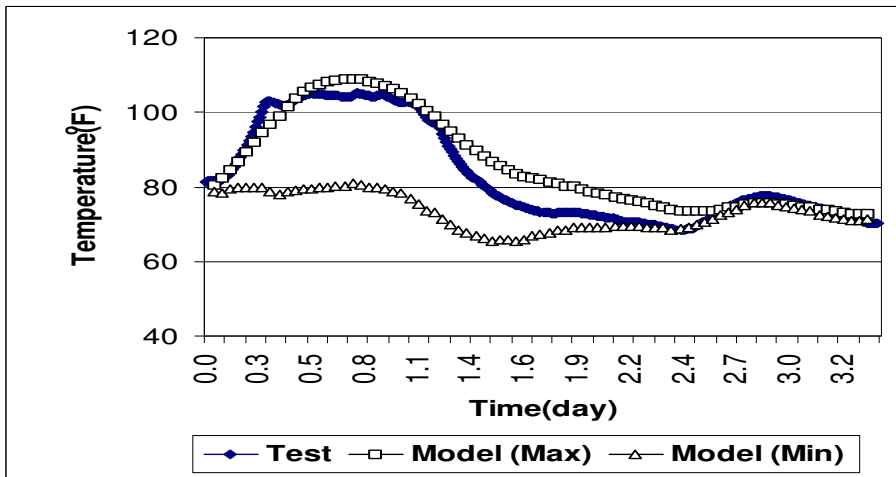


Figure V-8 Comparison for M-50 Bridge Temperature at S2 Bottom

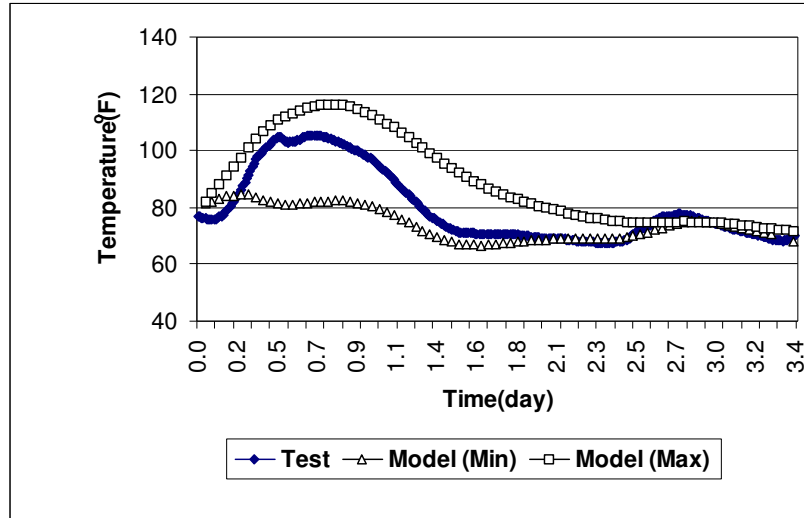


Figure V-9 Comparison for M-50 Bridge Temperature at S3 Top

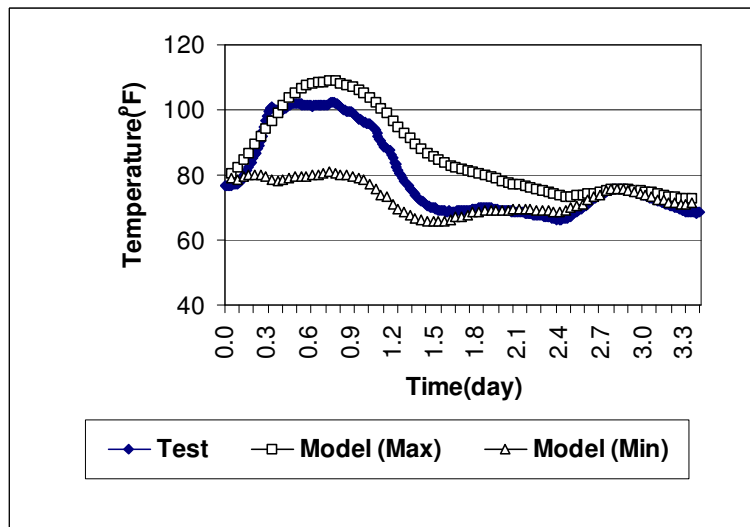


Figure V-10 Comparison for M-50 Bridge Temperature at S3 Bottom

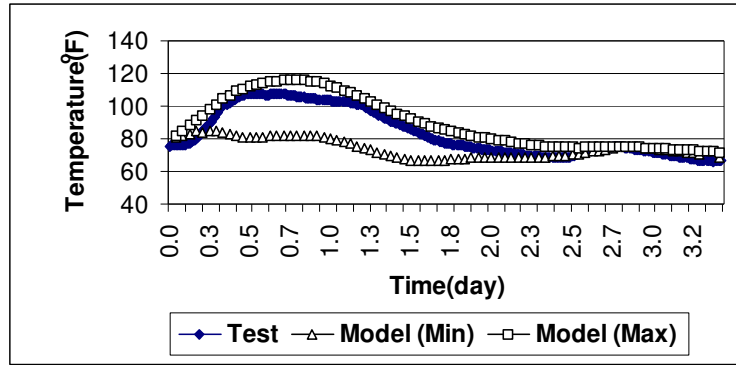


Figure V-11 Comparison for M-50 Bridge Temperature at S4 Top

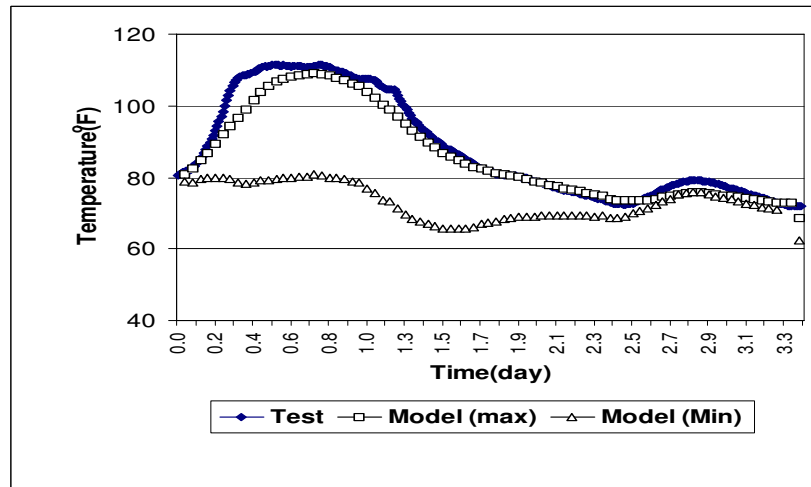


Figure V-12 Comparison for M-50 Bridge Temperature at S4 Bottom

These comparison results show that the FEA was able to produce reasonably reliable temperatures compared with the measured results. On the other hand, for the first 2 days of hydration, the range between the maximum and the minimum cases is relatively large and selecting appropriate material properties may become difficult if the material at the site is not rigorously tested. Beyond the first two days, it seems that the material property variation causes very little variation in the concrete temperature.

Figures V-13 to V-24 continues this comparison for the strains for the M-50 bridge during the same time period, obtained using FEA and physical measurement. The FEA again used the minimum and maximum cases defined earlier to indicate a range of the response strain. As seen, the FEA results for strain do not match with the test results as well as for the temperature, although the minimum and maximum cases do show that the measurement results are close to or within the range. Similarly to the temperature results, the strain results for the minimum and maximum cases also show a more significant difference during the first two days of hydration than the rest of time. Note also that Figures V-17 and V-20 show steady increase in strain after 1.5 days. This may be due to drifting of the strain measurement for a long period of time.

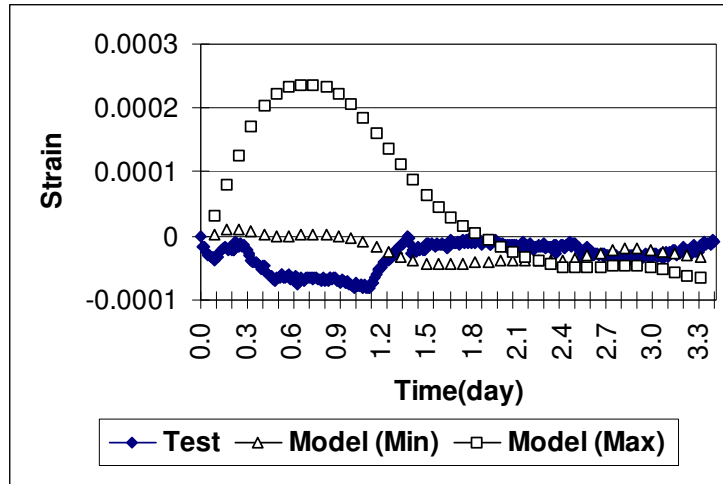


Figure V-13 Comparison for M-50 Bridge Strain at S1 Top Longitudinal

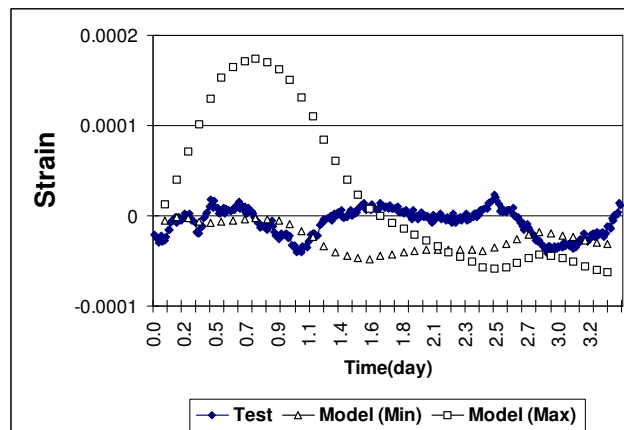


Figure V-14 Comparison for M-50 Bridge Strain at S1 Bottom Longitudinal

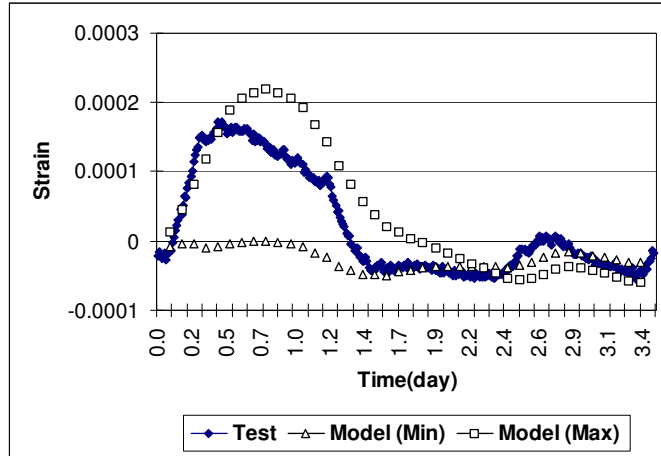


Figure V-15 Comparison for M-50 Bridge Strain at S1 Bottom Transverse

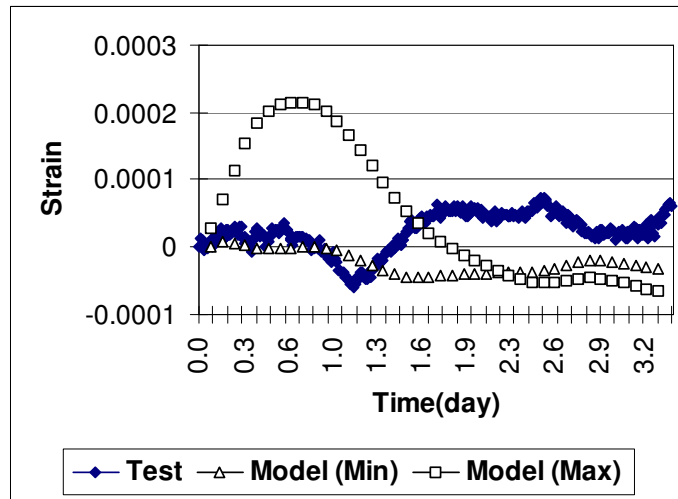


Figure V-16 Comparison for M50 Bridge Strain at S2 Top Longitudinal

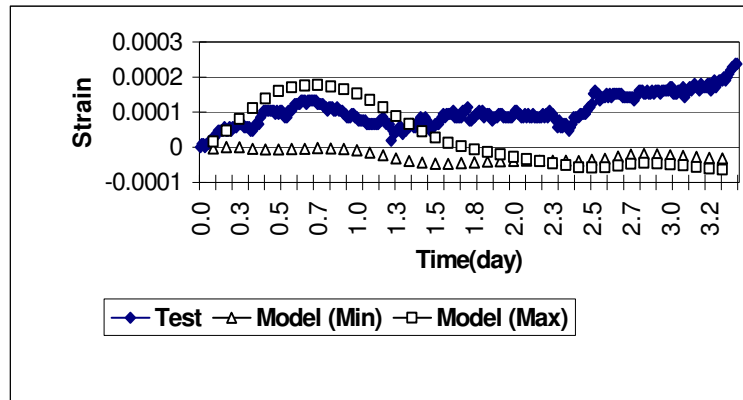


Figure V-17 Comparison for M-50 Bridge Strain at S2 Bottom Longitudinal

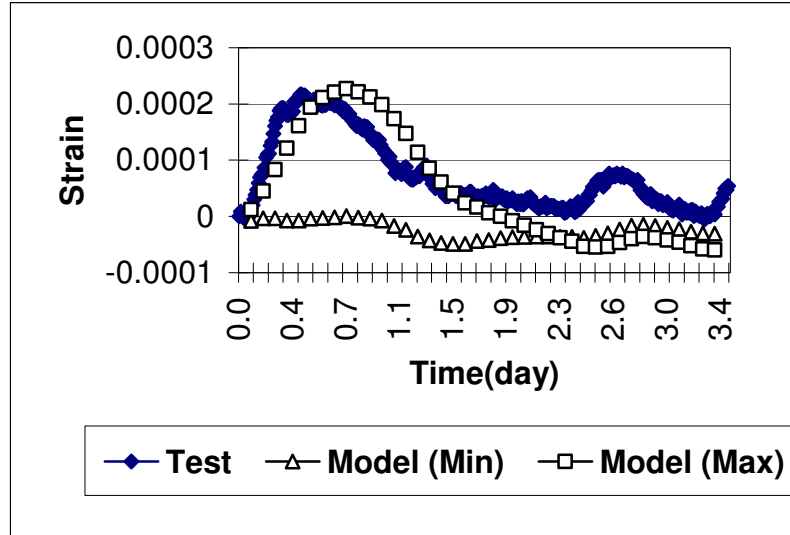


Figure V-18 Comparison for M-50 Bridge Strain at S2 Bottom Transverse

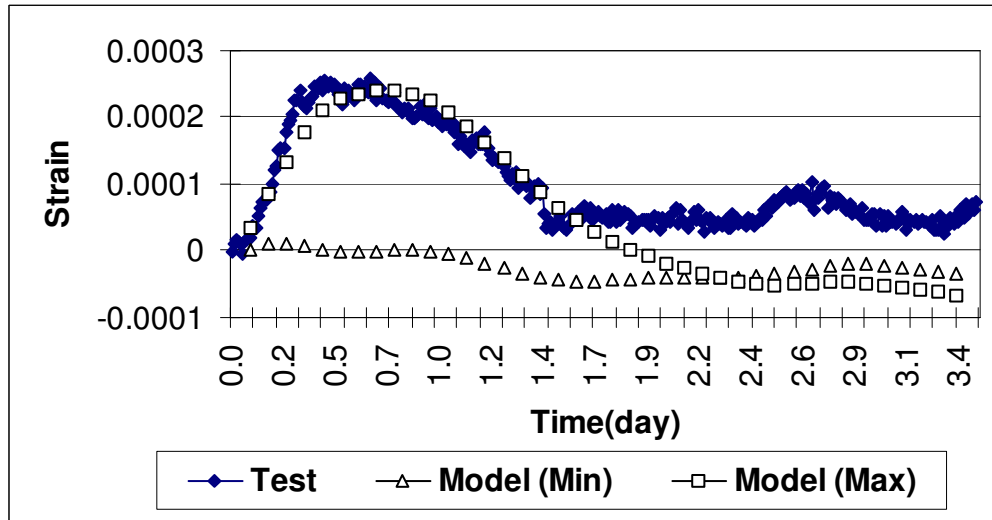


Figure V-19 Comparison for M-50 Bridge Strain at S3 Top Longitudinal

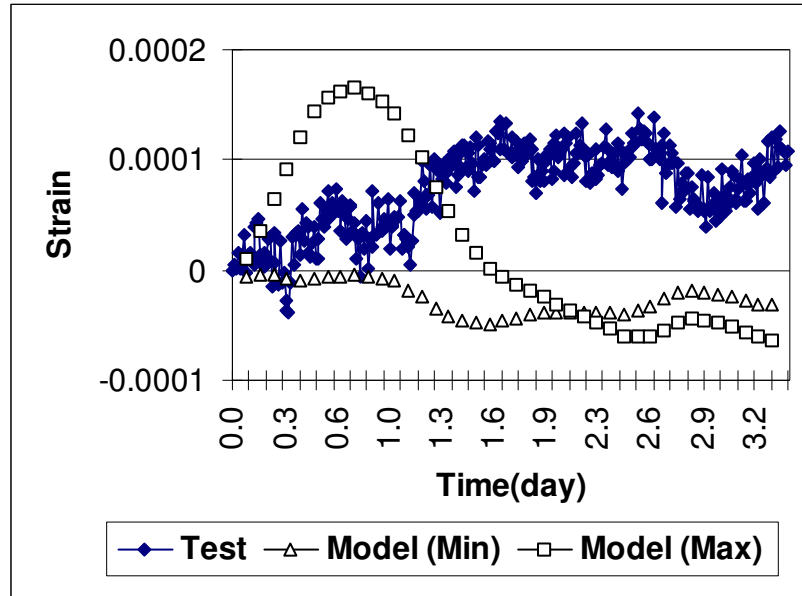


Figure V-20 Comparison for M-50 Bridge Strain at S3 Bottom Longitudinal

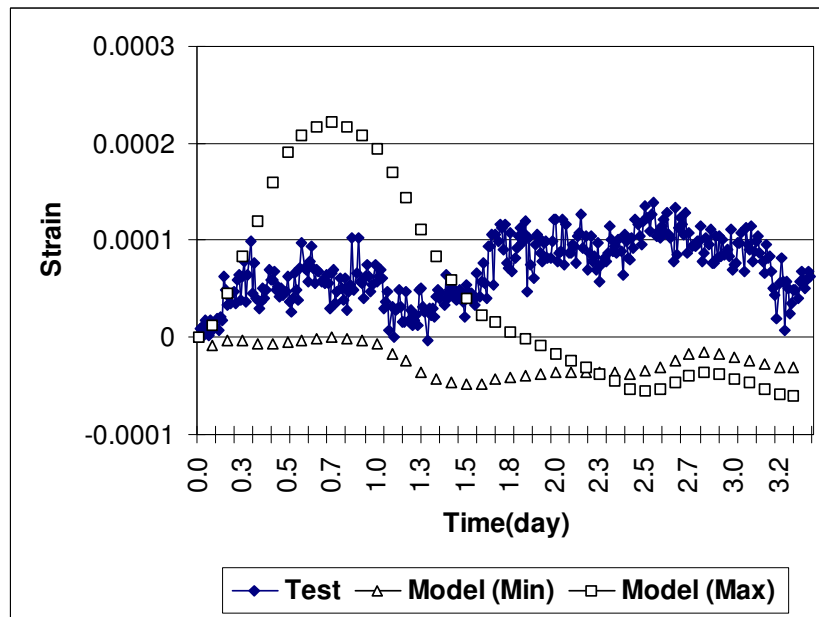


Figure V-21 Comparison for M-50 Bridge Strain at S3 Bottom Transverse

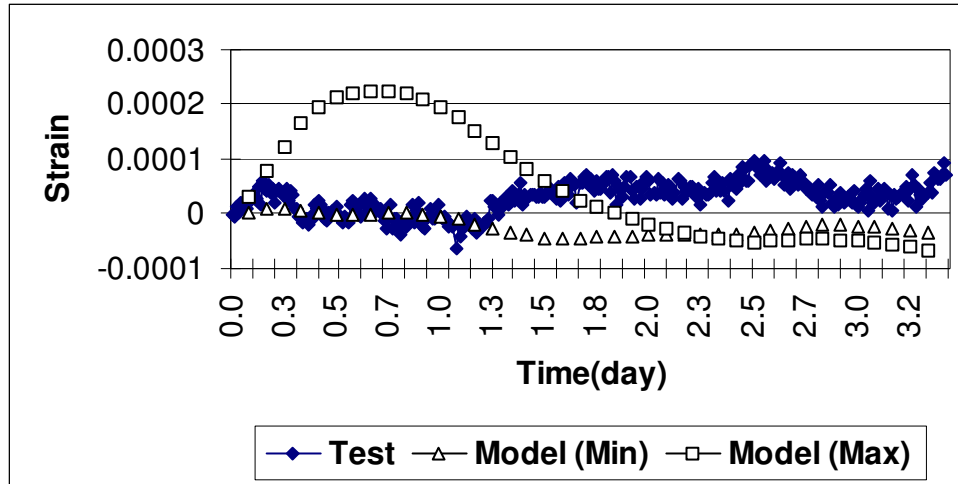


Figure V-22 Comparison for M-50 Bridge Strain at S4 Top Longitudinal

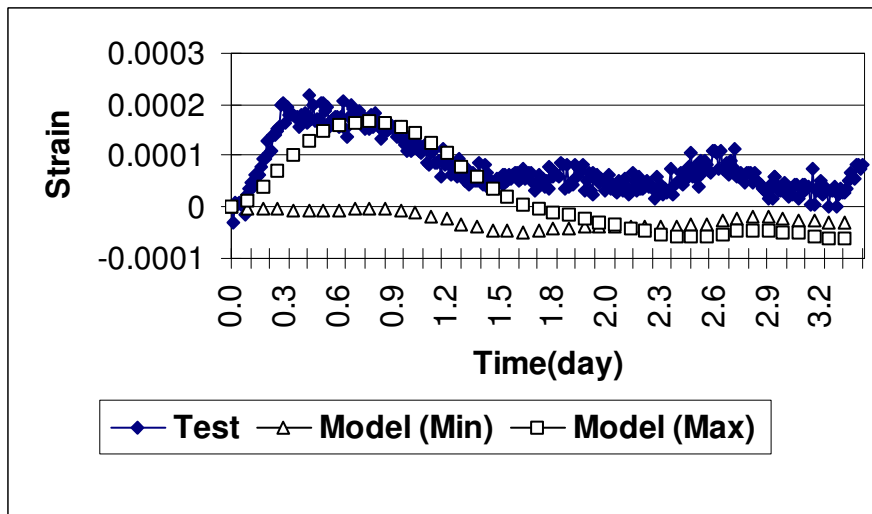


Figure V-23 Comparison for M-50 Bridge Strain at S4 Bottom Longitudinal

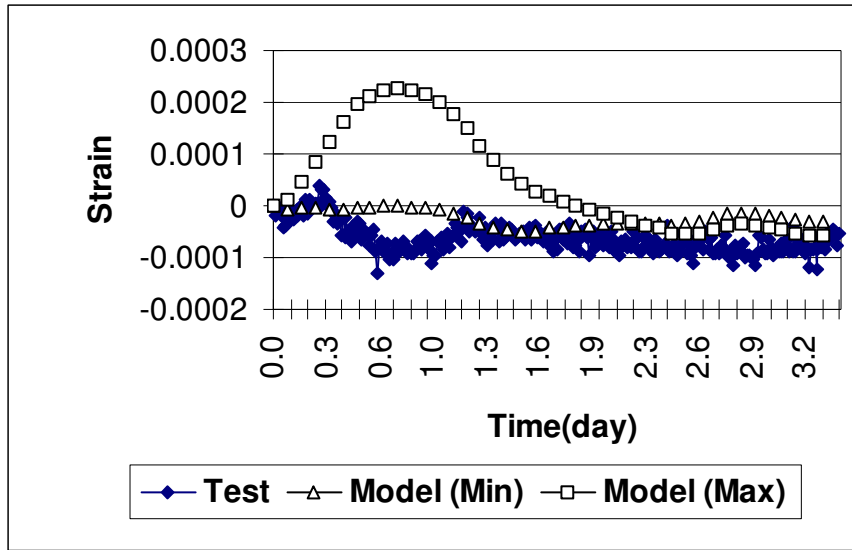


Figure V-24 Comparison for M-50 Bridge Strain at S4 Bottom Transverse

V-1.6.2 Grove Street Deck in Development (S02-81063)

Figures V-25 to V-28 compares the measured and computed temperatures for the first two and a half days of the Grove Street Bridge's East Bound side (Phase 1). This data acquisition period was slightly shorter than for the M-50 Bridge because the Omega Data Logbook system had to be removed after the first two and a half days of data acquisition to catch the opportunity of monitoring hydration process at the M-50 Bridge being constructed then.

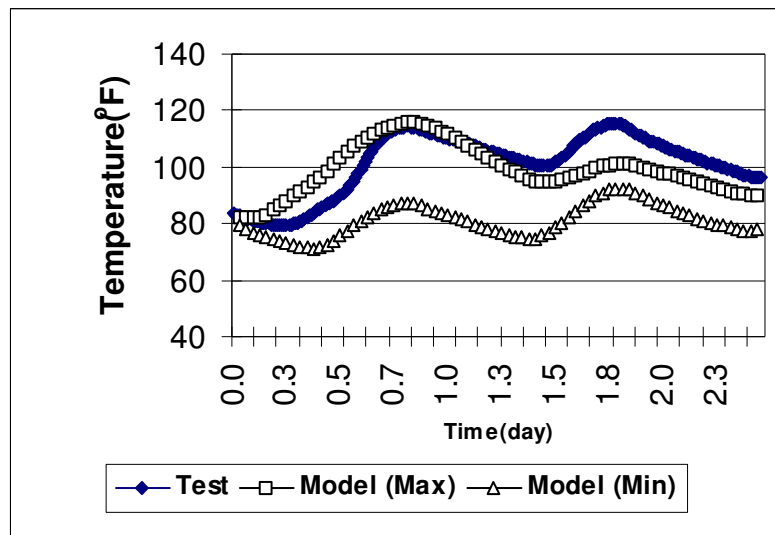


Figure V-25 Comparison for Grove Street Bridge Temperature at S3 Top

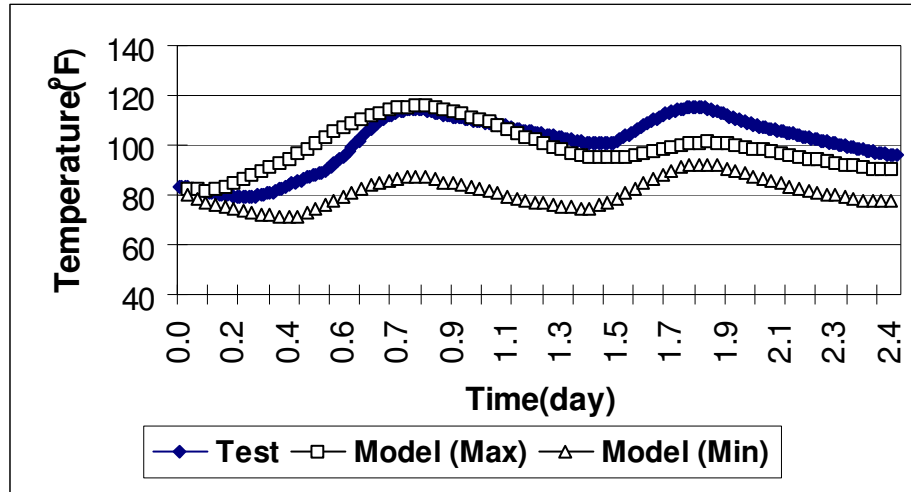


Figure V-26 Comparison for Grove Street Bridge Temperature at S3 Bottom

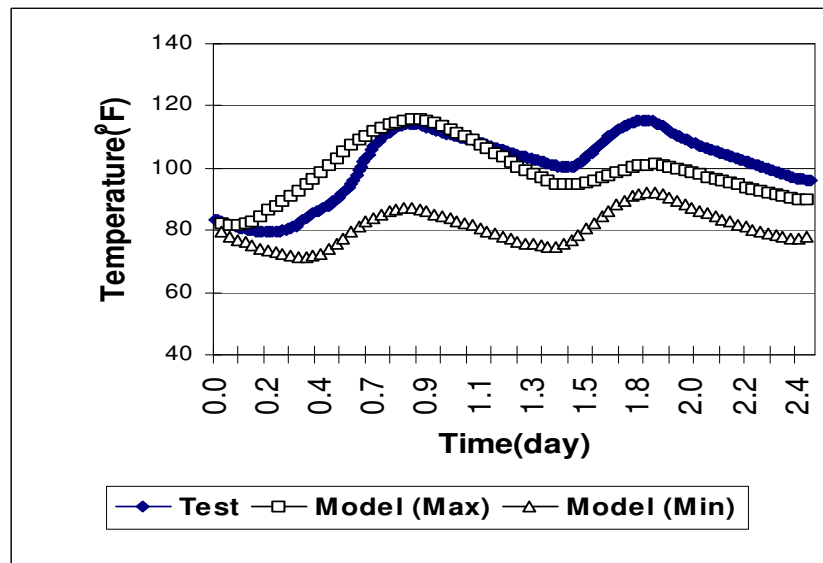


Figure V-27 Comparison for Grove Street Bridge Temperature at S4 Top

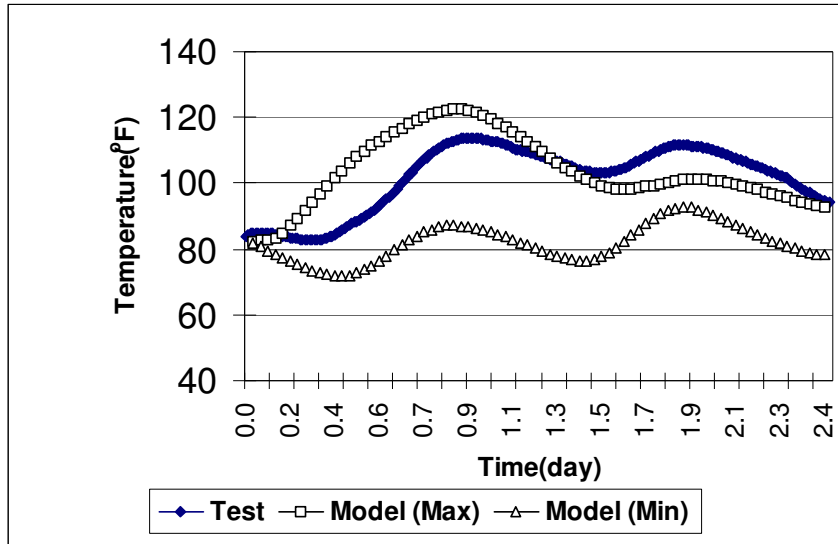


Figure V-28 Comparison for Grove Street Bridge Temperature at S4 Bottom

Temperature recorded at the Grove Street bridge deck exhibits more clearly the daily cycling as seen in Chapter IV. The perceived minimum and maximum responses are able to envelope the first one and a half days where the peak temperature was observed. Figures V-29 to V-32 show the same kind of comparison for the other half of the bridge deck poured later in Phase 2 (West Bound). Note that this half was constructed about a month later than Phase 1 and we were able to continue monitoring the temperature and strain for about 21 days. These four figures show that the minimum and maximum curves better envelope the measured temperature record, compared with Figures V-25 to V-28.

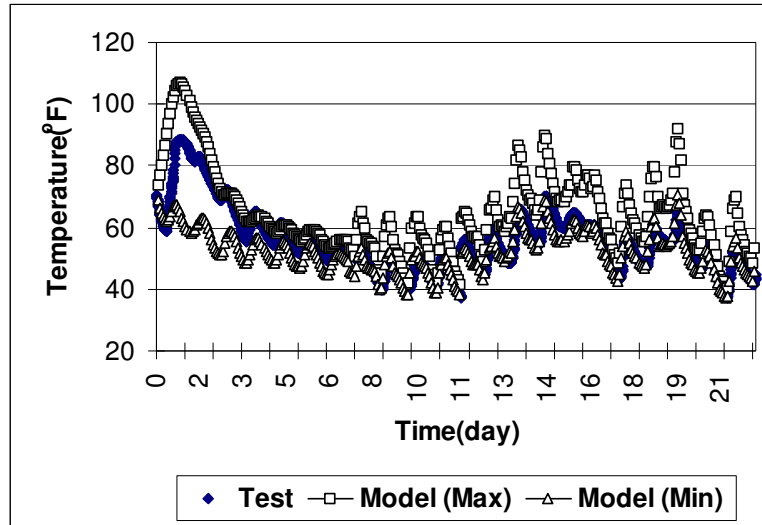


Figure V-29 Comparison for Grove Street Bridge Temperature at S1 Top

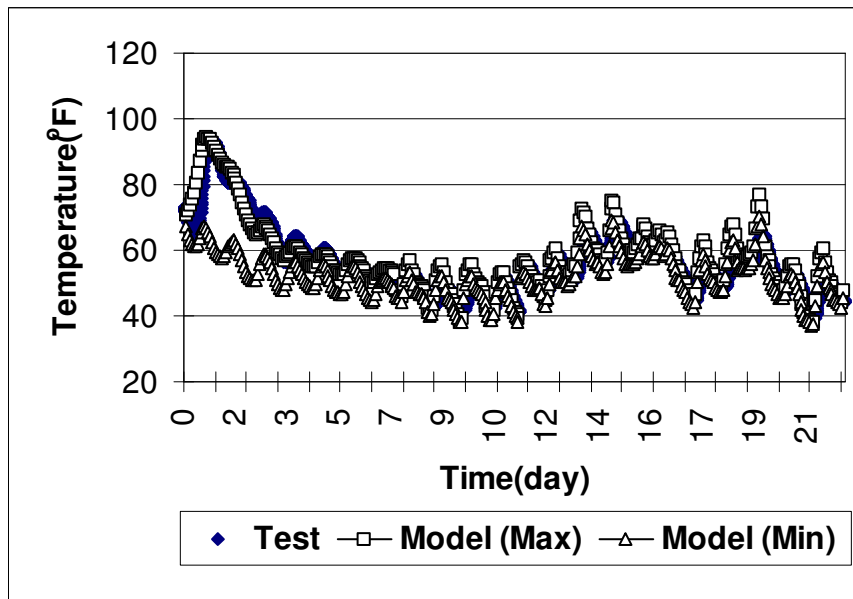


Figure V-30 Comparison for Grove Street Bridge Temperature at S1 Bottom

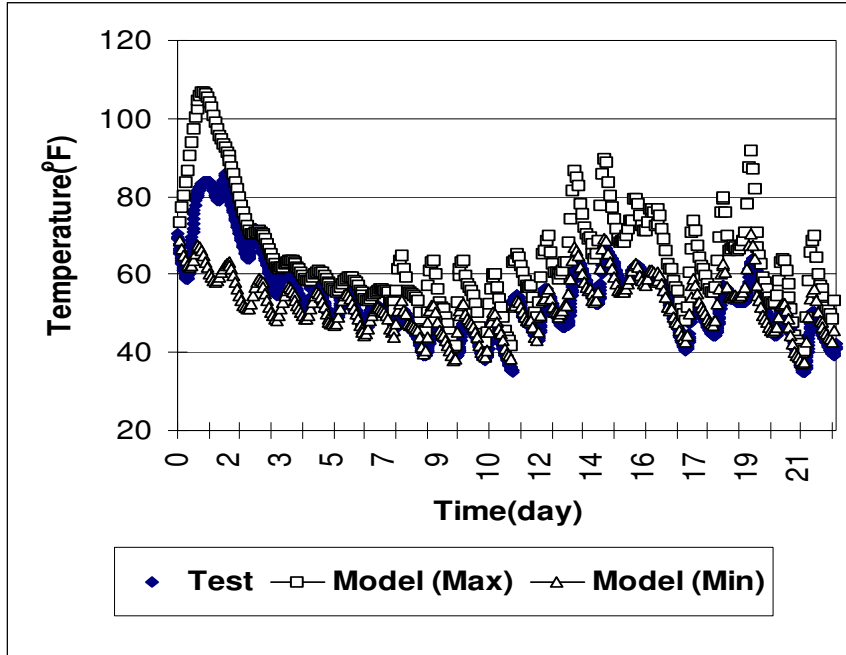


Figure V-31 Comparison for Grove Street Bridge Temperature at S2 Top

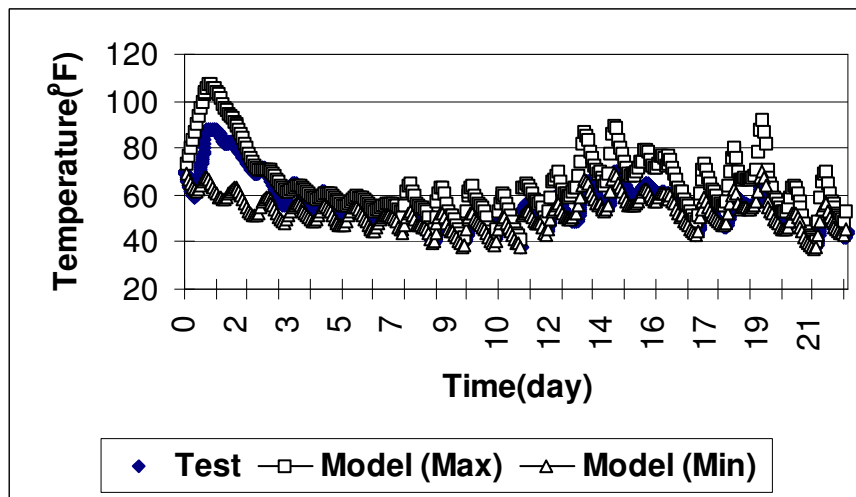


Figure V-32 Comparison for Grove Street Bridge Temperature at S2 Bottom

Figures V-33 to V-38 compare the strains in Phase 1 of the Grove Street bridge between measurement and FEA simulation using DIANA. The measured strains are enveloped between the maximum and minimum curves in Figures V-35 to V-38. In Figure V-35 the measured strain appears to be drifting up with time. Figures V-39 to V-44 shows similar comparison for strains for Phase 2 of the bridge deck. It is seen that during the first one and a half days, the measured strains were bounded by the envelopes shown. Beyond first 2 or 3 days, the envelopes did not do well. Also, it should be noted that the strain prediction by FEA is not as good as the temperature prediction, because the strain computation depends on the temperature as the input, which was discussed earlier in Section V-1.5. In addition, the strain-stress analysis is nonlinear, thus more difficult to model and predict.

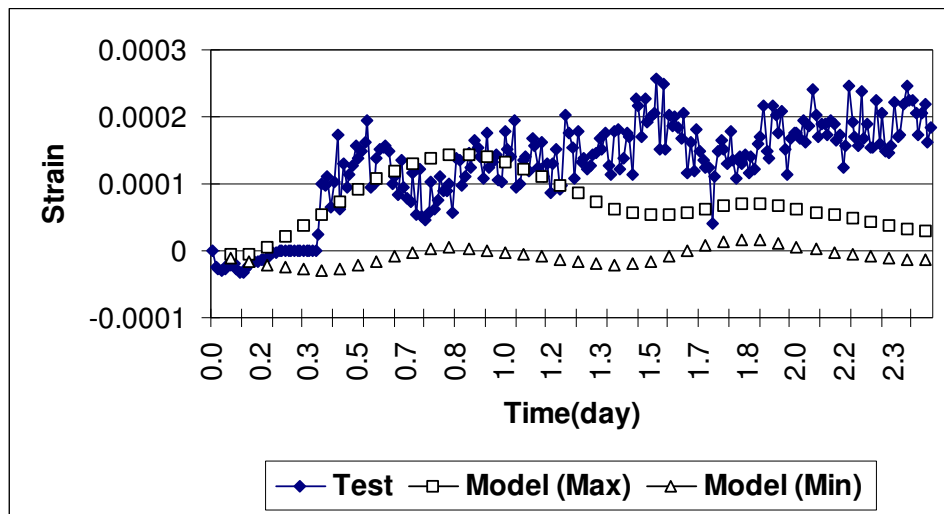


Figure V-33 Comparison for Grove Street Bridge Strain at S3 Top Longitudinal

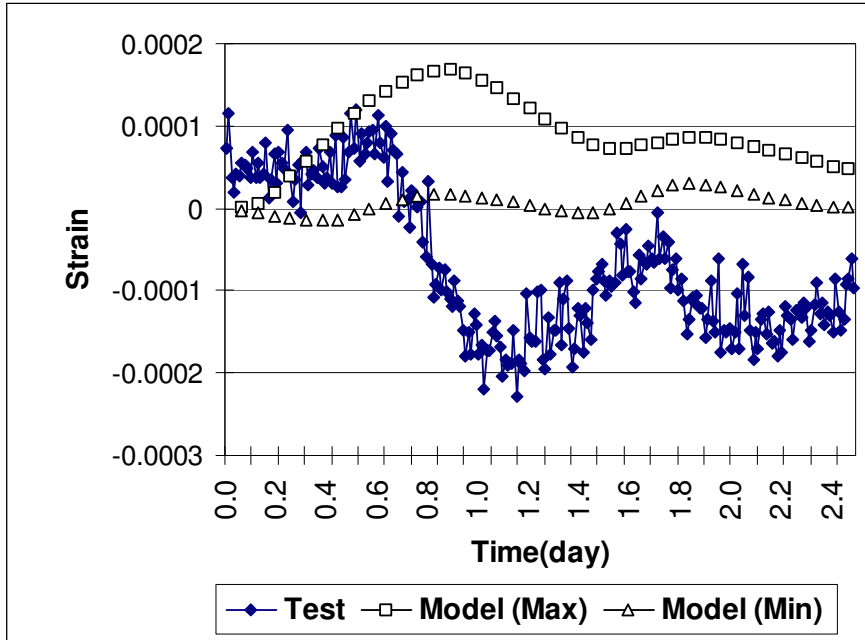


Figure V-34 Comparison for Grove Street Bridge Strain at S3 Bottom Longitudinal

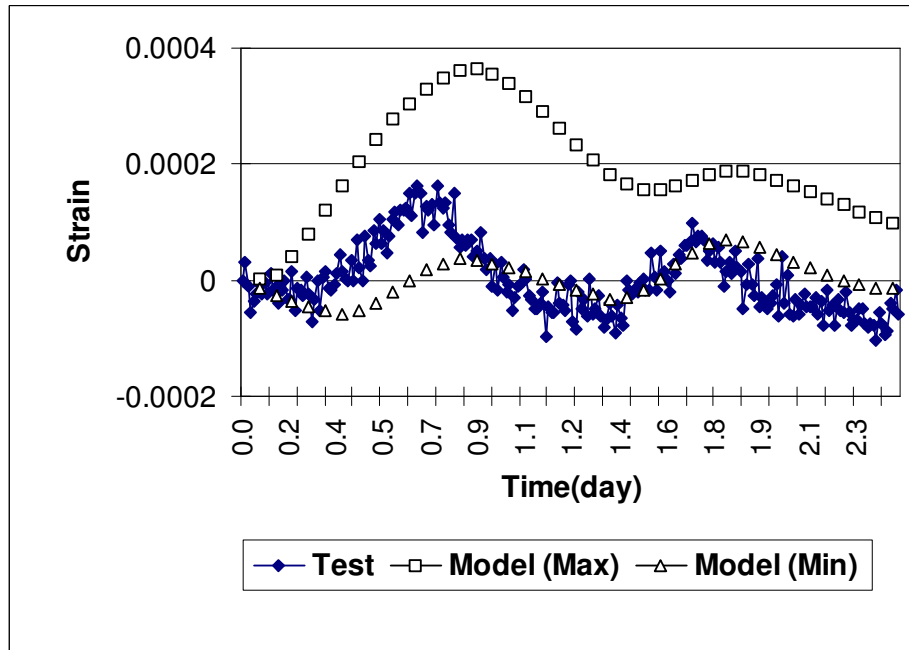


Figure V-35 Comparison for Grove Street Bridge Strain at S3 Bottom Transverse

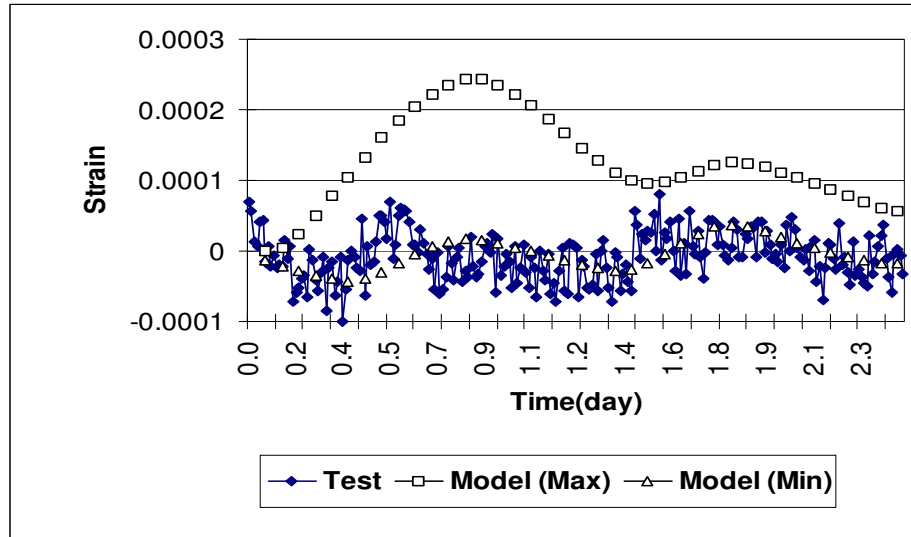


Figure V-36 Comparison for Grove Street Bridge Strain at S4 Top Longitudinal

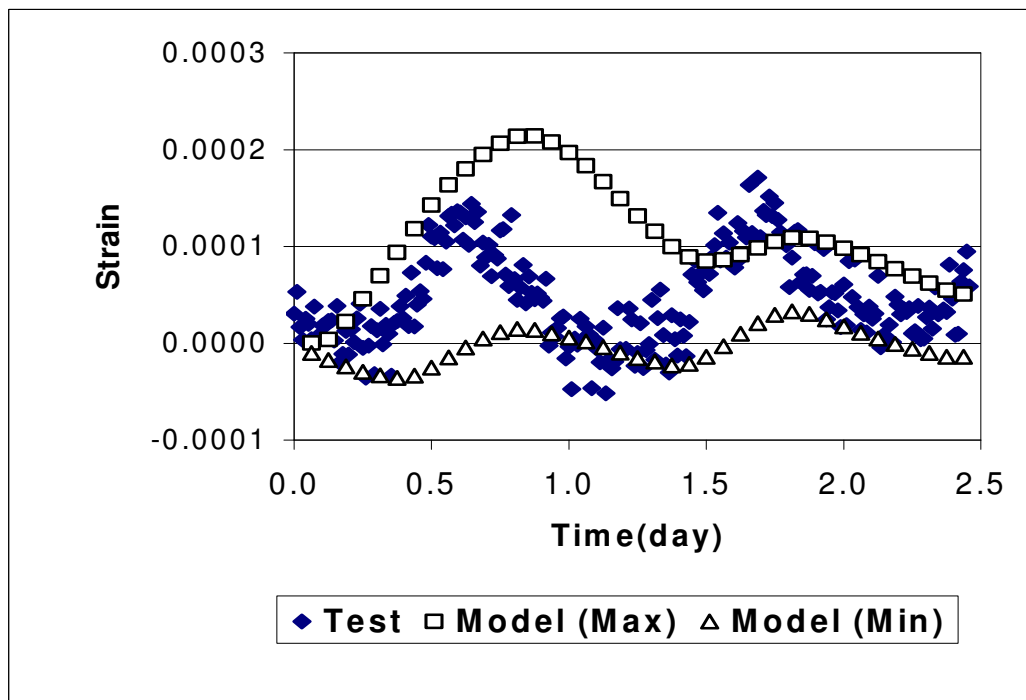


Figure V-37 Comparison for Grove Street Bridge Strain at S4 Bottom Longitudinal

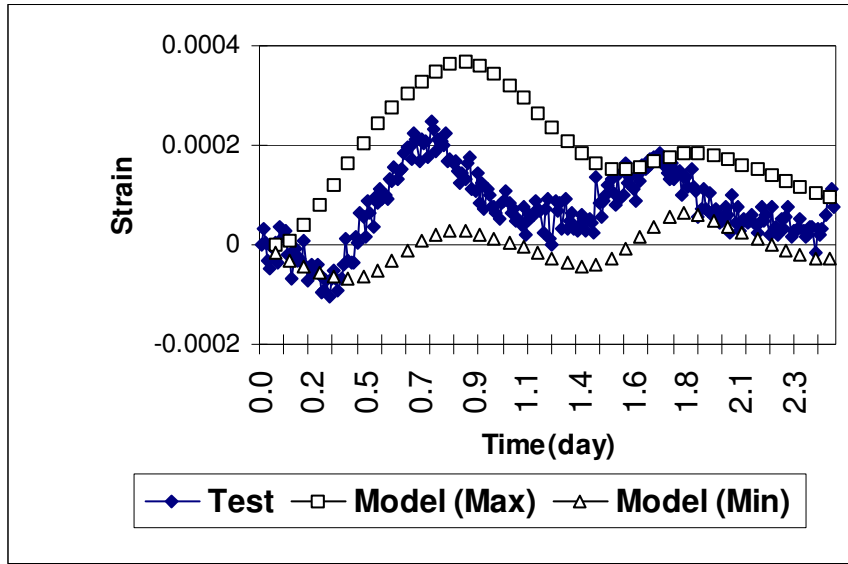


Figure V-38 Comparison for Grove Street Bridge Strain at S4 Bottom Transverse

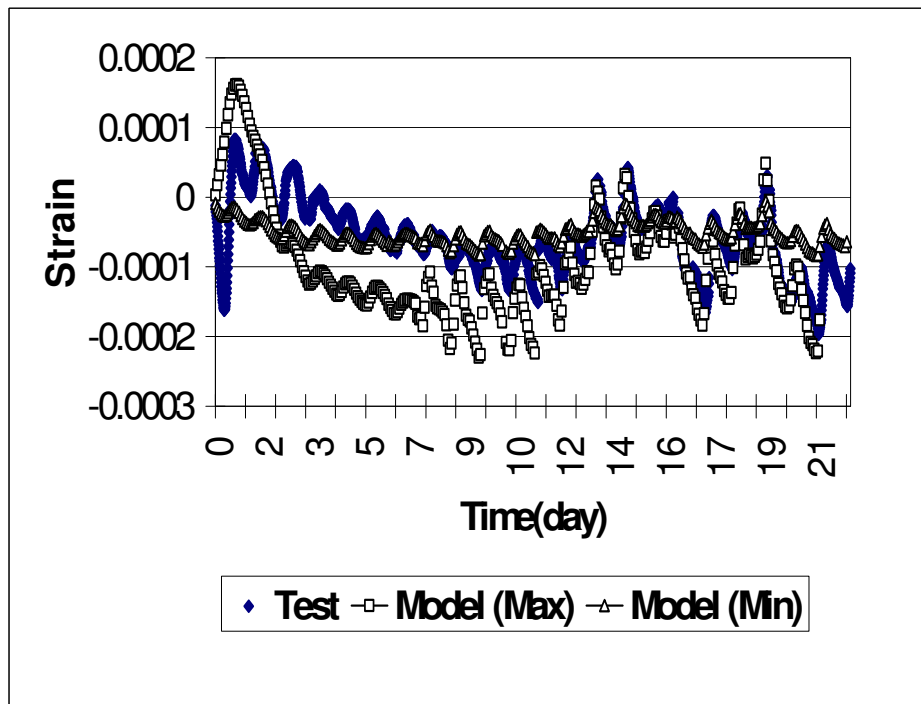


Figure V-39 Comparison for Grove Street Bridge Strain at S1 Top Longitudinal

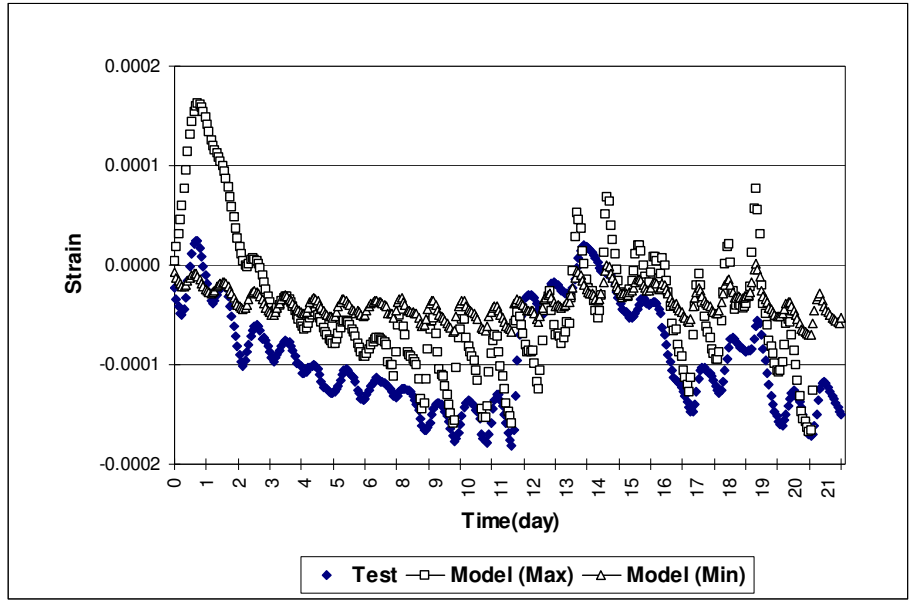


Figure V-40 Comparison for Grove Street Bridge Strain at S1 Bottom Longitudinal

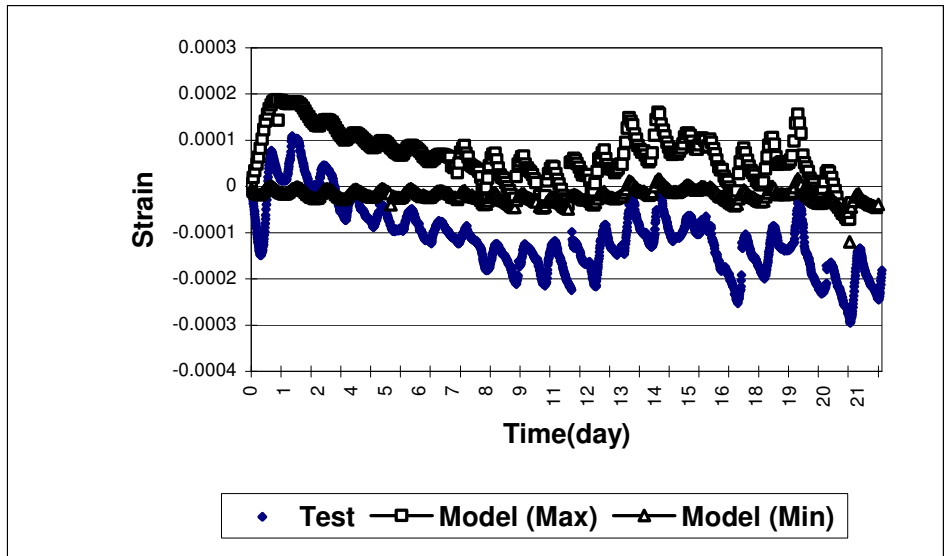


Figure V-41 Comparison for Grove Street Bridge Strain at S1 Bottom Transverse

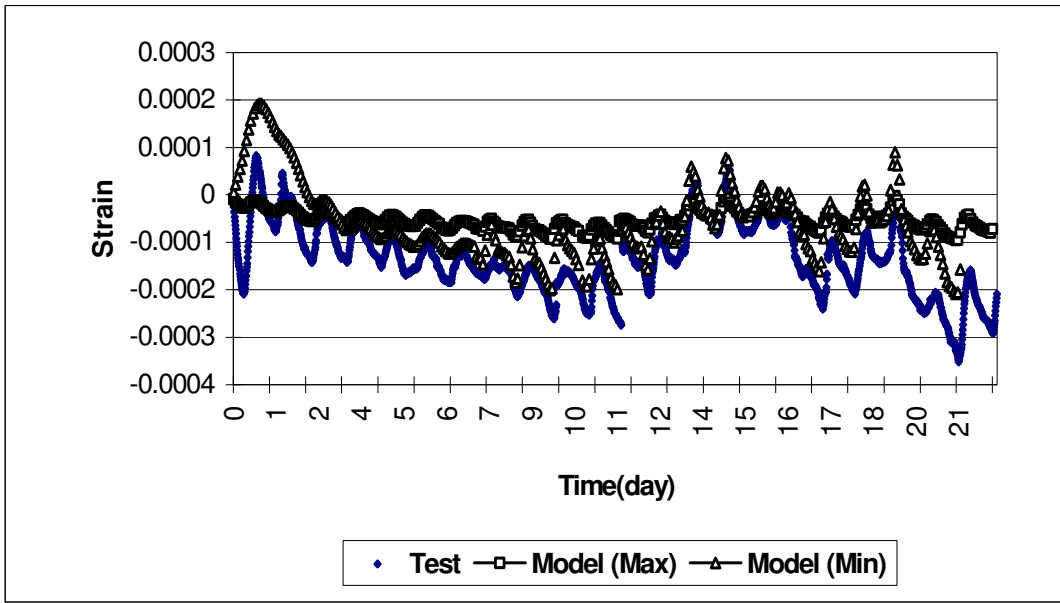


Figure V-42 Comparison for Grove Street Bridge Strain at S2 Top Longitudinal

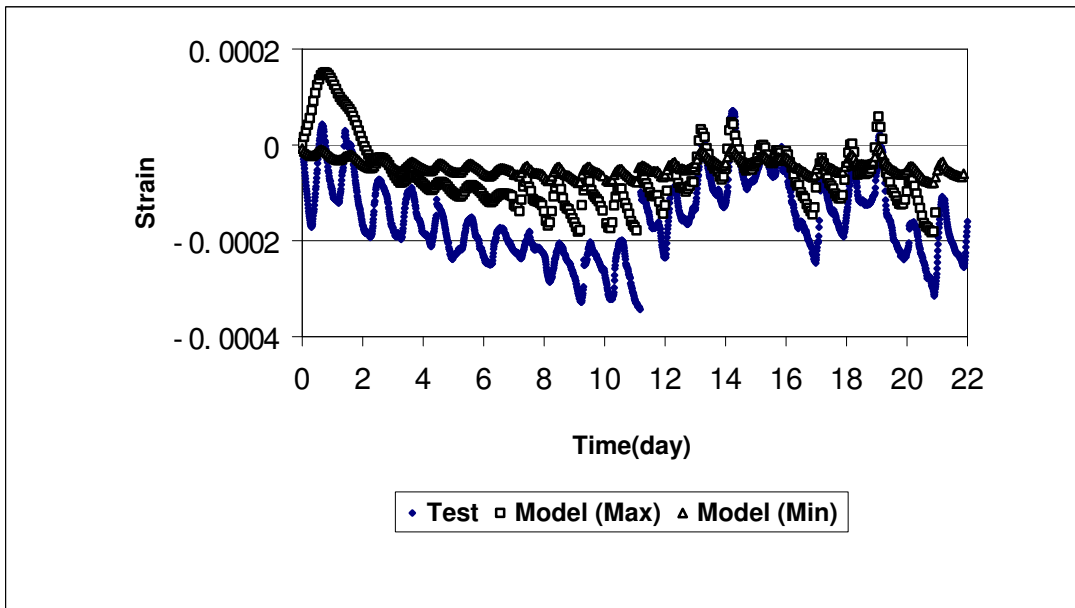


Figure V-43 Comparison for Grove Street Bridge Strain at S2 Bottom Longitudinal

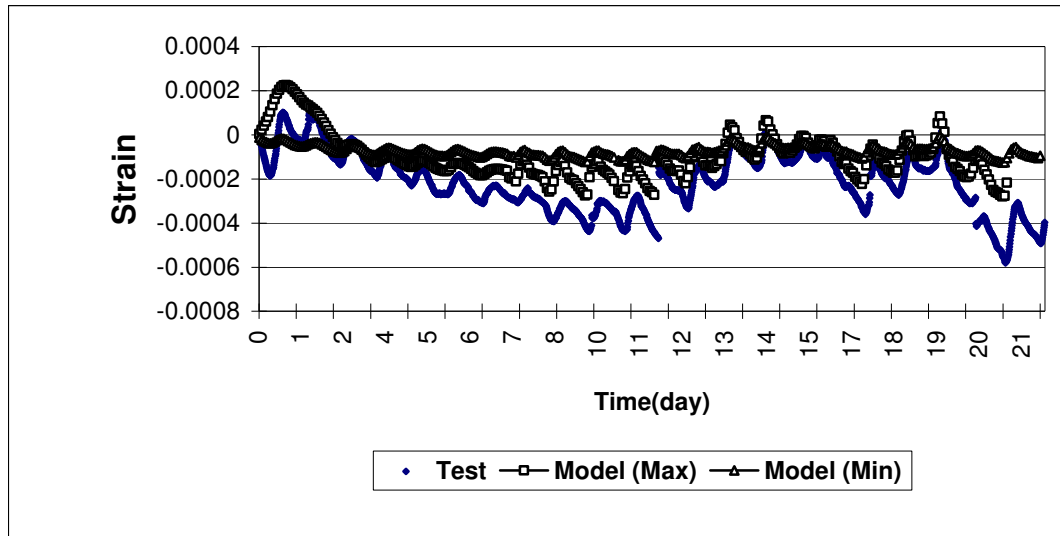


Figure V-44 Comparison for Grove Street Bridge Strain at S2 Bottom Transverse

V-1.6.3 Truck Load Test for Grove Street Bridge (S02-81063) and M50 Bridge (S02-38131)

The DIANA FEA models were also used to simulate the truck load tests performed on the two bridge decks. The comparison of the computed and measured strain for the Grove Street Bridge is shown in Figures V-45 to V-50 for the 6 strain gages in Phase 1 at locations S3 and S4. The computed strains are indicated as points marked with small triangles, and the measured strains are shown as continuous lines formed with filled diamond shapes with a higher resolution, because more data points were acquired and plotted here.

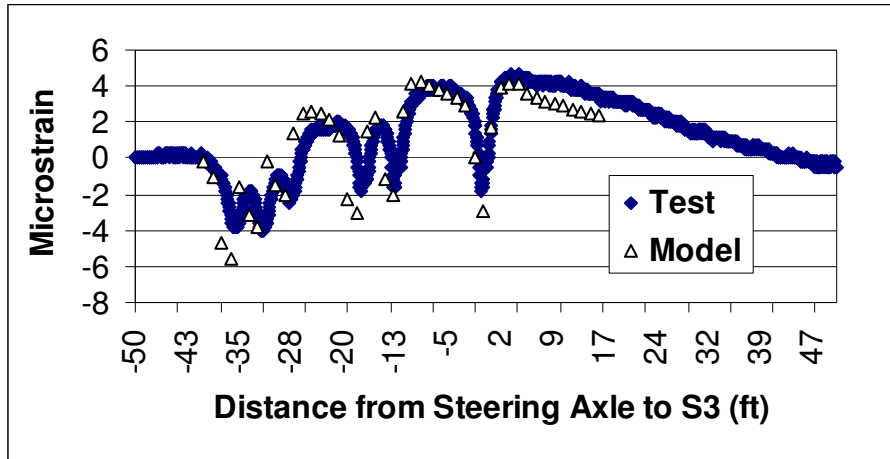


Figure V-45 Comparison of Truck Load Response for Grove Street Bridge S3 Top Longitudinal

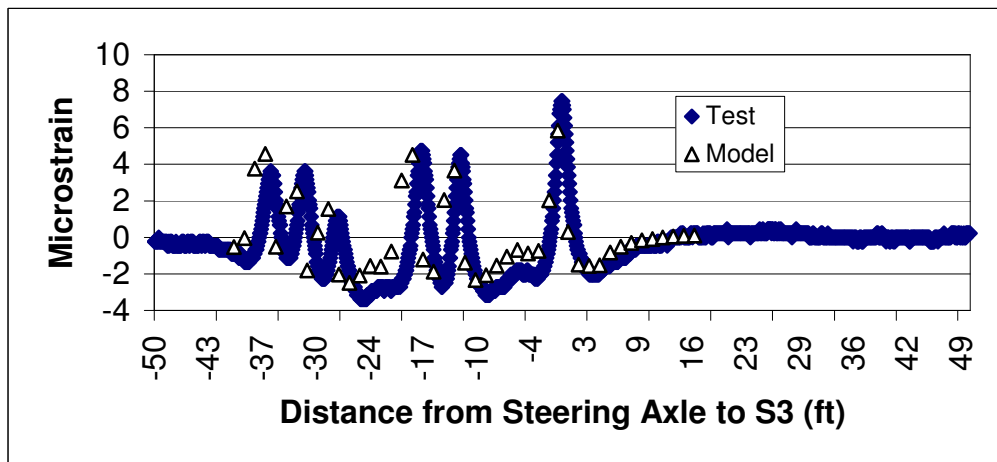


Figure V-46 Comparison of Truck Load Response for Grove Street Bridge S3 Bottom Longitudinal

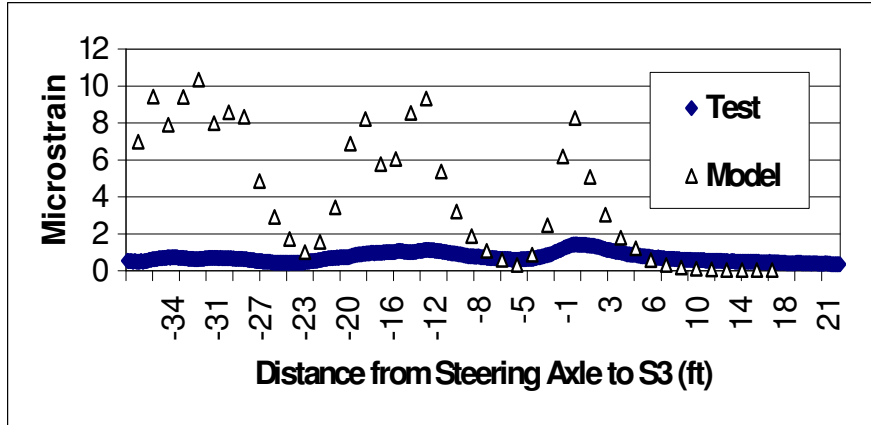


Figure V-47 Comparison of Truck Load Response for Grove Street Bridge S3 Bottom Transverse

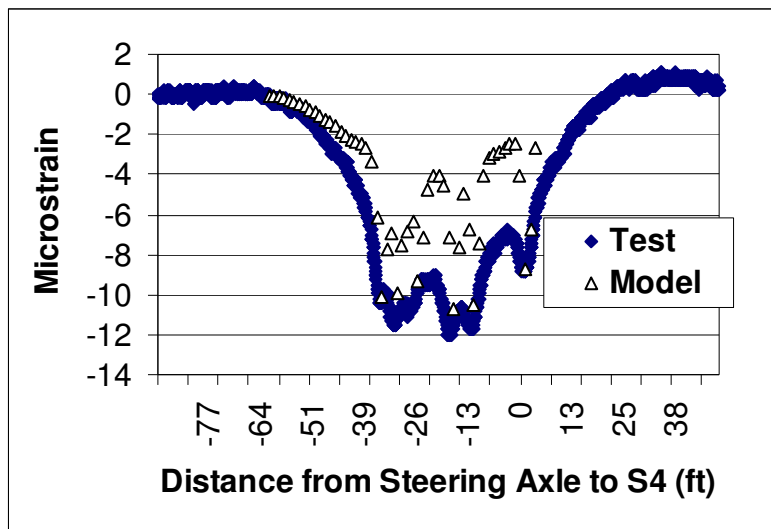


Figure V-48 Comparison of Truck Load Response for Grove Street Bridge S4 Top Longitudinal

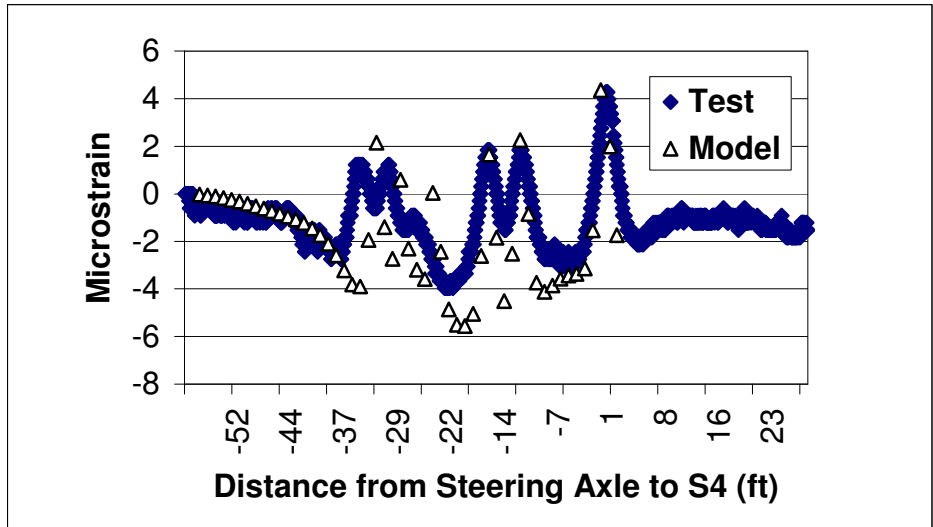


Figure V-49 Comparison of Truck Load Response for Grove Street Bridge S4 Bottom Longitudinal

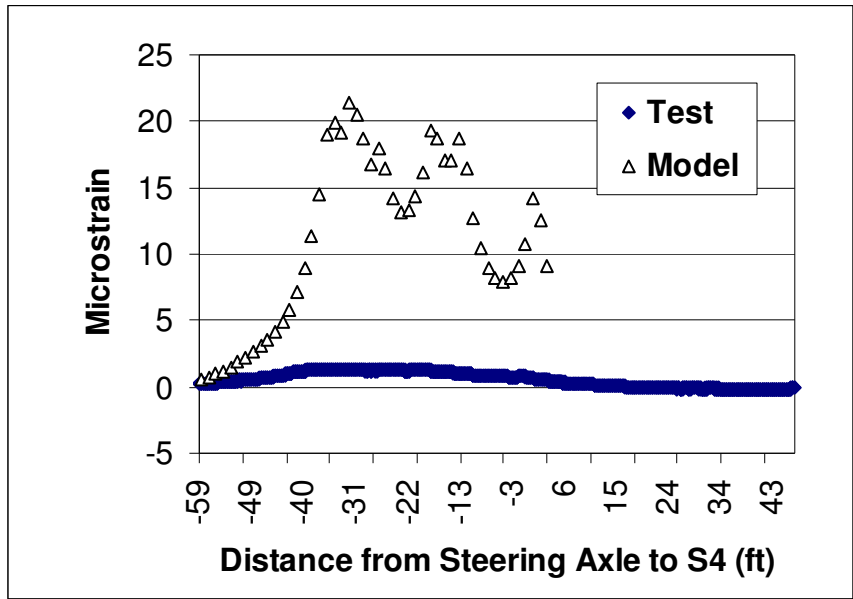


Figure V-50 Comparison of Truck Load Response for Grove Street Bridge S4 Bottom Transverse

In addition, these figures display longer data lines than the computed values, because the FEA model did not include the approach slab before the analyzed bridge span, nor the other spans beyond the first pin-and-hanger where measured data were also collected. The load was applied using a 6-axle truck as shown in Figure V-51, with axle weights of 14380, 15700, 15250, 11840, 14530, and 15850 lbs and spacing of 12, 4.67, 9.92, 3.75, and 4.75 ft.

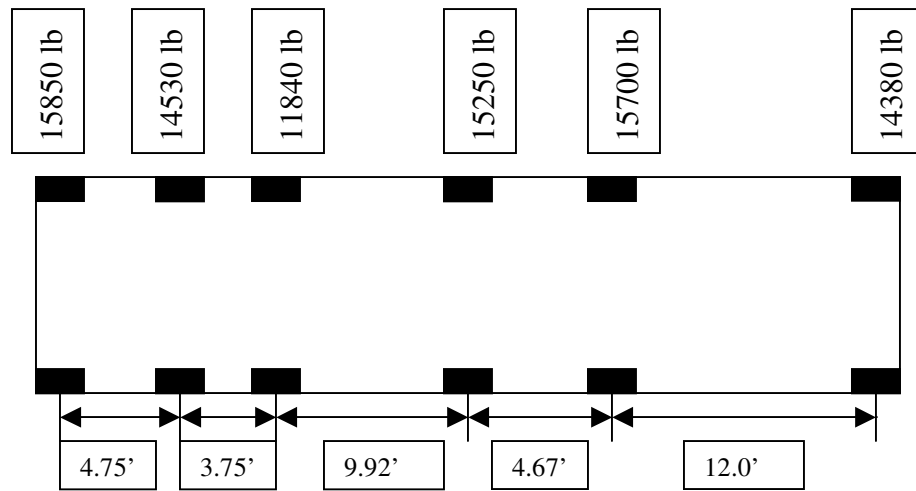
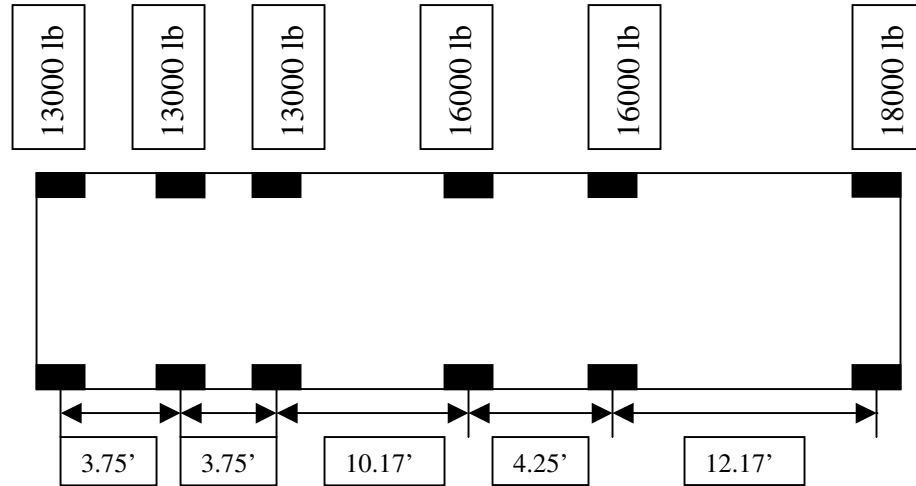


Figure V-51 6-axle Truck for Loading Grove Street Bridge Phase 1 (S3 and S4)

These comparison results show that the FEA model was able to produce reliable results compared with measured results for truck loading, except for the transverse bottom strains in the two locations. It has not been concluded exactly what factors have contributed to the large discrepancy between the measured and FEA calculated strains. One possible factor is that some of the strain gages' locations were moved from where intended during the process of concrete placement. This could result in inconsistency between the reality and the computer simulated condition. Another possible factor is that the truck wheels did not follow the marked line for direct loading the instrumented locations.



Error!

Bookmark not defined.

Figure V-52 6-axle Truck for Loading Grove Street Bridge Phase 2 (S1 and S3)

For Phase 2 (West Bound half) of the Grove Street bridge, load testing was performed about a month after Phase 1 construction was completed. A different 6-axle truck shown in Figure V-52 was used to load the deck, with axle weights of 18,000, 16,000, 16,000, 13,000, 13,000, and 13,000 lbs, and axle spacing of 12.17, 4.25, 10.17, 3.75, and 3.75 ft. Comparison of the measured strains and FEA computed strains is shown below in Figures V-53 to V-58. These figures all show good agreement between the measured and calculated strains. The bottom transverse strains are also predicted well, which were not so well predicted for the Phase 1 gages.

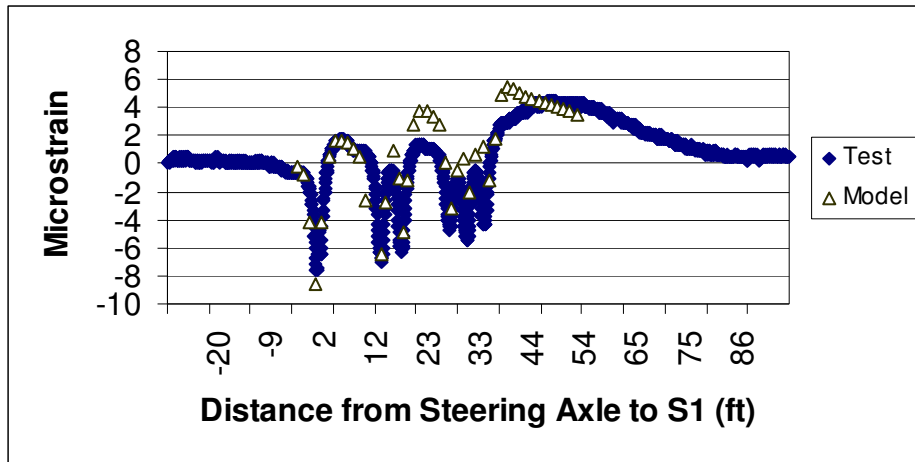


Figure V-53 Comparison of Truck Load Response for Grove Street Bridge S1 Top Longitudinal

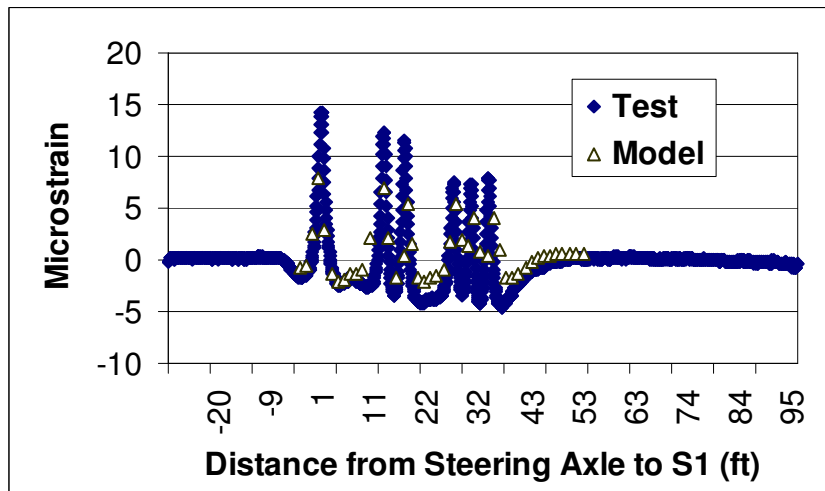


Figure V-54 Comparison of Truck Load Response for Grove Street Bridge S1 Bottom Longitudinal

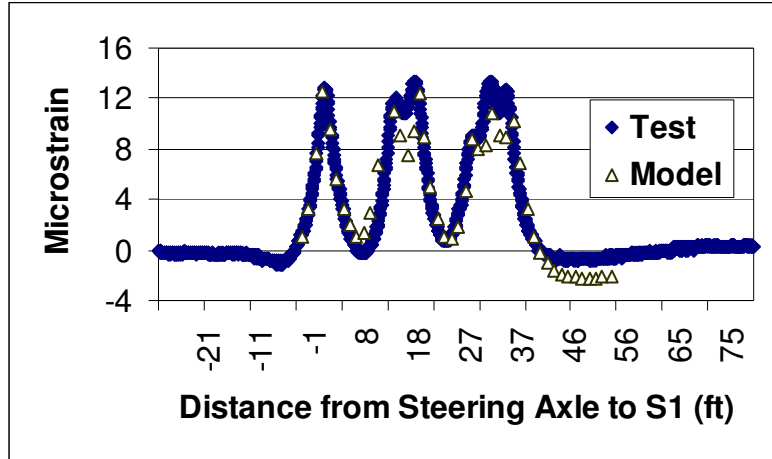


Figure V-55 Comparison of Truck Load Response for Grove Street Bridge S1 Bottom Transverse

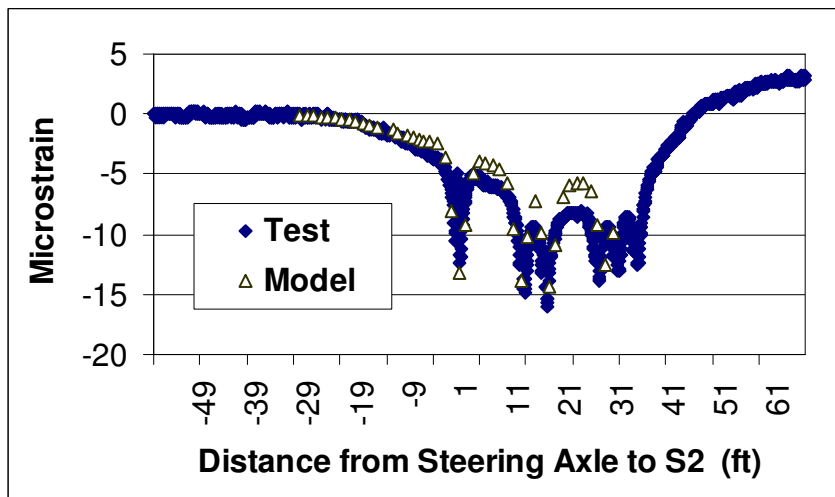


Figure V-56 Comparison of Truck Load Response for Grove Street Bridge S2 Top Longitudinal

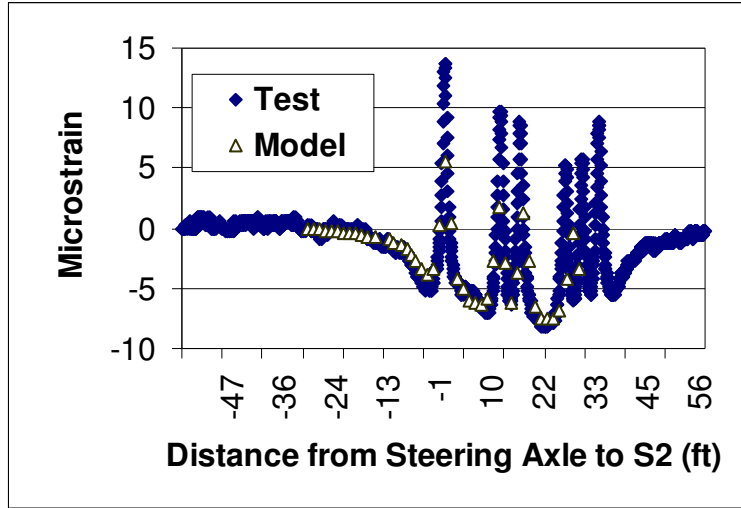


Figure V-57 Comparison of Truck Load Response for Grove Street Bridge S2 Bottom Longitudinal

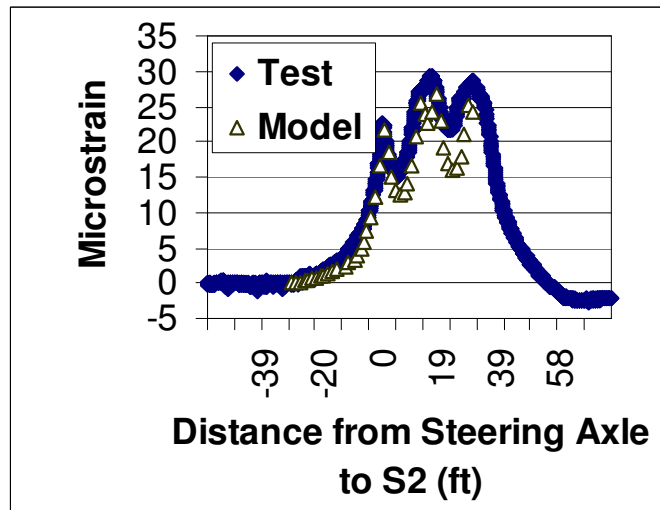


Figure V-58 Comparison of Truck Load Response for Grove Street Bridge S2 Bottom
Transverse

For the M-50 bridge deck, comparison between the measured and computed strains is exhibited in Figures V-60 to V-65 for strain gages at the S1 and S2 locations. A 5-axle truck, as shown in Figure V-59, was used to load the deck with axle weights of 18,000, 13,000, 13,000, 13,000, and 13,000 lbs, and axle spacings of 9.25, 3.83, 5.33, and 4.33 ft. It may be interesting to mention that these results show as good consistency for the bottom transverse strain gages as for other locations. However, this time the longitudinal bottom gage at location S2 shows more significant discrepancy. In Figures V-66 to V-71, comparison of the test results and the FEA results is presented for the locations of S3 and S4 in the M-50 Bridge. The same 5-axle truck in Figure V-59 was used to load this part of the deck. These results appear to also show good predictions of the FEA, except the transverse bottom strain at S4.

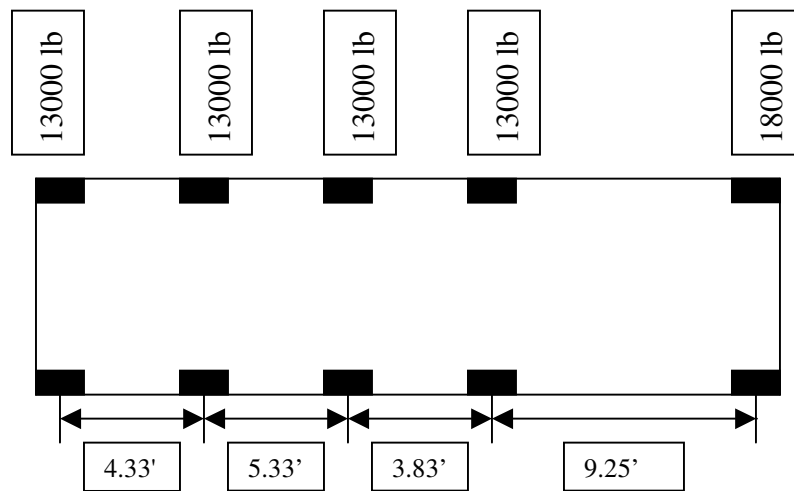
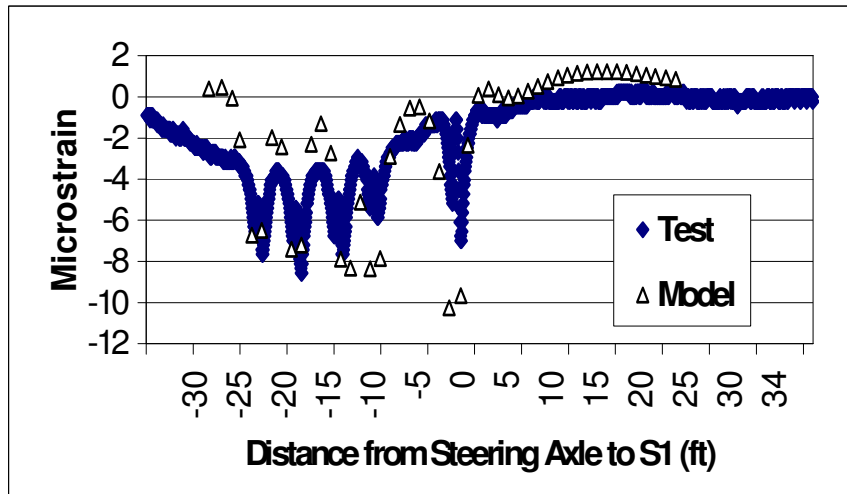


Figure V-59 5-axle Truck for Loading M-50 Bridge



Error! Bookmark not defined.

Figure V-60 Comparison of Truck Load Response for M-50 Bridge S1 Top Longitudinal

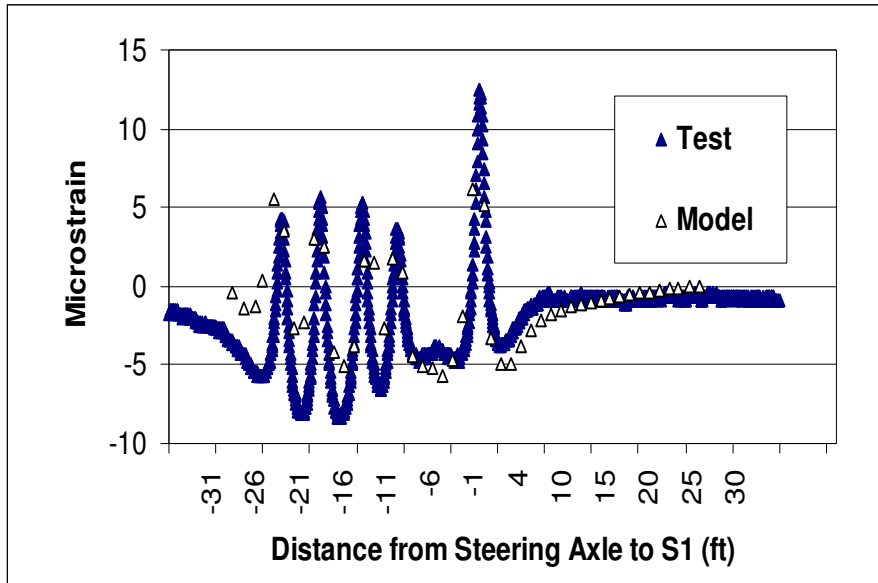


Figure V-61 Comparison of Truck Load Response for M-50 Bridge S1 Bottom Longitudinal

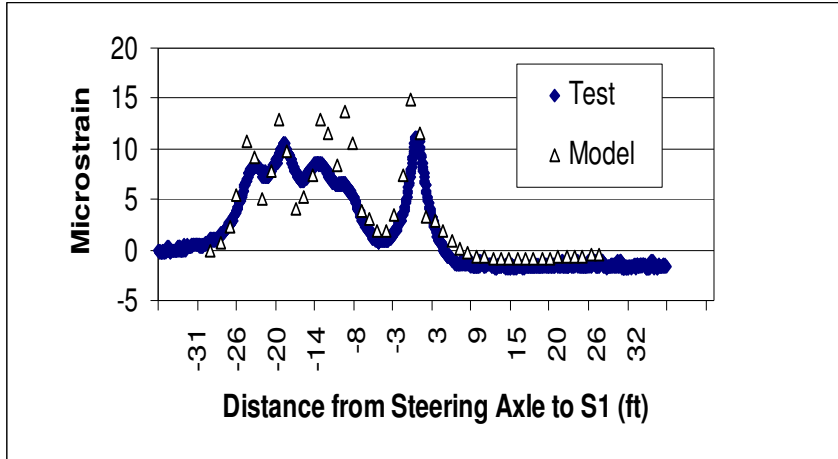


Figure V-62 Comparison of Truck Load Response for M-50 Bridge S1 Bottom Transverse

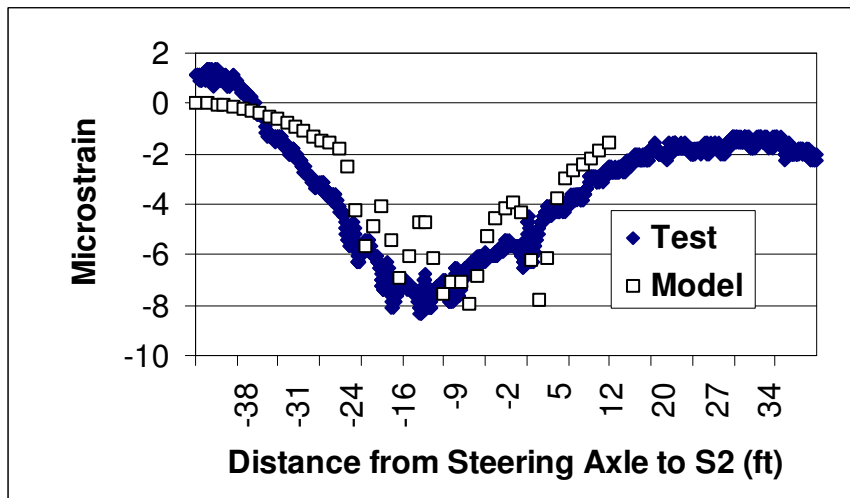


Figure V-63 Comparison of Truck Load Response for M-50 Bridge S2 Top Longitudinal

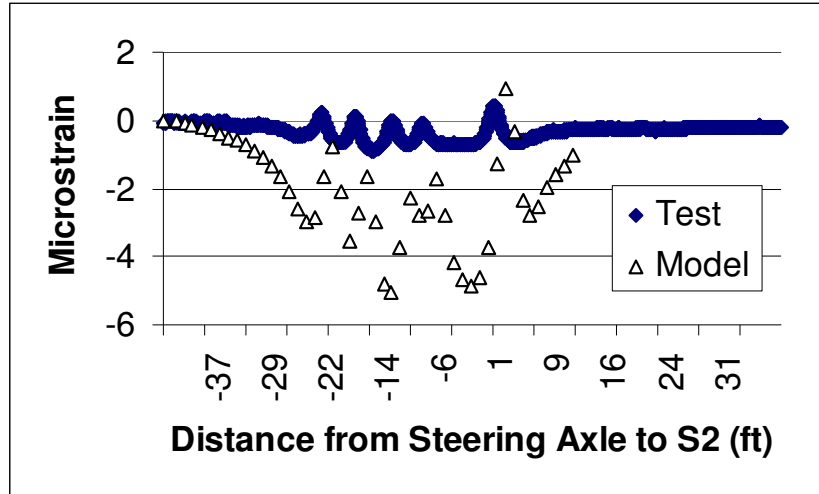


Figure V-64 Comparison of Truck Load Response for M-50 Bridge S2 Bottom Longitudinal

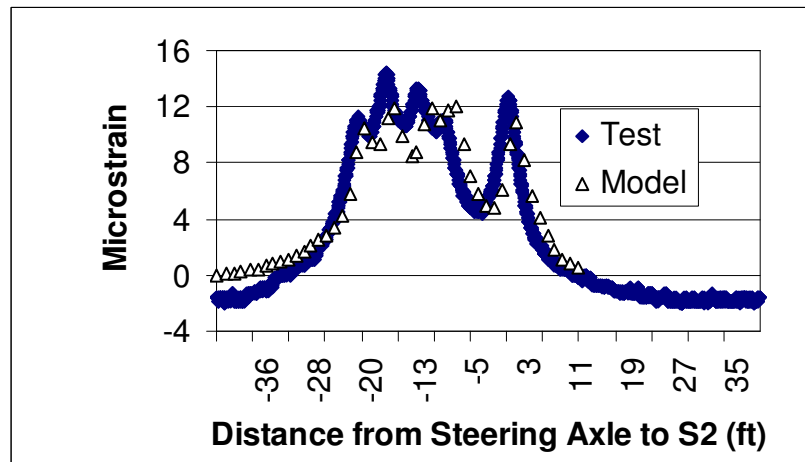


Figure V-65 Comparison of Truck Load Response for M-50 Bridge S2 Bottom Transverse

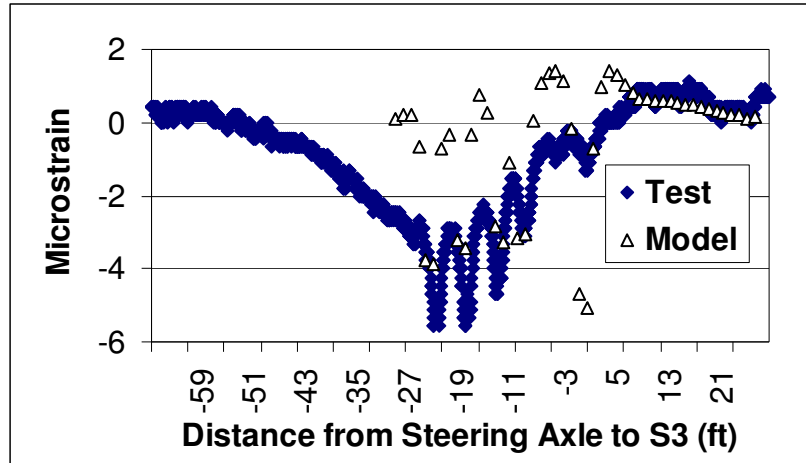


Figure V-66 Comparison of Truck Load Response for M-50 Bridge S3 Top Longitudinal

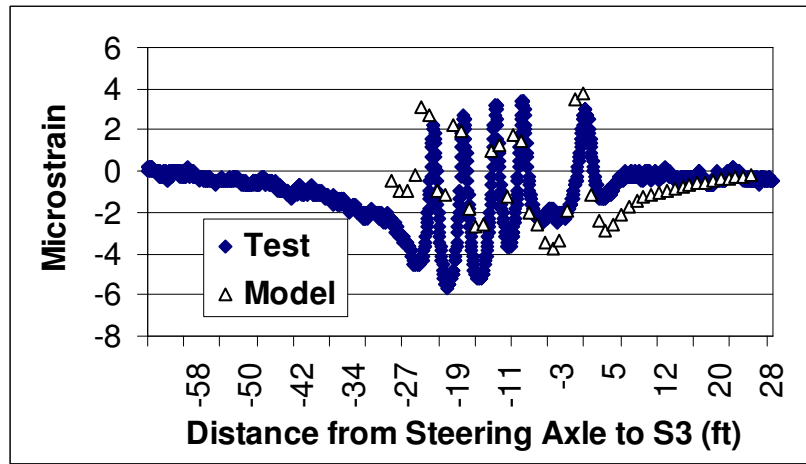


Figure V-67 Comparison of Truck Load Response for M-50 Bridge S3 Bottom Longitudinal

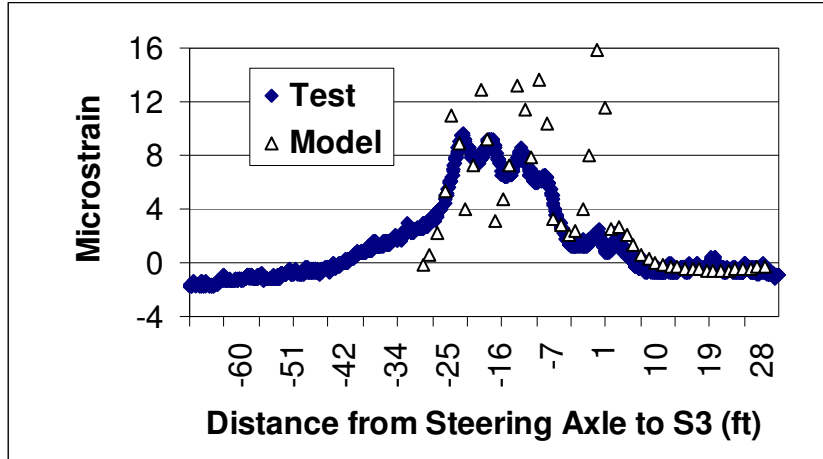


Figure V-68 Comparison of Truck Load Response for M-50 Bridge S3 Bottom Transverse

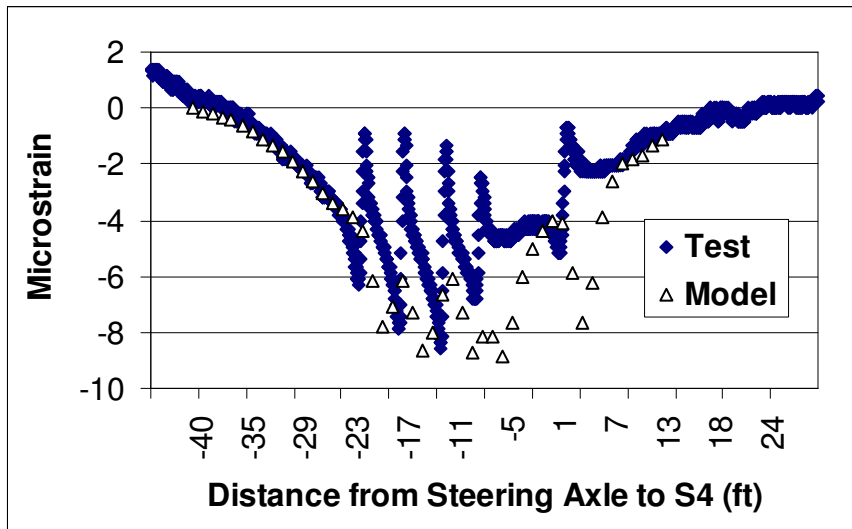


Figure V-69 Comparison of Truck Load Response for M-50 Bridge S4 Top Longitudinal

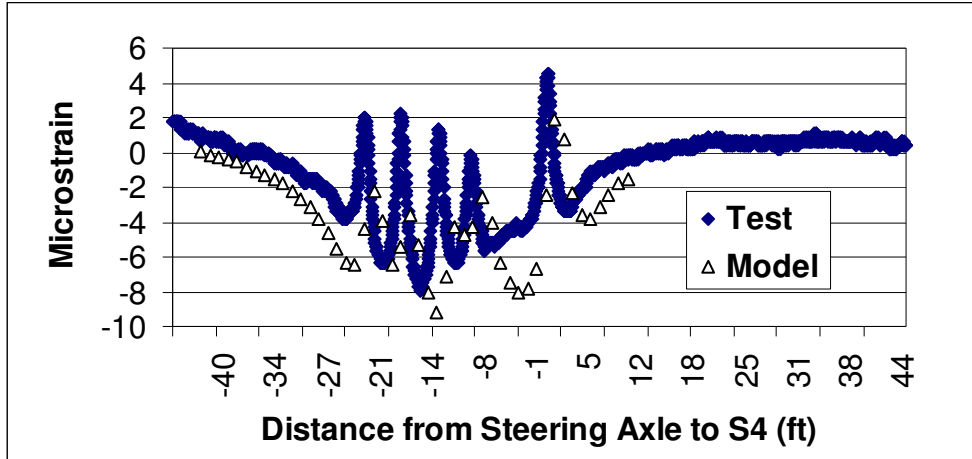


Figure V-70 Comparison of Truck Load Response for M-50 Bridge S4 Bottom Longitudinal

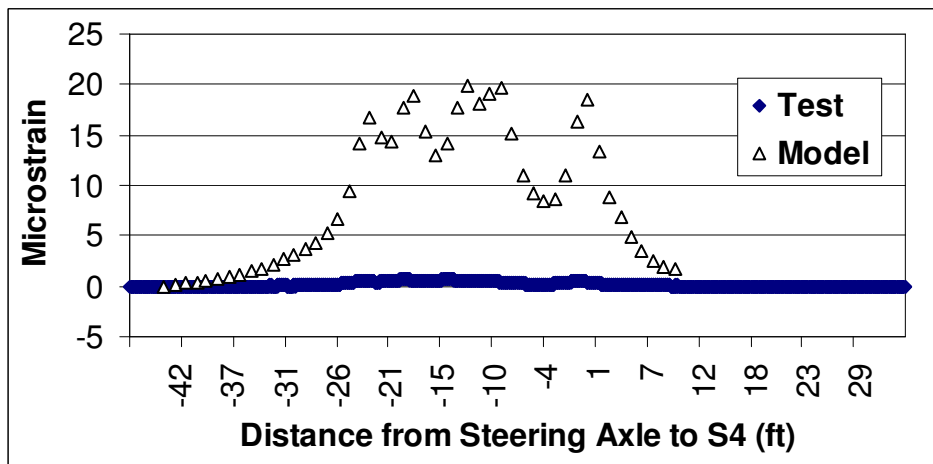


Figure V-71 Comparison of Truck Load Response for M-50 Bridge S4 Bottom Transverse

V-2. Analysis of Typical Skew Decks in Michigan

Upon completion of the model validation above, the FEA using DIANA was applied to 12 cases of concrete bridge decks. These cases included two superstructure arrangements (steel and

prestressed I-beams) with composite deck, three skew angles (0° , 30° , and 45°), and two beam spacings (6' and 10'). All possible combinations of these three sets of the parameter values result in the 12 cases. To limit the scope of work, these cases have one simply supported span length of 70 ft. Typical diaphragms at the span ends are also included, but for simplicity without loss of reliability the barriers are not included in the models. While this sample still represents a small section of possible designs for Michigan, it was felt that they could envelope a large majority of situations that are typical in Michigan.

Figures V-72 and V-73 show the cross section of the steel bridges for 10' and 6' beam spacings, respectively. Figures V-74 and V-75 show the prestressed I-beam counterparts. The simply supported condition was modeled using no constraint to the horizontal translations at one end of the span and hinge at the other end that is constrained in all three orthogonal directions. These generic spans were designed according to the current design specifications for MDOT (AASHTO 2002), to be consistent with current practice. To focus on the deck and its relation to the supporting beams, the barriers or guide rails are ignored in the FEA models.

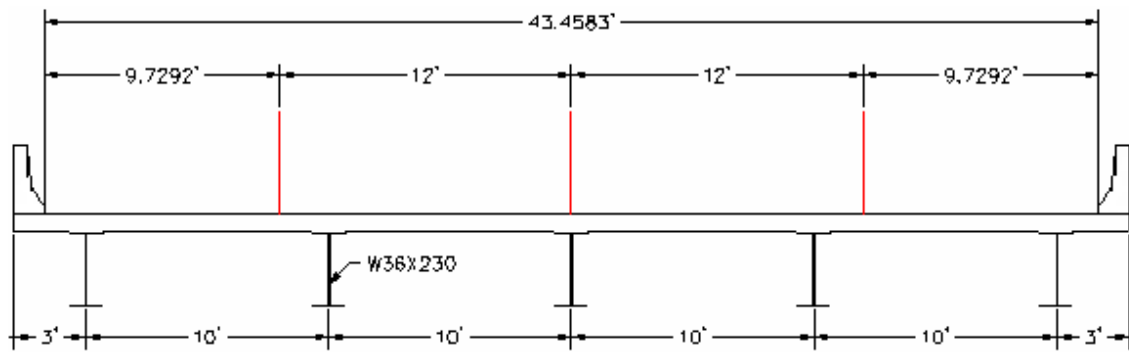


Figure V-72 Cross Section of Generic Steel Bridge with a 9" Concrete Deck on 10' Beam Spacing

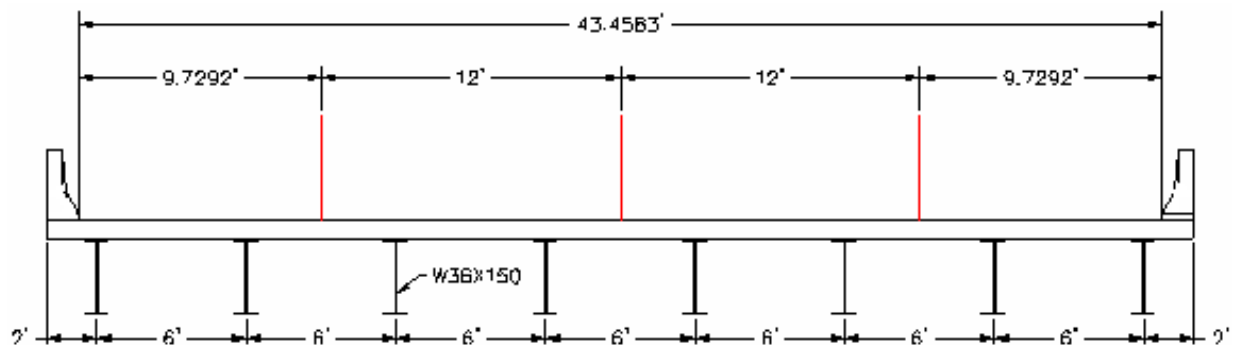


Figure V-73 Cross Section of Generic Steel Bridge with a 9" Concrete Deck on 6' Beam Spacing

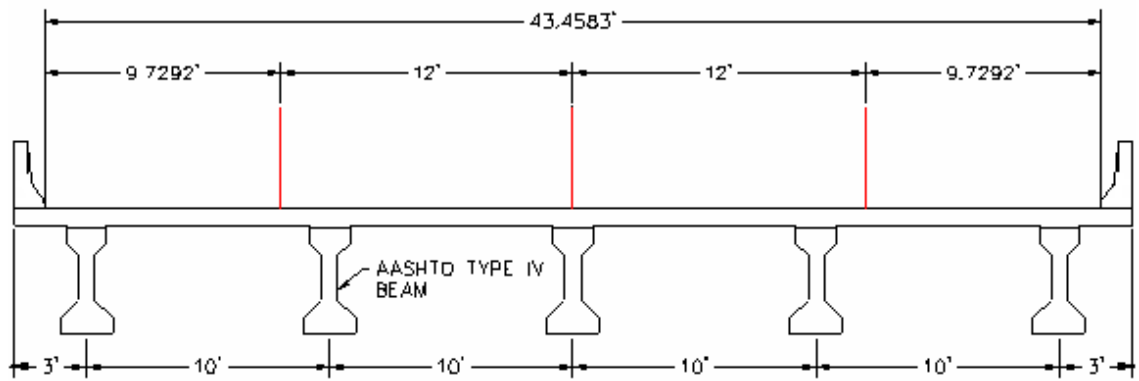


Figure V-74 Cross Section of Generic Prestressed I-Beam Bridge with a 9" Concrete Deck on 10' Beam Spacing

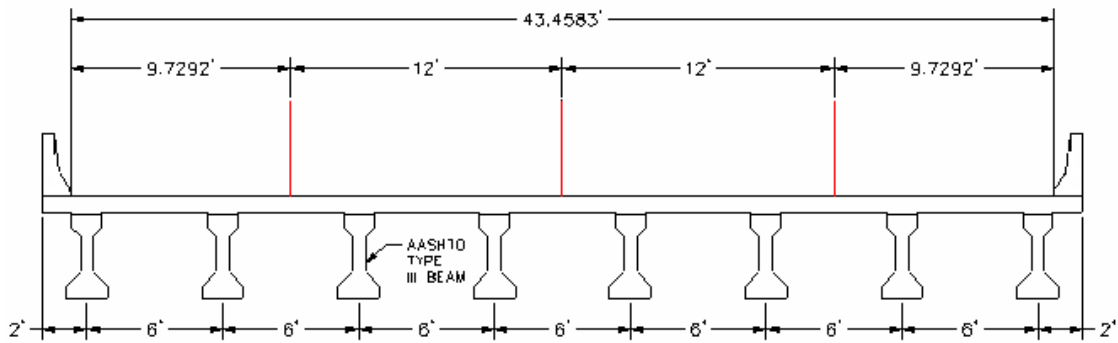


Figure V-75 Cross Section of Generic Prestressed I-Beam Bridge with a 9" Concrete Deck on 6' Beam Spacing

Table V-9 shows a summary of the FEA results for these 12 cases of typical bridge decks, with respect to the maximum principal stresses during the first three days. The input parameters discussed in Section V-1.3 are used to produce these results. These maximum values are found to occur usually between 0.8 to 1.2 days, according to the FEA. They appear in the deck end areas and close to the bottom surface. These areas connect the deck to a beam, end diaphragm (end back wall), or both. It is seen that these stress levels well exceed the concrete's cracking strength. With an estimated 400 psi cracking strength at 28 days, the cracking strength at 1 day can be as low as 100 psi. It is also seen that for the 8 skew deck cases (either 30 or 45 degrees), the maximum principal stress is generally higher than the straight counterparts, highlighting the effect of skew angle.

Table V-9 Maximum Computed Hydration-Induced Thermal Stresses in Concrete Decks Typical in Michigan (psi) (with the upper bound case designated as Max and lower bound case as Min)

6 ft beam spacing (steel beam)			10 ft beam spacing (steel beam)		
0°	Min	509	0°	Min	329
	Max	886		Max	568
30°	Min	656	30°	Min	693
	Max	1451		Max	1569
45°	Min	711	45°	Min	719
	Max	1596		Max	1596

6 ft beam spacing (concrete beam)			10 ft beam spacing (concrete beam)		
0°	Min	582	0°	Min	540
	Max	764		Max	840
30°	Min	606	30°	Min	635
	Max	953		Max	1265
45°	Min	690	45°	Min	686
	Max	1024		Max	1407

Figure V-76 shows the directions of the principal stresses on the deck top for the Grove Street bridge, which is typical for other decks analyzed. Note that these directions are seen following lines along the deck edge or the support line for the superstructure. Thus, cracks in this situation would appear perpendicular to the principal stress directions or the edge line. For comparison, a deck crack photograph for the Grove Street bridge is shown in Figure V-77. These cracks are seen consistent with the maximum principal stress directions found by FEA.

As also seen in Figure V-76, the absolutely maximum principal stresses occur at locations near the end of the deck. These principal stresses are larger at locations directly above the beams than between the beams. It appears that these larger stresses are caused by the constraint imposed by the beams during hydration.

For comparison, Table V-10 shows the maximum principal stresses in the same 12 decks due to a standard truck wheel load of 16 kips. It is seen that these stresses are much lower than those in the hydration stage. In addition, the concrete deck's strength is much higher at the time when truck loads are applied compared with early strengths. Therefore, it appears to be clear that initiation of skew deck corner cracking is not due to truck load. On the other hand, truck loads may result in more visible cracks due to fatigue of a cracked deck.

Table V-10 Maximum Computed Truck Wheel Load-induced Stresses (psi) in Concrete Decks Typical in Michigan

		Steel Beam	Steel Beam	Prestressed Beam	Prestressed Beam
Beam Spacing		6ft	10ft	6ft	10ft
Skew (degree)					
0		36	42	63	51
30		41	42	69	52
45		41	42	72	54

V-3. Discussions

This chapter has presented the process and results of the FEA using DIANA in this project. The modeling practice was first calibrated using two skew bridge decks constructed in Michigan, instrumented with strain, humidity, and temperature sensors. The calibration used the measured data from the processes of truck loading after hardening and thermal and shrinkage loading during concrete hydration. It is seen that the truck loading-induced stress is much lower than that caused in concrete hydration.

In addition, further analysis has shown that skew decks may develop much higher stresses than their straight counterparts.

It is thus concluded that cracking in skew concrete decks is mainly caused by thermal and shrinkage loading in concrete hydration. On the other hand, it should be noted that truck wheel load may form a fatigue loading that can gradually make cracking much more visible with time (Matsui 1985, Perdikaris 1993, Fu et al 2003).

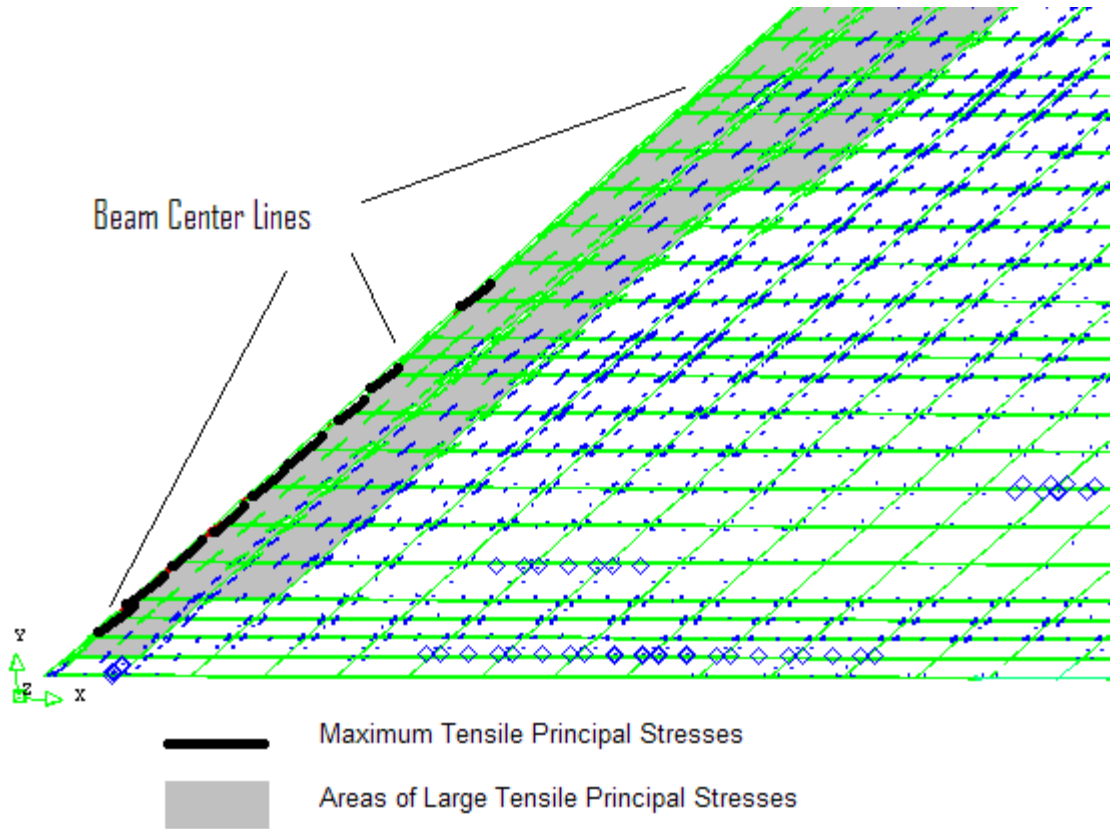


Figure V-76 Grove Street Bridge Principal Stress Directions on Deck Top
(Lines for tensile and diamonds for compressive principal stresses)



Figure V-77 Grove Street Bridge Deck Corner Cracking Observed
Perpendicular to Deck Edge
(Modeled in Figure V-76)

CHAPTER VI DISCUSSIONS AND RECOMMENDATIONS

As presented and discussed in Chapter V, skew deck corner cracking can be concluded as caused by large strain and stress generated due to thermal and shrinkage loading in the process of concrete hydration development. On the other hand, cracking can be made more visible by truck wheel loads.

VI-1. Recommended Cures for Skew Deck Corner Cracking

There appears to be several possible approaches that may be used to reduce the strain and stress in the concrete during the strength development stage. The stress and strain are mainly caused by the constraints to the deck induced by the beams and diaphragms (end walls). These approaches are listed and discussed below.

1) Reduction or relaxation of constraint. Changing the composite deck configuration to a non-composite or less composite one can be an option. At the end of a span, reducing the rigidity of the end diaphragm or backwall can reduce the constraint as well. For example, the concrete end diaphragm may be replaced by steel bracings for steel beam spans if this will not affect other considerations. For concrete bridges, smaller end diaphragms should be considered to reduce the stiffness of the constraint to the deck. In the case of backwall encasing the beam ends, the stiffness of the backwall should be minimized if possible.

2) Optimizing the ingredients in the concrete mix to reduce the potential of cracking, by reducing the heat to be generated in a short period of time and the tendency of shrinkage. One option is to change the type of cement used. However, since this study did not include testing for possibly optional mixes, it is not appropriate to recommend any quantitative changes, although this appears to be the most effective approach without requiring other things to change that may significantly change current practice.

3) Increasing the amount of steel reinforcement in the acute angle corner areas and the end areas of skewed decks, to reduce the stress in the concrete deck. These areas will benefit from such reinforcement in the direction along the skew for potential cracking perpendicular to it. Specifically, additional reinforcement along the deck edge (i.e., along the beam support line) is recommended over one beam spacing in the longitudinal direction, with a spacing of 4" in both top and bottom layers. To minimize possible complexity in construction, the top and bottom additional rebar sizes can be respectively the same as those regularly designed. This additional steel is recommended for those decks exceeding the skew threshold (25 degrees according to the AASHTO LRFD design specifications 2004, Article 9.7.13).

VI-2. Recommended Future Research Work

It also should be noted that this study has used an approach of calibrated numerical modeling and diagnosing, with limited physical testing. The approach was applied to a limited number of cases (12). In addition, a number of important parameters in the model were estimated using the general knowledge not necessarily specific for the tested decks. To fully understand the phenomenon and quantitatively prescribe the solution to the problem, more detailed analysis is required, and more physical testing to determine those important parameters will be very helpful.

In a future study, the following items deserve more attention and further investigation.

- 1) Improved understanding and better data for the parameters used in FEA modeling, especially where the minimum stress case and the maximum stress case do not envelope the test results.
- 2) Identification of potentially optimal mixes that have lower cracking potential than those concretes being used in current bridge deck construction practice. Experiment with these mixes in the laboratory condition to select candidates for field trial.
- 3) Further investigation of the recommended options above for reducing or eliminating deck corner cracking, using physical testing and computer simulation.

VI-3. Implementation Considerations

Based on the scope of this research project, the recommendation for additional steel reinforcement in the skew deck end area can be implemented with minimal effort. It is thus recommended that this recommendation be reviewed by design engineers. When the design is

finalized, a number of skew bridge decks (for example three decks) should be selected for experimental application. After concrete is placed for each of these decks, the deck should be inspected at ages of 7 days, 28 days, 2 months, and 6 months to detect cracking and record its pattern if any. These results should be used to determine whether the additional steel design is effective or needs any improvement.

VI-4. Cost- Benefit Analysis

The recommended additional steel is to reduce or eliminate corner cracking in skewed concrete bridge decks. This section presents an exercise of cost – benefit analysis based on estimation.

Assuming that, on average, the recommended additional steel is to cover an equivalent length approximately equal to one fifth of the deck span length (one beam spacing long on each end). Since the entire width will be covered using the additional steel, the additional cost for this steel is estimated at 20% of the total reinforcement cost for the span ($\$8/\text{ft}^2$) or $\$1.60/\text{ft}^2$. The unit cost $\$8/\text{ft}^2$ was obtained based on the MDOT 2007 price report. Let us further assume that this steel will reduce cracking so that the average deck life to first overlay is to be extended by about 15% (using a 6-year increase for a life to first overlay of 40 years). Therefore the potential benefit is estimated as 15% of average total deck cost of $\$24.86/\text{ft}^2$ equal to $\$3.73/\text{ft}^2$, with the total deck cost estimated according to the MDOT 2007 price report. Thus the cost/benefit ratio can be estimated at $\$1.60/\$3.73 = 0.43$. This represents a net benefit for the recommendation to be implemented.

REFERENCES

AASHTO "Standard Specifications for Highway Bridges" 17th Ed. 2002, Washington D.C.

AASHTO "LRFD Bridge Design Specifications", 4th Ed, 2007, Washington, DC

Abel, J., Moore, W. P., and Associates Hover, K., (1998) "Effect of Water-Cement Ratio on the Early Age Tensile Strength of Concrete" *TRB Annual Meeting practical papers*

ACI 209 Prediction of Creep, Shrinkage, and Temperature Effects in Concrete Structures. Tech. Rep. ACI 209R-82, American Concrete Institute, 1982

ACI Committee 224, 224.IR-84, (1984) "Causes, Evaluation and Repair of Cracks in Concrete" *ACI Manual of Concrete Practice*, American Concrete Institute, Detroit, Michigan

ACI Committee 308, (Revised 1986) "Standard Practice for Curing Concrete" *ACI Manual of Concrete Practice*, American Concrete Institute, Detroit, Michigan, ACI 308-81

Aktan, H., Fu, G., Attanayaka, U., and Dekelbab, W. "Investigate Causes and Develop Methods to Minimize Early-age Deck Cracking on Michigan Bridge Decks" Final Report to Michigan Department of Transportation, Wayne State University, 2003

Allan, M. L., (1995) "Probability of Corrosion Induced Cracking in Reinforced Concrete" *Cement and concrete Research*, Vol. 25, No. 6, pp.1179-1190

Almusallam, A. A., (2001) "Effect of Environmental Conditions on the Properties of Fresh and Hardened Concrete" *Cement and Concrete Composites*, Vol. 23, pp. 353

Babaei, K. and Fouladgar, A. M., (1997) "Solutions to Concrete Bridge Deck Cracking" *Concrete International*, Vol. 19, No. 7, pp. 34.

Babaei, K. and Hawkins, N. M., (1987) "Evaluation of Bridge Deck Protective Strategies" *NCHRP Report 297*, Transportation Research Board, National Research Council, Washington, D.C.

Berke, N. S. and Roberts, L. R., (1989) "Use of Concrete Admixtures to Provide Long-Term Durability from Steel Corrosion" *ACI SP 119-20*, pp.384-403

Bolander, J.E. and Le, B.D., (1999) "Modeling Crack Development in Reinforced Concrete Structures Under Service Loading" *Journal of Construction and Building Materials*

Borrowman, P. E., Seeber, K. E., and Kesler, C. E., (1977) "Behavior of Shrinkage-Compensating Concretes Suitable for use in Bridge Decks" *Department of Theoretical and Applied Mechanics*, University of Illinois, Urbana, Illinois, T. and A.M. Report No. 416

Boulware, B. L. and Nelson, B. H., (November 1979) "Factors Affecting the Durability of Concrete Bridge Decks: Shrinkage Compensated Cement Concrete in Bridge Deck-Interim Report No. 5" *California Department of Transportation*, FHWA/CA/SD-79/18

Burke, M. P. Jr., (1999) "Cracking of Concrete Decks and Other Problems with Integral-type Bridges" *Transportation Research Record*, pp. 131

Cady, P. D. and Carrier, R. E., (1971) "Final Report on Durability of Bridge Deck-concrete-Part 2: Moisture Content of Bridge Decks" *Department of Civil Engineering*, Pennsylvania State University

Cady, P. D., Carrier, R. E., Bakr, T., and Theisen, J., (1971) "Final Report on the Durability of Bridge Decks-Part 1: Effect of Construction Practices on Durability" *Department of Civil Engineering*, Pennsylvania State University

Campbell-Allen, D. and Lau, B., (1978) "Cracks in Concrete Bridge Decks" *University of Sydney School of Civil Engineering*, Research Report R313

Carlson, R. W., (June 1940) "Attempts to Measure the Cracking Tendency of Concrete" *Journal of the ACI*, Vol. 36, No. 6, pp.533-540

Castaneda, D.E. "Causes of Mechanical Damage to Alabama Bridge Decks" Report to Alabama Department of Transportation, 1995

Cheng, T. T. and Johnston, D. W., (June 1985) "Incidence Assessment of Transverse Cracking in Bridge Decks: Construction and Material Considerations" *North Carolina State University*, Department of Civil Engineering, Raleigh, North Carolina, FHWA/NC/85-002 Vol. 1

Committee on the Comparative Costs of Rock Salt and Calcium Magnesium Acetate (CMA) for Highway Deicing, (1991) "Highway Deicing Comparing Salt and Calcium Magnesium Acetate" *NCHRP Special Report 235*, Transportation Research Board

Cook, H.K. "Thermal Properties" Significance of Tests and Properties of Concrete and Concrete-making Materials, 1966

Coutinho, A. de S., (December 1959) "The Influence of the Type of Cement on its Cracking Tendency" *Rilem*, New Series No. 5

Cusick, R. W. and Kesler, C. E., (1980) "Behavior of Shrinkage Compensating Concretes Suitable for Use in Bridge Decks" *American Concrete Institute*, Detroit, Michigan, ACISP 64-15, pp.293-310

Dakhil, F. H., Cady, P. D., and Carrier, R. E., (August 1975) "Cracking of Fresh Concrete as Related to Reinforcement" *Journal of the ACI*, pp. 421-428

DIANA User's Manual: Material Library, 2003

Dry, C. M., (1999) "Repair and Prevention of Damage Due to Transverse Shrinkage Cracks in Bridge Decks" *Proceedings of SPIE - The International Society for Optical Engineering*, Vol. 3671, pp. 253

Ebeido, T., and Kennedy J., "Shear and Reaction Distributions in Continuous Skew Composite Bridges" *J. J. Bridge Eng.* 1996, Vol. 1, No. 4, pp. 155-165

Feng, J. "Reinforced Concrete Bridge Deck Fatigue Under Truck Wheel Load" PhD dissertation, Department of Civil and Environmental Engineering, Wayne State University, 2004

Fouad, F. H. and Furr, H. L., (1986) "Behavior of Portland Cement Mortar in Flexure at Early Ages" *ACI SP 9-5-6*, American Concrete Institute, Detroit, Michigan, pp. 93-113

Freidin, C., (2001) "Effect of Aggregate on Shrinkage Crack-Resistance of Steam Cured Concrete" *Magazine of Concrete Research*, Vol. 53, pp. 85

French, C., Eppers, L., Le, Q., and Hajjar, J., (1998) "Transverse Cracking in Bridge Decks" *TRB Annual Meeting practical papers*

Fu, G., J. Feng, W. Dekelbab, F. Moses, H. Cohen, D. Mertz, and P. Thompson "Effect of Truck Weight on Bridge Network Costs", NCHRP Report 495 (Project 12-51), Department of Civil and Environmental Engineering, Wayne State University, 2003

Fu, G., S. Alampalli, and F. P. Pezze "Lightly Reinforced Concrete Bridge Deck Slabs on Steel Stringers: A Summary of Field Experience", Final Report on R142 to FHWA, FHWA/NY/RR-94/161, Engineering Research and Development Bureau, New York State Department of Transportation, June 1994

Furr, H. L. and Fouad, F. H., (1982) "Effect of Moving Traffic on Fresh Concrete During Bridge-Deck Widening." *Transportation Research Record 860*, pp. 28-36

Furtak, K., (1999) "Assessment of Crack State in RC Slabs of Composite Bridges" *Archives of Civil Engineering*, Vol. 45, pp. 59

Gilbert, R. I., (March-April 1992) "Shrinkage Cracking in Fully Restrained Concrete Members" *ACI Structural Journal*, Vol. 89, No. 2, pp. 141-149

Hansen, T. C. and Mattock, A. H., (February 1966) "Influence of Size and Shape of Member on the Shrinkage and Creep of Concrete" *Journal of the ACI*, Vol. 63 [Also *PCA Development Department Bulletin D103*, Portland Cement Association]

Hanson, J. A., Elstner, R. C., and Clore, R. H., (1973) "The Role of Shrinkage Compensating Cement in Reduction of Cracking of Concrete" *American Concrete Institute*, Detroit, Michigan, ACI SP 38-12, pp. 251-271

Healy, R. J. and Lawrie, R. A. (1998) "Bridge Cracking: A Dot Experience and Perspective" *Concrete International*, Vol. 20, No. 9, pp. 37-40

Holt, E.E. and Janssen, D. J., (1998) "Influence of Early Age Volume Changes on Long-Term Concrete Shrinkage" *TRB Annual Meeting practical papers*

Horn, M. W., Stewart, C. F., and Boulware, R. L., (1972) "Factors Affecting the Durability of Concrete Bridge Decks: Normal vs. Thickened Deck-Interim Report No. 3" Bridge Department, California Division of Highways, CA-HY-4101-3-72-11

Horn, M. W., Stewart, C. F., and Boulware, R. L., (1972) "Webber Creek Deck Crack Study-Final Report." State of California, Business and Transportation Agency, Department of Public Works, in Cooperation with the FHWA, Research Report CA-HWY-BD-624102 (2)-72-2

Horn M. W., Stewart, C. F., and Boulware R. L., (March 1975) "Factors Affecting the Durability of Concrete Bridge Decks." Construction Practices-Interim Report No. 4. Bridge Department, California Division of Highways, CA-DOT-ST-4104-4-75-3

Hue, F., Serrano, G., and Bolano, J. A., (2000) "Oresund Bridge Temperature and Cracking Control of the Deck Slab Concrete at Early Ages" *Automation in Construction*, Vol. 9, pp. 437

Irwin, R. J. and Chamberlin, W. P., (September 1981) "Performance of Bridge Decks with 3-inch Design Cover" *New York State Department of Transportation*, Report No FHWA/NY/RR-81/93

Issa, M. A., (1999) "Investigation of Cracking in Concrete Bridge Decks at Early Ages" *Journal of Bridge Engineering*, pp. 116

Issa, M.A., Yousif, A.A., and Issa, M.A., (August 2000) "Effect of Construction Loads and Vibrations on New Concrete Bridge Decks" *Journal of Bridge Engineering*

Jauregui, D.V., (2001)" A Field-Testing System for Experimental Bridge Evaluation" *Experimental Techniques*, Vol. 25, pp.37

Jovall, O., (2001) "Avoiding Early Age Cracking." *Concrete Engineering International*, Vol. 5, pp. 41

Khaloo, A., and Mirzabozorg, H., "Load Distribution Factors in Simply Supported Skew Bridges." *J. Bridge Eng.* Vol. 8, No. 4, pp241-244, 2003

Kosel, H. C. and Michois, K. A., (January 1985) "Evaluation of Concrete Deck Cracking for Selected Bridge Deck Structures of the Ohio Turnpike, Report to Ohio Turnpike Commission" *Construction Technology Laboratories (CTL)*

Kraai, P., (September 1985) "A Proposed Test to Determine the Cracking Potential Due to Drying Shrinkage of Concrete" *Concrete Construction*, Vol. 30, No. 9, pp. 775-779

Krauss, P. D. and Rogalla, E.A, (1996) "Transverse Cracking in Newly Constructed Bridge Decks" NCHRP Report No. 380. Washington, D.C.

Ksomatka, S. H. and Panarese, W. C., (1990) "Design and Control of Concrete Mixtures" Thirteenth edition, *Portland Cement Association*

Kumaat, E. and Lorrain, M., (1996) "Cracking of Plain or Reinforced High Performance Concrete Slabs" *International Journal of Structures*, Vol. 16, pp. 1

Kwak, H. G., Seo, Y. J., and Jung, C. M., (2000) "Effects of the Slab Casting Sequences and the Drying Shrinkage of Concrete Slabs on the Short-Term and Long-Term Behavior of Composite Steel Box Girder Bridges. Part 2" *Engineering Structures*, Vol. 22, pp. 1467

Kwak, H. G., and Seo, Y. J., (2002) "Shrinkage Cracking at Interior Supports of Continuous Pre-Cast Pre-Stressed Concrete Girder Bridges" *Construction and Building Materials*, Vol. 16, pp. 35

La Fraugh, R. W. and Perenchio, W. F., (October 1989) "Phase I Report of Bridge Deck Cracking Study West Seattle Bridge" *Wiss, Janney, Elstner Associates*, Report No. 890716

Lebet, J. P. and Ducret, J.M., (1998) "Experimental and Theoretical Study of the Behavior of Composite Bridges During Construction" *Proceedings of the 1998 2nd World Conference on Steel in Construction*, Journal of Constructional Steel Research

Lerch, W., (February 1957) "Plastic Shrinkage" *Journal of the ACI*, Vol. 53, No. 2, pp. 803-802

Lower, D. O., (1980) "Summary Report on Type K Shrinkage-Compensating Concrete Bridge Deck Installations in the State of Ohio" *American Concrete Institute*, Detroit, Michigan, ACI SP 64-10, pp. 181-192

Maleki, S. "Deck Modeling for Seismic Analysis of Skewed Slab-girder Bridges" *Engineering Structures*, 24, pp1315–1326, 2002

Manning, D. G., (December 1981) "Effect of Traffic-Induced Vibrations on Bridge Deck Repairs" *NCHRP Synthesis 86*, Transportation Research Board, National Research Council Washington, D.C.

Mendelson, A. *Plasticity: Theory and Application*. Second Edition 1970

McDonald, J. E., (1992) "The Potential for Cracking of Silica-Fume Concrete" *Concrete Construction*

Meyers, C., (1982) "Survey of Cracking on Underside of Classes B-1 and B-2 Concrete Bridge Decks in District 4" Investigation 82-2, Missouri Highway and Transportation Department, Division of Materials and Research

Nevelle, A. M. Properties of Concrete, 4th Ed, 1995

Newmark, N. M., Siess, C. P., and Penman, R. R. "Studies of Slab and Beam Highway Bridges, Part I Tests of Simple Span Right I- Beam Bridges", University of Illinois Bulletin, Vol. 43, No.42. 1946

Newmark, N. M., Siess, C. P., and Peckham, R. M. "Studies of Slab and Beam Highway Bridges, Part II Tests of Simple Span Skew I-Beam Bridges", University of Illinois Bulletin Series, No.375. 1947

Nishida, N., Ushioda, K., Dobashi, Y., and Matsui, K., (1995) "Evaluation of Thermal cracking Index in Slab-Concrete Under Uncertain Parameters" *Transactions of the Japan Concrete Institute*, Vol. 17, pp. 127

Ohama, Y., Demura, K., Satoh, Y., Tachibana, K., and Miyazaki, Y., (1989) "Development of Admixtures for Highly Durable Concrete" *ACI SP 119-17*, pp. 321-342

Ottosen, N. S. "A Failure Criterion for Concrete" ASCE Journal of the Engineering Mechanics Division, Vol.103, EM4, pp. 527-535, 1977

Perfetti, G. R., Johnson. D. W., and Bingham, W. L., (June 1985) "Incidence Assessment of Transverse Cracking in Concrete Bridge Decks" *Structural Consideration*, FHWA/NC/85-002 Vol. 2

Perragaux, G. R. and Brewster, D. R., (June 1992) "In-Service Performance of Epoxy-Coated Steel Reinforcement in Bridge Decks-Final Report" New York State Dept. of Transportation Technical Report 92-3

Pettersson, D. and Thelandersson, S., (2001) "Crack Development in Concrete Structures Due to Imposed Strains - Part I: Modelling" *Materials and Structures/Material Constructions*, Vol. 34, pp. 7

Phillips, M.V., Ramey, G.E., and Pittman, D.W., (November 1997) "Bridge Deck Construction Using Type K cement" *Journal of Bridge engineering*

Popovic, P., Rewerts, T. L., and Sheahen, D. J., (January 1988) "Deck Cracking Investigation of the Hope Memorial Bridge" *Ohio Department of Transportation*

Portland Cement Association, (1970) Final Report-Durability of Concrete Bridge Deck--A Co-operative Study

Purvis, R. L., (1989) "Prevention of Cracks in Concrete Bridge Decks" *Wilbur Smith Associates, Report on Work in Progress*

Purvis, R. L. and Babaei, K., (1995) "Premature Cracking of Concrete Bridges: Causes and Method of Prevention" *Conference Proceedings 7, Vol. 1, pp. 163-175*

Ramey, G. E., Stallings, J. M., and Oliver, R. S., (1999) "Cracking Damage/Deterioration and Rehabilitation Considerations of Some Birmingham, Alabama, Interstate Bridge Decks" *Transportation Research Record*, pp. 33

Randall, F. A., (1980) "Field Study of Shrinkage Compensating Cement Concrete" *American Concrete Institute, Detroit, Michigan, ACI SP 64-13, pp. 239-257*

Rawi, R. S. A. and Kheder, G. F., (July-August 1990) "Control of Cracking Due to Volume Change in Base-Restrained Concrete Members" *ACI Structural Journal, Vol. 87, No. 4, pp. 397-405*

Reis, E. E., Jr., Mozer, J. D., Bianchini, A. C., and Kesler, C.E., (1964)" Causes and Control of Cracking in Concrete Reinforced with High Strength Steel Bars-A Review of Research." *T. & A.M. Report No. 261, Department of Theoretical and Applied Mechanics, University of Illinois, Urbana, Illinois*

Rhodes, C. C., (1950) "Curing Concrete Pavements with Membranes" *Journal of the ACI, Vol. 57, No. 12, pp. 277-295*

Russell, H. G., (1980) "Performance of Shrinkage-Compensating Concretes in Slabs" *American Concrete Institute, Detroit, Michigan, ACI SP 65-6, pp. 81-114*

Schmitt, T.R and Dawin, D., (February 1999) "Effect of Material Properties on Cracking in Bridge Decks" *Journal of Bridge Engineering*

Shah, S. P., Weiss, W. J., and Yang, W., (1998)" Shrinkage Cracking - Can It Be Prevented?" *Concrete International, Vol. 20, pp. 51*

Shah, S. P., Marikunte, S., Yang, W., and Aldea, C., (1996) "Control of Cracking with Shrinkage-Reducing Admixtures" *Transportation Research Record*, pp. 25

Shi, Z.; Nakano, M., (2001) "Application of a 3-D Crack Analysis Model to RC Cantilever Decks of Excessive Cracking" *Structural Engineering and Mechanics, Vol. 12, pp.377*

Spellman, D. L., Woodstrom, J. H., and Baily, S. N., (June 1973) "Evaluation of Shrinkage Compensated Cement" Materials and Research Department, California Division of Highways, CA-HY-MR-5216-1-73-15

Stewart, C. F. and Gunderson, B. J., (November 1969) " Factors Affecting the Durability of Concrete Bridge Decks-Interim Report #2" Report by the Research and Development Section of the Bridge Department, State of California

Suh, Y. and McCullough, B. F., (1994) "Factors Affecting Crack Width of Continuously Reinforced Concrete Pavement" *Transportation Research Record*, pp. 134

Tindal, T. T. and Yoo, C. H. "Thermal Effects on Skewed Steel Highway Bridges and Bearing Orientation", *ASCE Journal of Bridge Engineering*, Vol. 8, No. 2, March 1, 2003.

Van der Veen, C., Koenders, E. A. B., and Kaptijn, N., (1996) "Thermal Cracking in a Cantilever Bridge Made of HSC" *Computing in Civil Engineering (New York)*, pp. 892

Wang, Q., Zhang, T., and Zhao, G., (2001) "Analysis of Biaxial Bending of Reinforced Concrete Slabs with Simply Support Under Concentrated Loads" *Journal of Dalian University of Technology*, Dalian Ligong Daxue Xuebao, Vol. 41, pp. 481

Weiss, W.J. Prediction of Early-age Shrinkage Cracking in Concrete Elements, 1999